Analysis of Axisymmetric Structures and Tanks by the Program *ELPLA*

Part II: Verification Examples

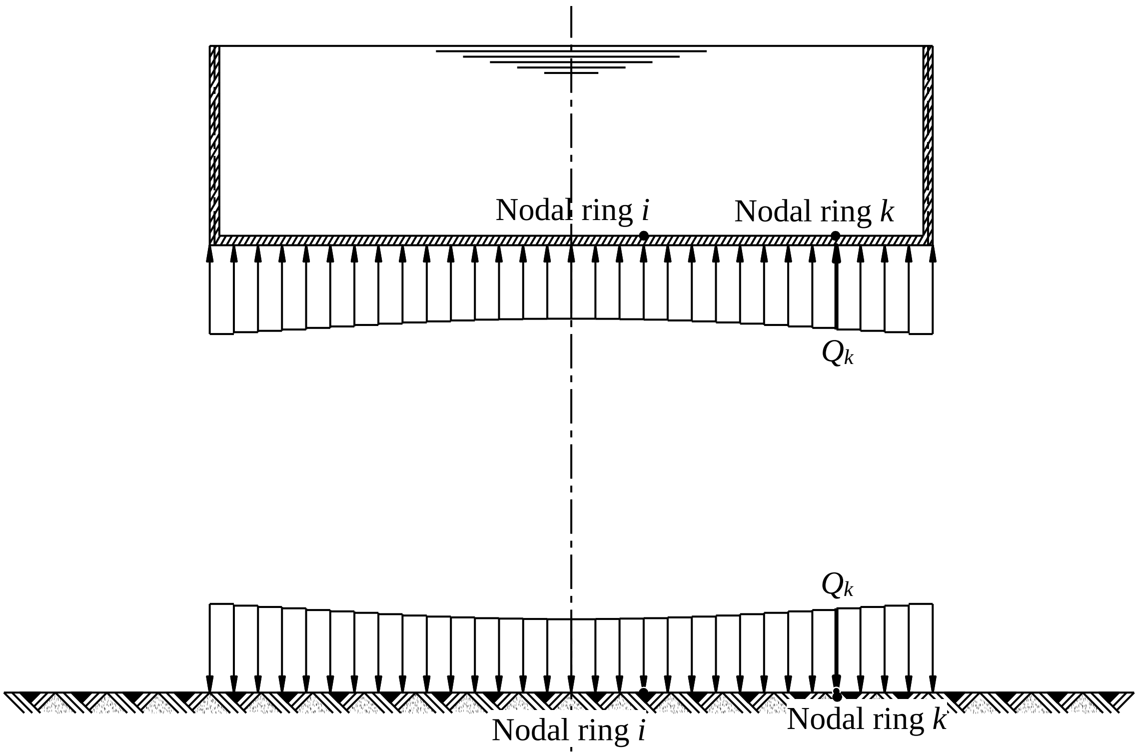

M. El Gendy
O. El Gendy

GEOTEC Software Inc.
PO Box 14001 Richmond Road PO, Calgary AB, Canada T3E 7Y7
Tele.:+1(587) 332-3323
geotec@geotecsoftware.com
www.geotecsoftware.com

2022

Table of Contents

Page

Preface

Various problems in geotechnical Engineering can be investigated by the program *ELPLA*. The original version of *ELPLA* was developed by the father of elastic foundation Prof. M. Kany, Prof. M. El Gendy and Dr. A. El Gendy. After the death of Prof. Kany, Prof. M. El Gendy and Dr. A. El Gendy further developed the program to meet the needs of practice.

This book describes procedures and methods available in *ELPLA* to analyze circular cylindrical shells structures. It is also considered, circular cylindrical tank resting on any layered compressible soil as one unit taking into account the soil-structure interaction effect.

The purpose of this text is to present the methods, equations, procedures, and techniques used in the formulation and development of the *ELPLA* function for analyzing tanks on different subsoil models. It is of value to be familiar with this information when using the software.

An understanding of these concepts will be of great benefit in applying the software, resolving difficulties and judging the acceptability of the results.

Two familiar types of subsoil models are considered, *Winkler*'s model and Continuum model. In addition, the simple assumption model is also considered. This model assumes linear contact pressure on the base of the tank.

The mathematical solution of the circular cylindrical tanks is based on the Finite Element Method using axi-symmetric circular cylindrical shell elements.

In which, axi-symmetric shell finite elements represent the tank wall and tank base according to the nature geometry of the structure.

Based on his MSc research, *El Gendy, O.* (2016) had carried out a numerical modification on the methods in *ELPLA* for analyzing rafts to be applicable for analyzing cylindrical water storage tanks. Many tested examples are presented to verify and illustrate the available methods. Some of verification examples for analyzing cylindrical water storage tanks carried out by *El Gendy, O.* (2016) are presented in this book.

2 Verification Examples

2.1 Introduction

Most of mathematical models used in the analysis of circular cylindrical tanks resting on layered soil under static loading are new developed in the program *ELPLA*. *ELPLA* is a user-friendly computer program. It can analyze structures with different types of subsoil models. To verify the validity of this computer program, some problems published previously by researchers using different methods of analyses and models are compared with the results obtained by the analysis used in this book. A verification study is carried out using the computer program to analyze circular cylindrical tanks with different subsoil models. The mathematical solution of the circular cylindrical tanks is based on the Finite Element Method using circular cylindrical shell elements.

The verification analyses are focused on the validity of the structural analysis of circular cylindrical tanks. The mathematical model of the structural analysis is based on the Finite Element Method using circular cylindrical shell elements. Items to be checked under deferent conditions are internal forces, deformations and rotations in the tank wall and base.

2.2 Axisymmetric structure problems

The analysis of axisymmetric structure problems is now available in *ELPLA* (Figure 2.1). This book presents many examples for this type of problems. It is recommended to read this book to understand the procedures used by the program before starting to create any practical problem analysis.

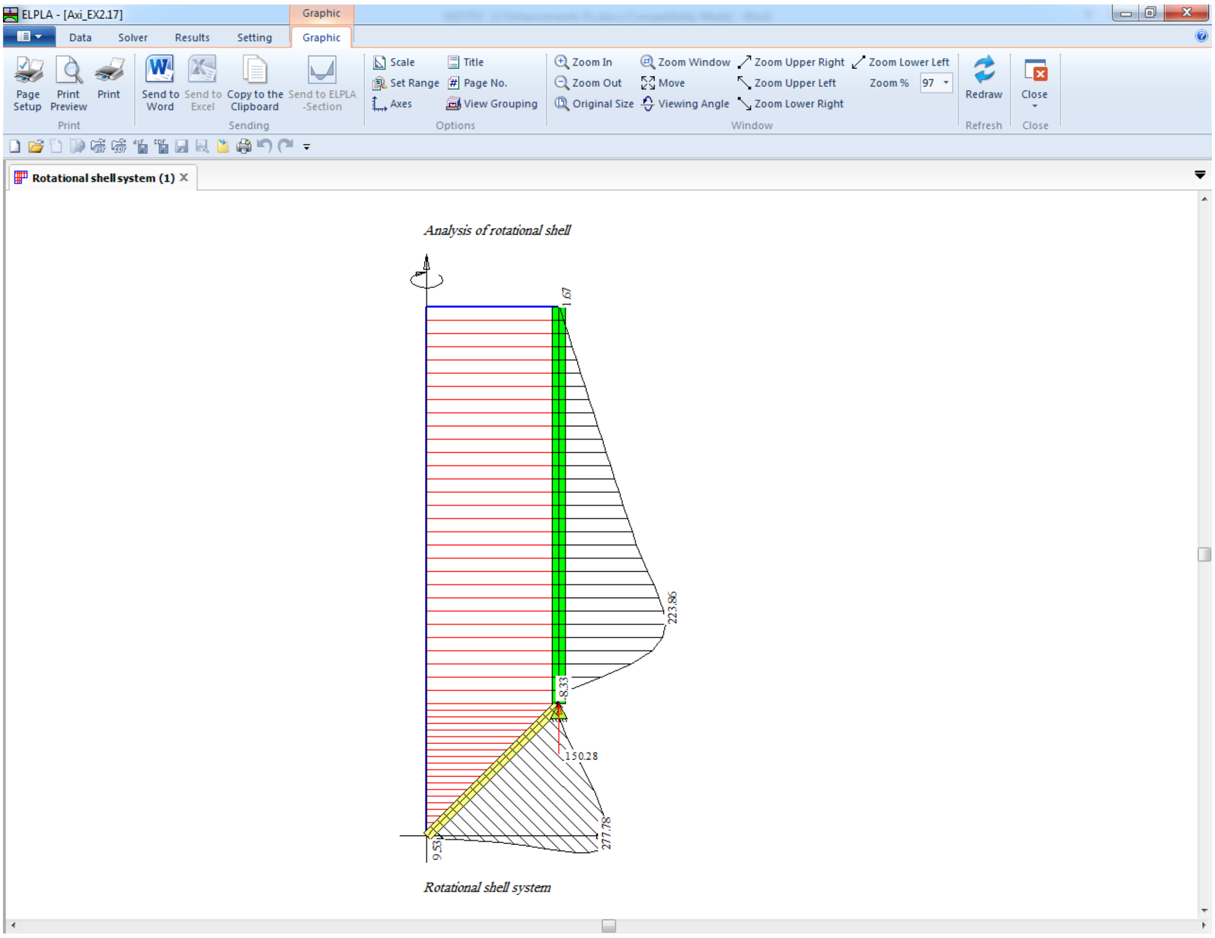

Figure 2.1 Analysis of a water container

2.2.1 Coordinate Systems

There are two different coordinates for axisymmetric structure problems; global coordinate system and local coordinate system (Figure 2.2). Each of these coordinate systems is used to describe certain data such as the location of nodes or the direction of loads, displacements, internal forces and reactions. Understanding these different coordinate systems is essential for the user to define correctly the problem.

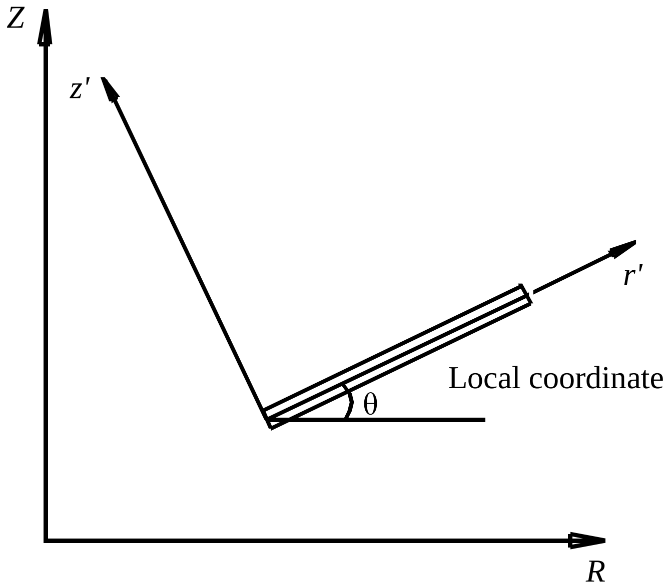

Figure 2.2 System Coordinates

2.2.2 Element Loads

As shown in Figure 2.3, *ELPLA* uses a different vertical direction for defining loads. The positive value of load means that it is a downward load. Nodal loads are applied on global coordinates while element loads are applied in three different cases as follow:

i. Self weight: A vertical uniform load distributed along the length of the element.
ii. Snow load: A vertical uniform load distributed along the horizontal projection of the element.
iii. Wind load: A uniform load distributed along the length of the element with a direction perpendicular to the element (local r` axis).

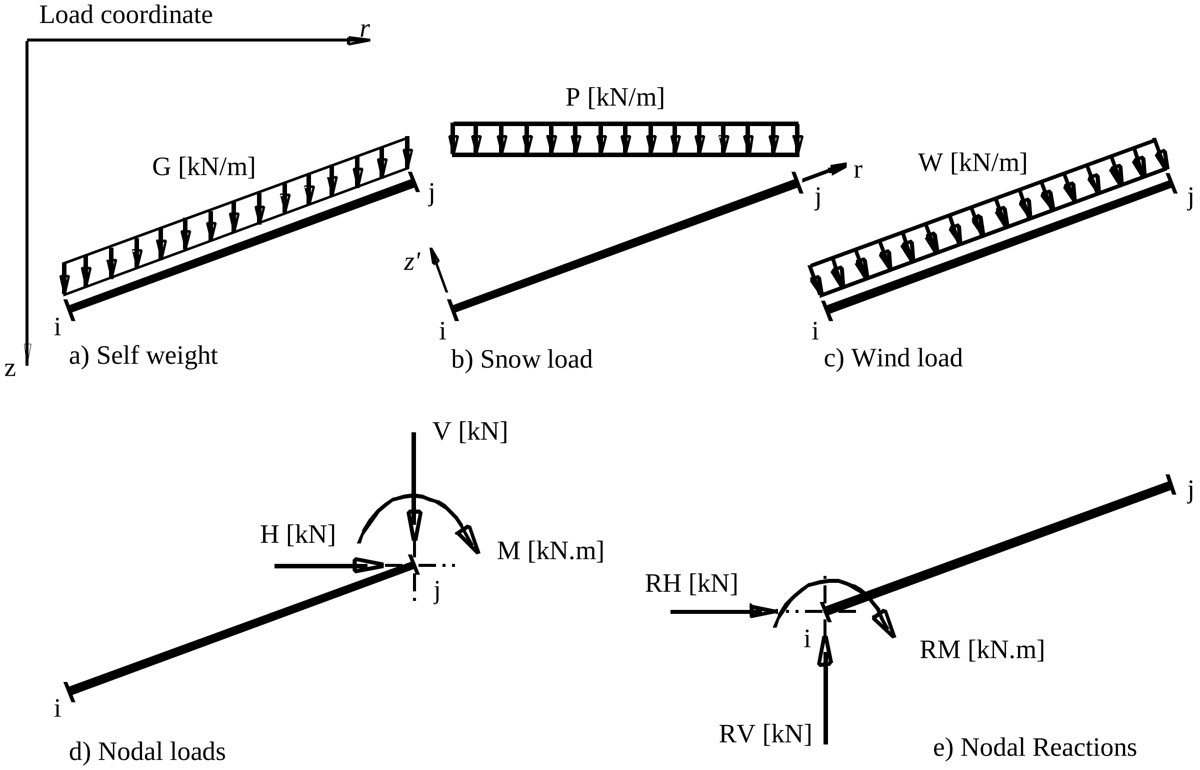

Figure 2.3 Cases of element loads, nodal loads and nodal reactions with directions

2.2.3 Graphical output

The graphical output of results such as displacements, rotations and internal forces (bending moments, shear forces and normal forces) are drawn in locale coordinate.

2.3 Example 1: Circular loaded area resting on a thin clay layer

2.3.1 Description of the problem

To verify the settlement of a loaded area resting on a relative thin clay layer calculated by *ELPLA* using circular and annular elements, a hand calculation of a settlement for a relative thin soil layer under a circular loaded area is compared with that obtained by *ELPLA*.

A circular loaded area of a load q = 150 [kN/m^2] and radius a = 4 [m] is acting on a relative thin clay layer as shown in Figure 2.4. Find the settlement of the clay layer under the center of the loaded area.

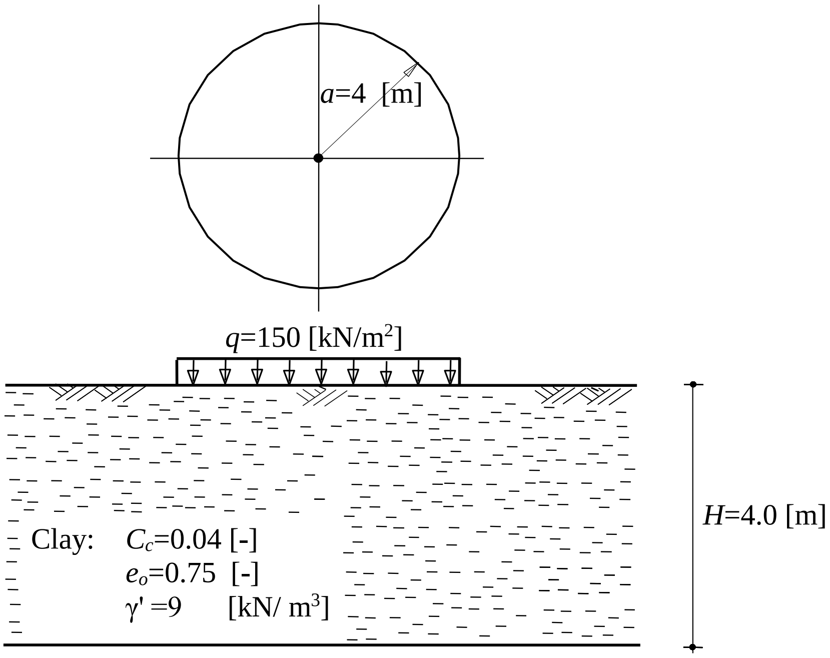

Figure 2.4 Soil profile under the circular loaded area

2.3.2 Hand calculation

If the clay layer is relatively thin and its thickness does not exceed on the footing length H<2a, *Quick ELPLA* deals with the clay layer as one unit and considers the stress for the whole layer. The average stress $\Delta\sigma_{va}$ in a relative thin clay layer of thickness H under the center of a circular loaded area q of a radius a is given by:

$$\Delta\sigma_{va} = \frac{q}{H}\left(H - \frac{H^2 + 2a^2}{\sqrt{H^2 + a^2}} + 2a \right)$$

The average stress $\Delta\sigma_{va}$ in the entire clay layer:

$$\Delta\sigma_{va} = \frac{150}{4}\left(4 - \frac{4^2 + 2\times 4^2}{\sqrt{4^2 + 4^2}} + 2\times 4\right)$$

$$\Delta\sigma_{va} = 131.8\,[\text{kN/m}^2]$$

Overburden stress σ_o at the middle of the clay layer (*z*=2 [m]):

$$\sigma_o = \gamma' z_2 = 9\times 2 = 18\ [\text{kN/m}^2]$$

Settlement S_c of the clay layer:

$$S_c = \frac{C_c H}{1+e_o}\log\frac{\Delta\sigma_{va} + \sigma_o}{\sigma_o} = \frac{0.04\times 4}{1+0.75}\log\frac{131.8+18}{18} = 0.0841\,[\text{m}] = 8.41[\text{cm}]$$

2.3.3 Settlement by *ELPLA*

The settlement obtained from *ELPLA* at the center *c* of the circular loaded area is 8.40 [cm]. It is same as that of the hand calculation. The input data and results of *ELPLA* are presented on the next pages.

Method (9) (Layered soil model)
Flexible Foundation

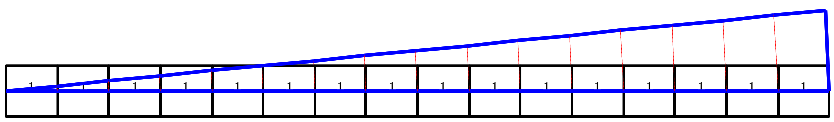

Elements of the loaded area

GEOTEC Software Inc
PO Box 14001 Richmond Road PO, Calgary AB, Canada T3E 7Y7

Scale 1:28	**Title: Settlement of a circular loaded area resting on a thin clay layer**
File: CircLoadedArea	**Date: 05/01/2020**
Page No.:	**Project: Verification Examples**

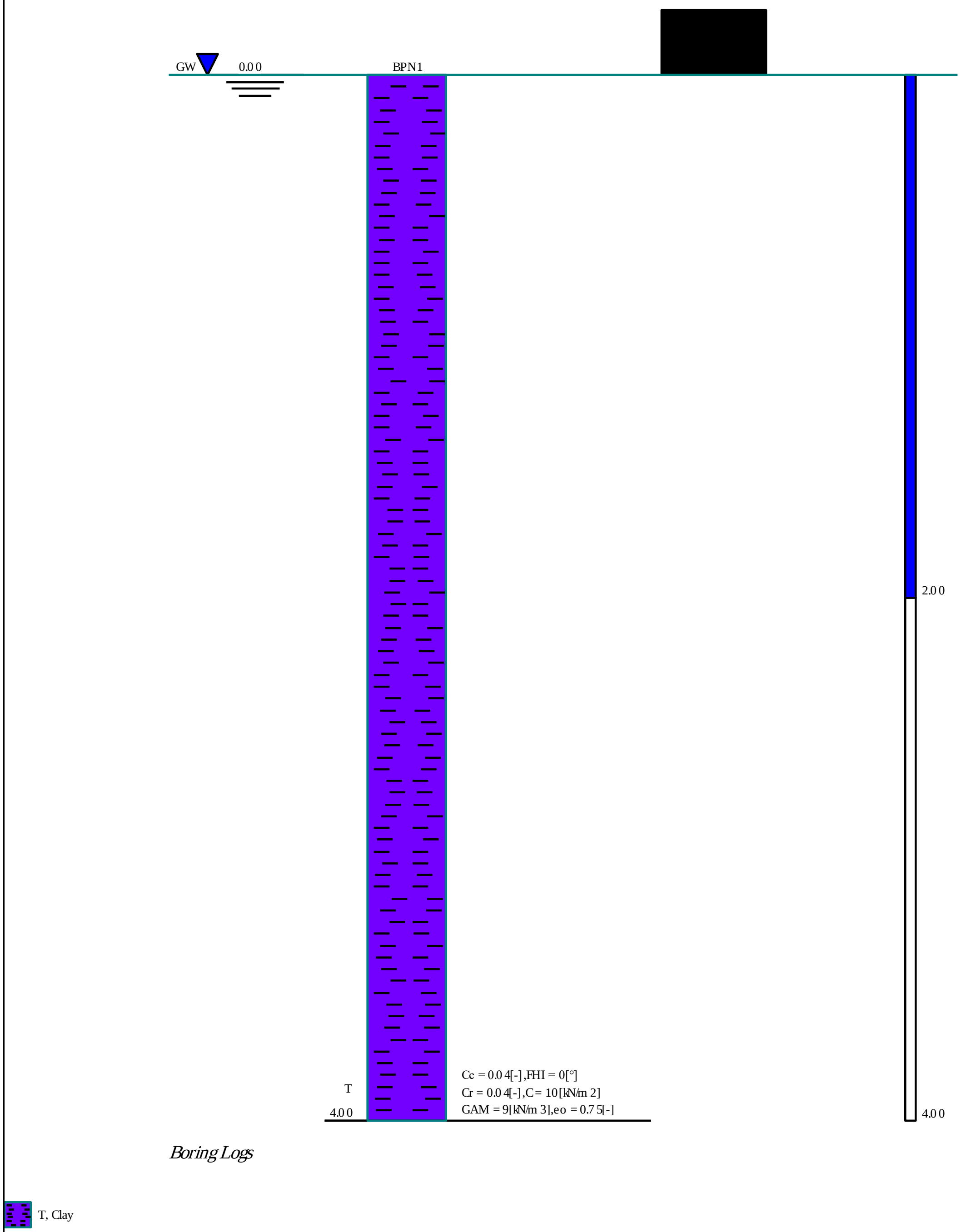

GEOTEC Software Inc PO Box 14001 Richmond Road PO, Calgary AB, Canada T3E 7Y7	
Scale 1:20	**Title: Settlement of a circular loaded area resting on a thin clay layer**
File: CircLoadedArea	**Date: 05/01/2020**
Page No.:	**Project: Verification Examples**

Method (9) (Analysis of rotational shell)
Flexible Foundation (Layered soil model)

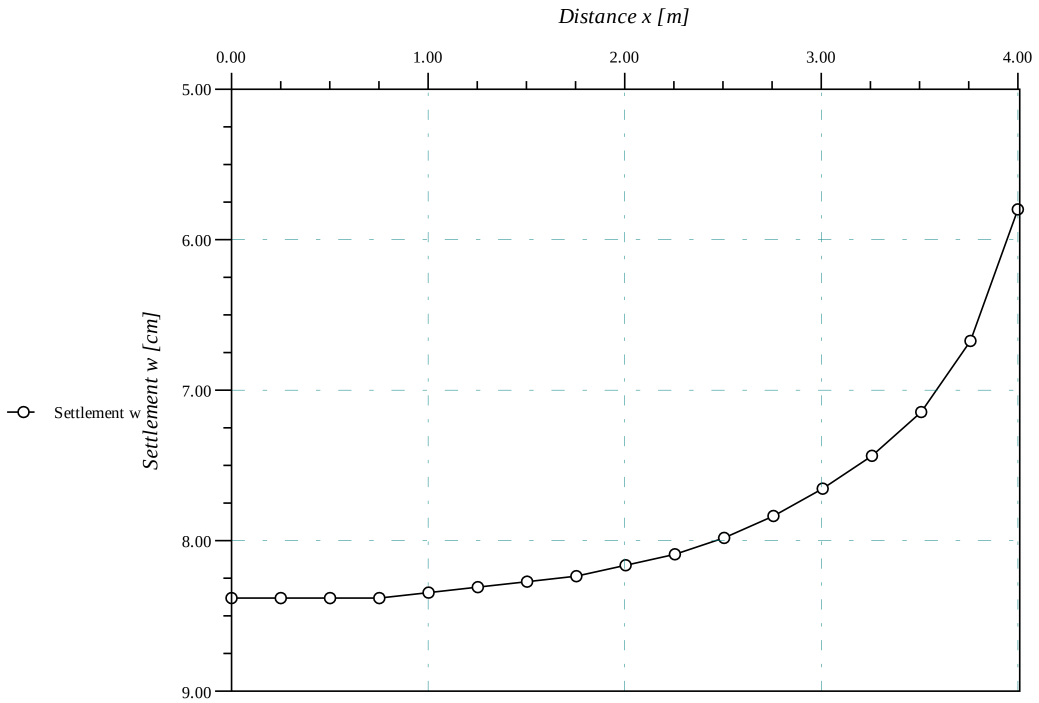

Base settlements
Section in shell base

GEOTEC Software Inc PO Box 14001 Richmond Road PO, Calgary AB, Canada T3E 7Y7	
Scale: 28	**Project: Verification Examples**
File: CircLoadedArea	**Date: 05/01/2020**
Page No.:	**Title: Settlement of a circular loaded area resting on a thin clay layer**

2.4 Example 2: Circular loaded area resting on a thick clay layer

2.4.1 Description of the problem

To verify the settlement of a loaded area resting on a thick clay layer calculated by *ELPLA* using circular and annular elements, a hand calculation of a settlement for a thick soil layer under a circular loaded area is compared with that obtained by *ELPLA*.

A circular loaded area of a load q = 150 [kN/m^2] and radius a = 4 [m] is acting on a thick clay layer as shown in Figure 2.5. Find the settlement of the clay layer under the center of the loaded area.

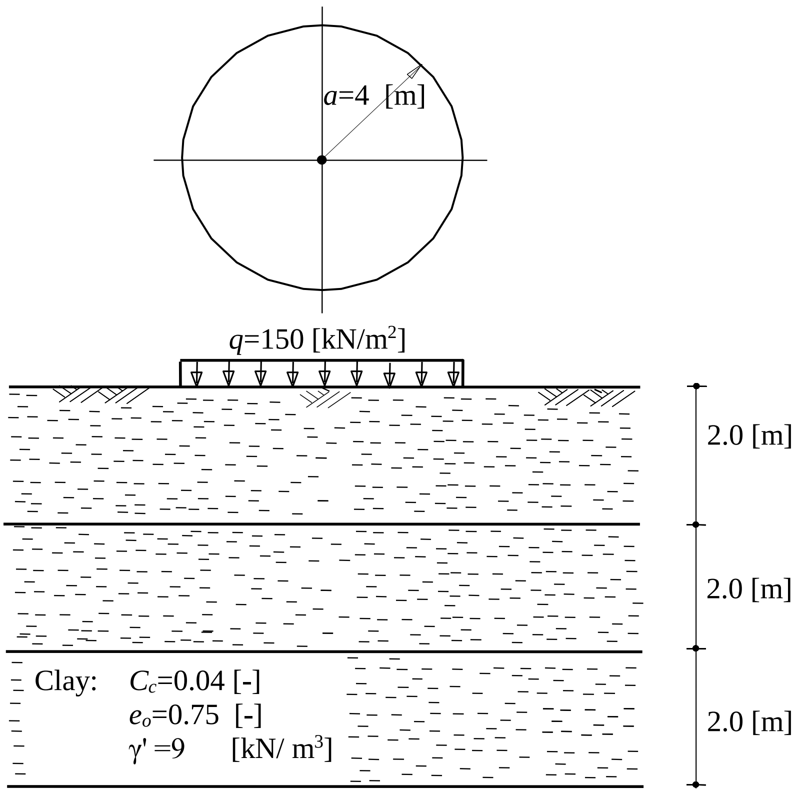

Figure 2.5 Soil profile under the circular loaded area

2.4.2 Hand calculation

ELPLA subdivides the thick clay layer into sub-layers, then the average stress in each sub-layer is determined. Here, for simplifying the solution by the hand calculation, the stress is calculated at the middle of each sub-layer.

Stress σ_z at a depth z in the soil under the center of a circular loaded area q of radius a is given by:

$$\sigma_z = q\left[1 - \frac{z^3}{(a^2 + z^2)^{3/2}}\right]$$

Stress σ_z at the middle of the first sub layer (z=1 [m]):

$$\sigma_1 = 150\left[1 - \frac{1^3}{(16+1^2)^{3/2}}\right] = 147.86 \text{ [kN/m}^2\text{]}$$

Stress σ_z at the middle of the second sub layer (z=3 [m]):

$$\sigma_2 = 150\left[1 - \frac{3^3}{(16+9)^{3/2}}\right] = 117.6 \text{ [kN/m}^2\text{]}$$

Stress σ_z at the middle of the third sub layer (z=5 [m]):

$$\sigma_3 = 150\left[1 - \frac{5^3}{(16+25)^{3/2}}\right] = 78.58 \text{ [kN/m}^2\text{]}$$

Overburden stress σ_o at the middle of the first sub layer (z=1 [m]):

$$\sigma_o = \gamma' z_1 = 9 \times 1 = 9 \text{ [kN/m}^2\text{]}$$

Overburden stress σ_o at the middle of the second sub layer (z=3 [m]):

$$\sigma_o = \gamma' z_2 = 9 \times 3 = 27 \text{ [kN/m}^2\text{]}$$

Overburden stress σ_o at the middle of the third sub layer (z=5 [m]):

$$\sigma_o = \gamma' z_3 = 9 \times 5 = 45 \text{ [kN/m}^2\text{]}$$

Settlement S_c of the first sub layer:

$$s_3 = \frac{C_c h}{1+e_o}\log\frac{\Delta\sigma + \sigma_o}{\sigma_o} = \frac{0.04 \times 2}{1+0.75}\log\frac{147.86+9}{9} = 0.0567 \text{ [m]} = 5.67 \text{[cm]}$$

Settlement s of the second sub layer:

$$s_3 = \frac{C_c h}{1+e_o}\log\frac{\Delta\sigma + \sigma_o}{\sigma_o} = \frac{0.04 \times 2}{1+0.75}\log\frac{117.6+27}{27} = 0.0333 \text{ [m]} = 3.33 \text{[cm]}$$

Settlement *s* of the third sub layer:

$$s_3 = \frac{C_c h}{1+e_o}\log\frac{\Delta\sigma+\sigma_o}{\sigma_o} = \frac{0.04\times 2}{1+0.75}\log\frac{78.58+45}{45} = 0.02 \text{ [m]} = 2.00\text{[cm]}$$

Total settlement *s* of all layers:

$$S_{ct} = s_1 + s_2 + s_3 = 5.67 + 3.33 + 2.00 = 11.01\text{[cm]}$$

2.4.3 Settlement by *ELPLA*

The exact settlement obtained from *ELPLA* at the center *c* of the circular loaded area is 10.65 [cm]. It is nearly same as that of the hand calculation with a difference of 0.35 [cm]. The input data and results of *ELPLA* are presented on the next pages.

Method (9) (Layered soil model)
Flexible Foundation

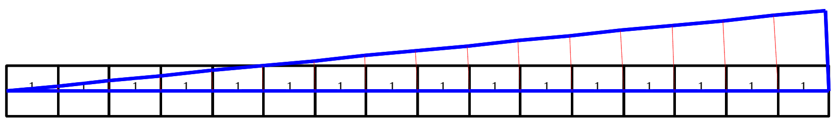

Elements of the loaded area

GEOTEC Software Inc
PO Box 14001 Richmond Road PO, Calgary AB, Canada T3E 7Y7

Scale 1:28	**Title: Settlement of a circular loaded area resting on a thick clay layer**
File: LoadedAreaThick	**Date: 05/01/2020**
Page No.:	**Project: Verification Examples**

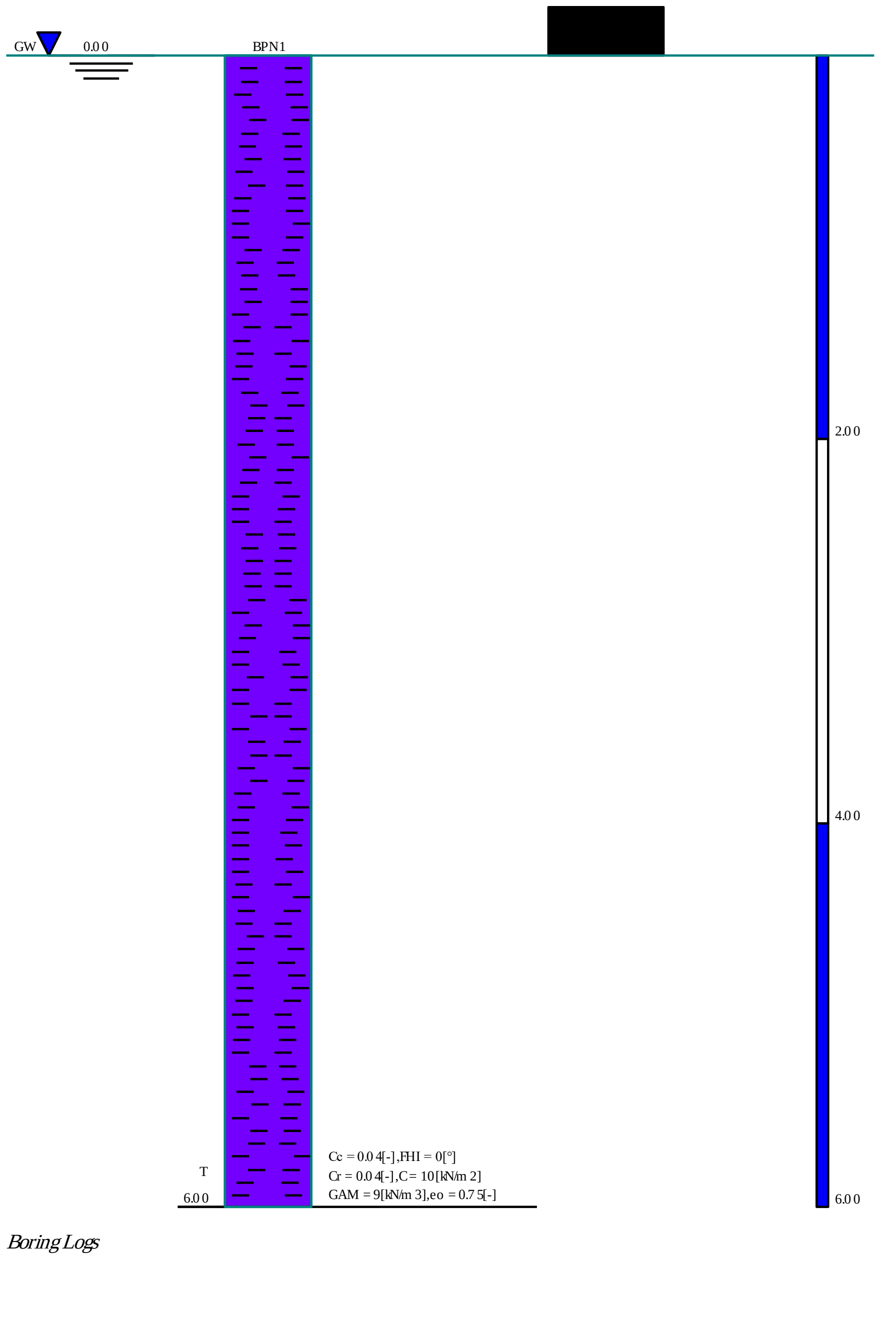

GEOTEC Software Inc PO Box 14001 Richmond Road PO, Calgary AB, Canada T3E 7Y7	
Scale 1:30	**Title: Settlement of a circular loaded area resting on a thick clay layer**
File: LoadedAreaThick	**Date: 05/01/2020**
Page No.:	**Project: Verification Examples**

Method (9) (Analysis of rotational shell)
Flexible Foundation (Layered soil model)

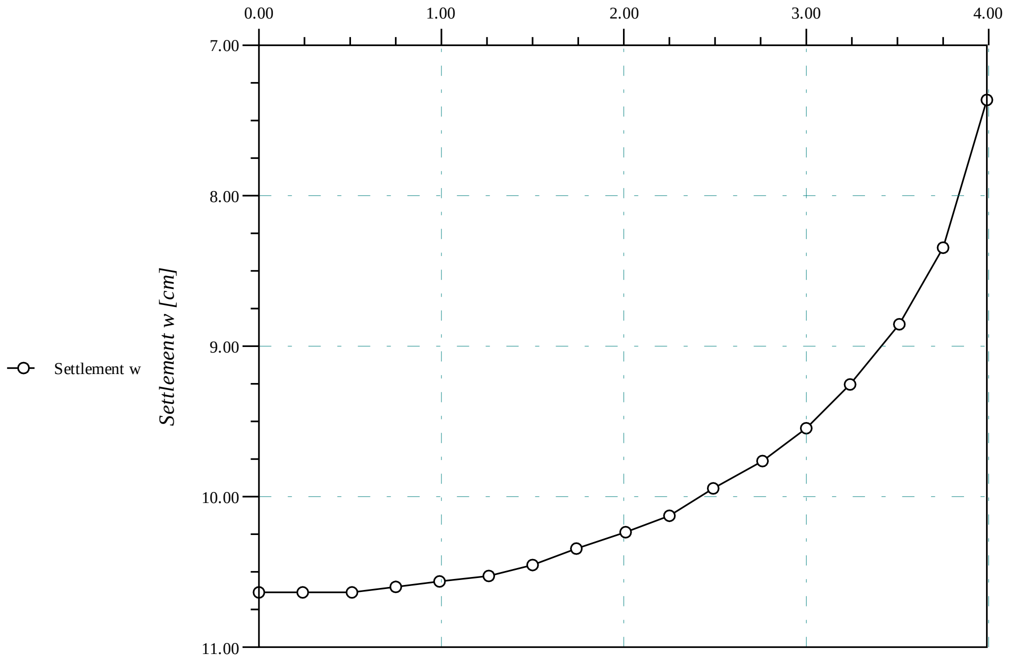

Base settlements
Section in shell base

GEOTEC Software Inc PO Box 14001 Richmond Road PO, Calgary AB, Canada T3E 7Y7	
Scale: 30	**Project: Verification Examples**
File: LoadedAreaThick	**Date: 05/01/2020**
Page No.:	**Title: Settlement of a circular loaded area resting on a thick clay layer**

2.5 Example 3: Circular loaded area resting on different soil layers

2.5.1 Description of the problem

To verify the settlement of a loaded area resting on different soil layers calculated by *ELPLA* using circular and annular elements, a hand calculation of a settlement for a three different soil layers under a circular loaded area is compared with that obtained by *ELPLA*.

A circular loaded area of a radius a=5 [m] acting on three different soil layers as shown in Figure 2.6. Find the total settlement of the three layers at the center of the loaded area.

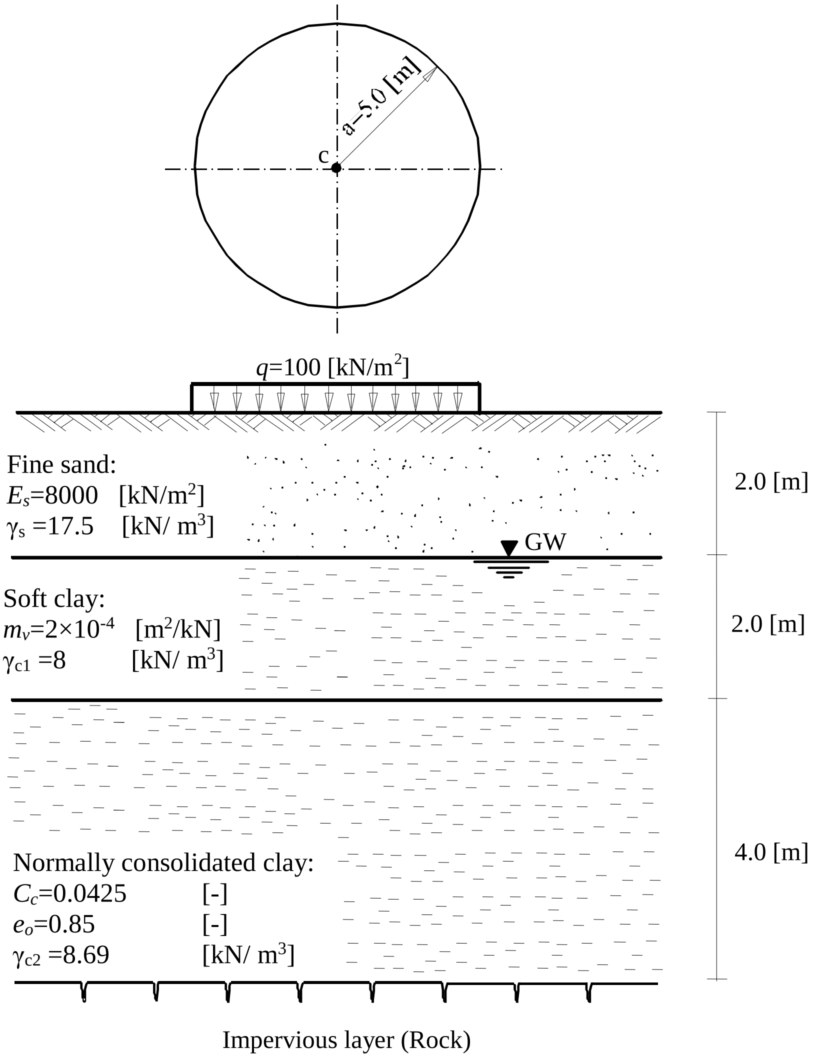

Figure 2.6 Soli profile under the circular loaded area

2.5.2 Hand calculation

Stress σ_z at a depth z in the soil under the center of a circular loaded area is given by:

$$\sigma_z = q\left[1 - \frac{z^3}{(a^2 + z^2)^{3/2}}\right] \tag{1}$$

Stress σ_z at the middle of the first layer (z=1 [m]):

$$\sigma_1 = 100\left[1 - \frac{1^3}{(25+1^2)^{3/2}}\right] = 99.25 \text{ [kN/m}^2\text{]}$$

Stress σ_z at the middle of the second layer (z=3 [m]):

$$\sigma_2 = 100\left[1 - \frac{3^3}{(25+9)^{3/2}}\right] = 86.38 \text{ [kN/m}^2\text{]}$$

Stress σ_z at the middle of the third layer (z=6 [m]):

$$\sigma_3 = 100\left[1 - \frac{6^3}{(25+36)^{3/2}}\right] = 54.66 \text{ [kN/m}^2\text{]}$$

Overburden stress σ_o at the middle of the third layer:

$$\sigma_o = 2\times 17.5 + 2\times 8 + 1.5\times 8.69 = 64.035 \text{ [kN/m}^2\text{]}$$

$$\sigma_o = 2\times 17.5 + 2\times 8 + 2.5\times 8.69 = 72.725 \text{ [kN/m}^2\text{]}$$

$$\sigma_o = 2\times 17.5 + 2\times 8 + 3.5\times 8.69 = 81.415 \text{ [kN/m}^2\text{]}$$

$$\sigma_o = 2\times 17.5 + 2\times 8 + 4.5\times 8.69 = 90.105 \text{ [kN/m}^2\text{]}$$

Settlement s of the first layer:

$$s_1 = \frac{1}{E_s}\Delta\sigma h = \frac{1}{8000}\times 99.25\times 2 = 0.0248 \text{ [m]} = 2.48 \text{ [cm]}$$

Settlement s of the second layer:

$$s_2 = m_v \Delta\sigma h = 2\times 10^{-4}\times 86.38\times 2 = 0.0346 \text{ [m]} = 3.46 \text{ [cm]}$$

Settlement s of the third layer:

$$s_3 = \frac{C_c h}{1+e_o}\log\frac{\Delta\sigma + \sigma_o}{\sigma_o} = \frac{0.0425\times 4}{1+0.85}\log\frac{54.66+68.38}{68.38} = 0.0234\,[\text{m}] = 2.34\ [\text{cm}]$$

$$s_3 = \frac{C_c h}{1+e_o}\log\frac{\Delta\sigma + \sigma_o}{\sigma_o} = \frac{0.0425\times 4}{1+0.85}\log\frac{54.66+68.38}{68.38} = 0.0234\,[\text{m}] = 2.34\ [\text{cm}]$$

Total settlement s of all layers:

$$s_t = s_1 + s_2 + s_3 = 2.48 + 3.46 + 2.34 = 8.28\ [\text{cm}]$$

2.5.3 Settlement by *ELPLA*

The exact settlement obtained from *ELPLA* at the center c of the circular loaded area is 8.09 [cm]. It is nearly same as that of the hand calculation with a difference of 0.19 [cm]. The input data and results of *ELPLA* are presented on the next pages.

Method (9) (Layered soil model)
Flexible Foundation

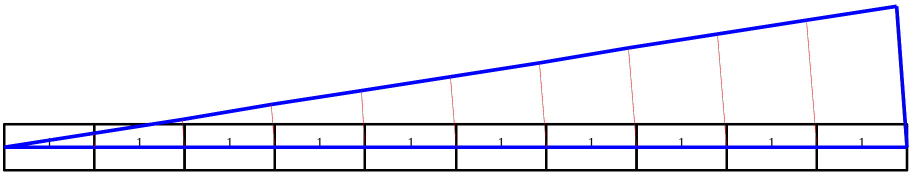

Elements of the loaded area

GEOTEC Software Inc PO Box 14001 Richmond Road PO, Calgary AB, Canada T3E 7Y7	
Scale 1:32	**Title: Settlement of a circular loaded area resting on different soil layers**
File: LoadedAreaLayeres	**Date: 05/01/2020**
Page No.:	**Project: Verification Examples**

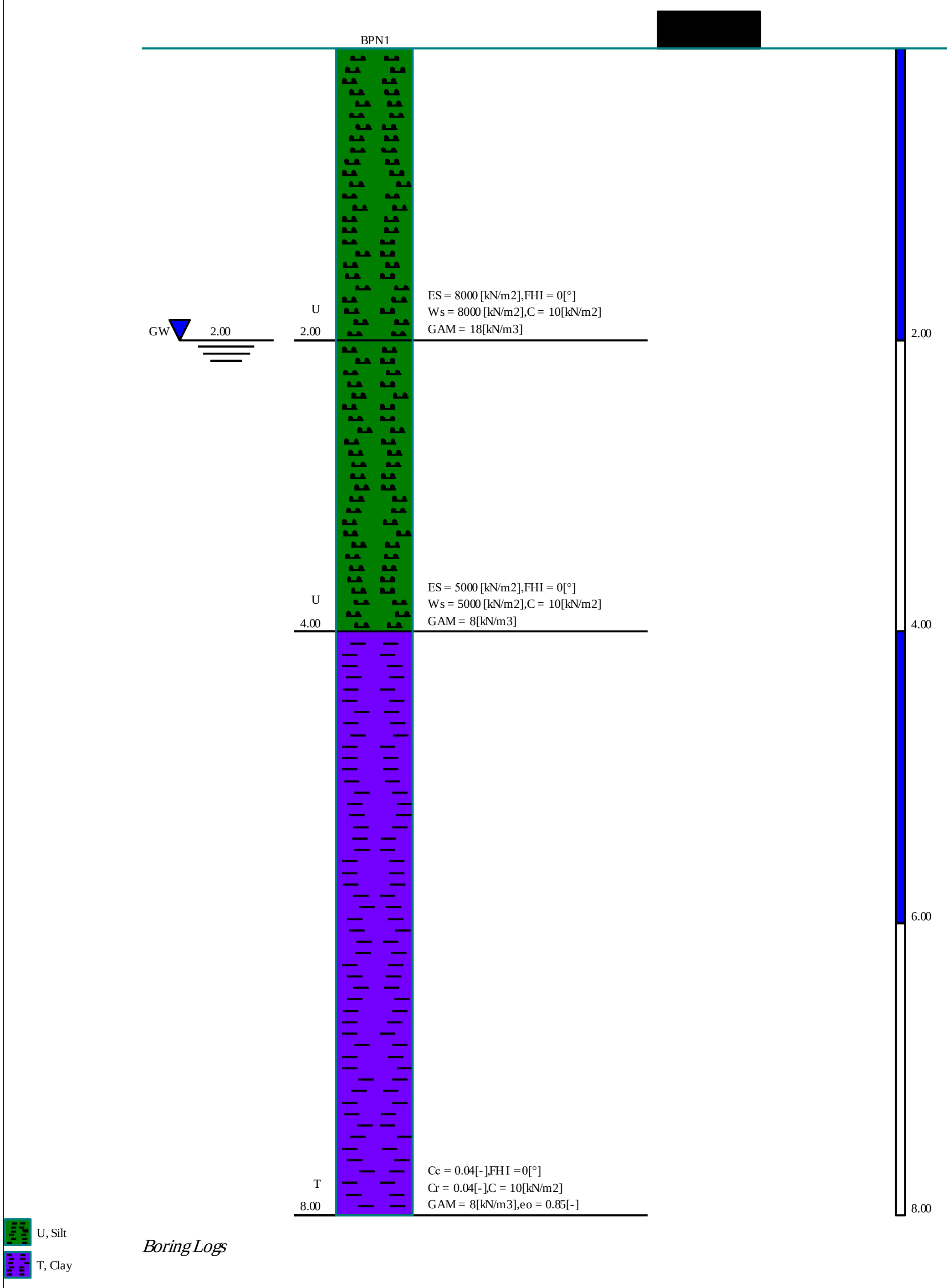

GEOTEC Software Inc

PO Box 14001 Richmond Road PO, Calgary AB, Canada T3E 7Y7

Scale 1:35	**Title: Settlement of a circular loaded area resting on different soil layers**
File: LoadedAreaLayeres	**Date: 05/01/2020**
Page No.:	**Project: Verification Examples**

Method (9) (Analysis of rotational shell)
Flexible Foundation (Layered soil model)

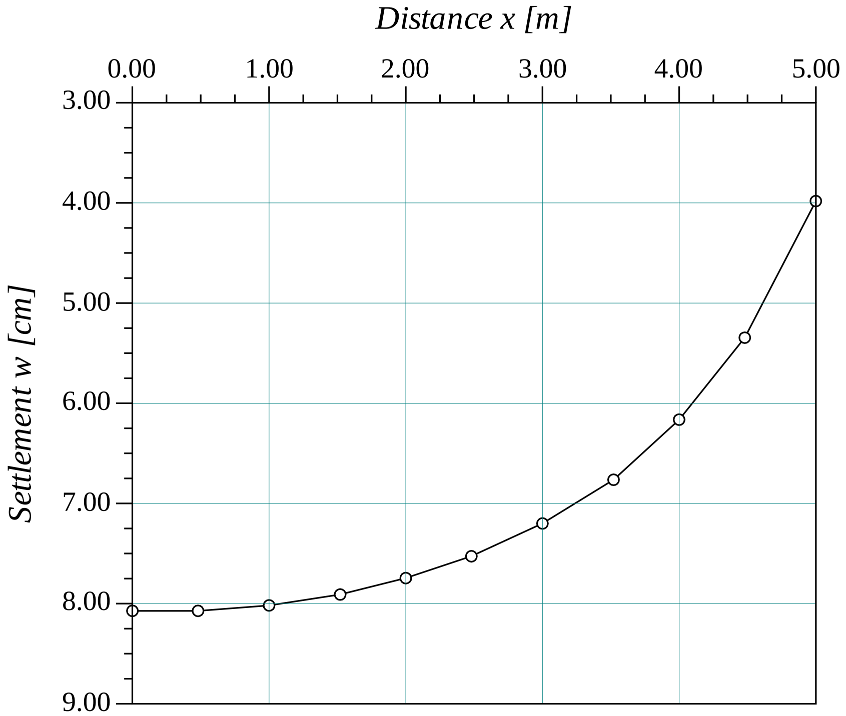

Base settlements
Sections in shell base

GEOTEC Software Inc PO Box 14001 Richmond Road PO, Calgary AB,Canada T3E 7Y7	
Scale: 40	**Project: Verification Examples**
File: Axi_EX2.4	**Date: 05/01/2020**
Page No.:	**Title: Circular loaded area resting on different soil layers**

2.6 Example 4: Circular plate subjected to a uniform load

2.6.1 Description of the problem

To verify the maximum deflection of the circular plate subjected to uniform load calculated by *ELPLA* using circular and annular elements, a hand calculation of a maximum deflection of a plate with simply supported edge and clamped edge under a uniform load is compared with that obtained by *ELPLA*.

According to theory of plate (*Ventsel, E./ Krauthammer, T.* (2001)), the maximum deflection w_{max} [m] of the plate with simply supported edge under a uniform load, which occurs at the center, is given by:

$$w_{\max} = \frac{P\,r^4\,(5+\nu_c)}{64\ D\ (1+\nu_c)}$$

while the maximum deflection w_{max} [m] of the plate with clamped edge under a uniform load, which occurs at the center, is given by:

$$w_{\max} = \frac{P\,r^4}{64\ D}$$

where:

ν_c	*Poisson's* ratio of the plate material [-]
E_c	*Young's* modulus of the plate material [kN/m^2]
r	Plate radius [m]
p	Load intensity on the plate [kN/m^2]
D	Flexural rigidity of the plate [-]

Flexural rigidity of the plate D is given by following equation:

$$D = \frac{E_c\,t^3}{12\ (1-\nu_c^2)}$$

where t is the plate thickness [m]

A circular plate subjected to a uniform load is chosen and subdivided into 10 equal annular regions. Load on the plate, plate radius and the elastic properties of the plate material are:

Radius of the plate	r	= 5	[m]
Thickness of the plate	t	= 0.25	[m]
Uniform load on the raft	p	= 100	[kN/m^2]
Young's modulus of the plate material	E_c	= 2.7×10^7	[kN/m^2]
Poisson's ratio of the plate material	ν_c	= 0.2	[-]

2.6.2 Hand calculation

Flexural rigidity of the plate D is calculated from:

$$D = \frac{E_c\ t^3}{12\ (1 - \nu_c^2)}$$

$$D = \frac{2 \times 10^7 \times 0.25^3}{12\ (1 - 0.25^2)} = 27777.77\ \text{[kN.m]}$$

The maximum deflection w_{max} [m] of the plate with simply supported edge under a uniform load is calculated from:

$$w_{\max} = \frac{P\ r^4\ (5 + \nu_c)}{64\ D\ (1 + \nu_c)}$$

$$w_{\max} = \frac{100 \times 5^4\ (5 + 0.25)}{64 \times 27777.77\ (1 + 0.25)} = 0.1476\ \text{[m]}$$

$$w_{\max} = 14.76\ \text{[cm]}$$

The maximum deflection w_{max} [m] of the plate with clamped edge under a uniform load is calculated from:

$$w_{\max} = \frac{P\ r^4}{64\ D}$$

$$w_{\max} = \frac{100 \times 5^4}{64 \times 27777.77} = 0.0352\ \text{[m]}$$

$$w_{\max} = 3.52\ \text{[cm]}$$

2.6.3 Maximum deflection by *ELPLA*

The maximum deflection obtained from *ELPLA* at the center of the plate with simply supported edge is 14.59 [cm], while that of the plate with clamped edge is 3.56 [cm], Table 2.1. It is nearly same as that of the hand calculation with a difference of 0.17 [cm] and 0.04 [cm], respectively. The input data and results of *ELPLA* are presented on the next pages.

Table 2.1 Comparison of the maximum deflection obtained by *ELPLA* with those obtained by hand calculation using plate theory

	Simply supported edge		Clamped edge	
	Plate theory	*ELPLA*	Plate theory	*ELPLA*
Maximum deflection *w* [cm]	14.76	14.59	3.52	3.56

w=0

Analysis of rotational shell

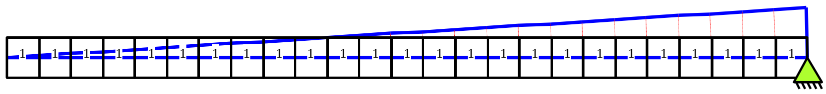

Boundary conditions

GEOTEC Software Inc

PO Box 14001 Richmond Road PO, Calgary AB, Canada T3E 7Y7

Scale 1:35	Title: Plate with simply supported edge under a uniform load
File: SimplySupportedPlate	Date: 11/01/2020
Page No.:	Project: Verification Examples

Analysis of rotational shell

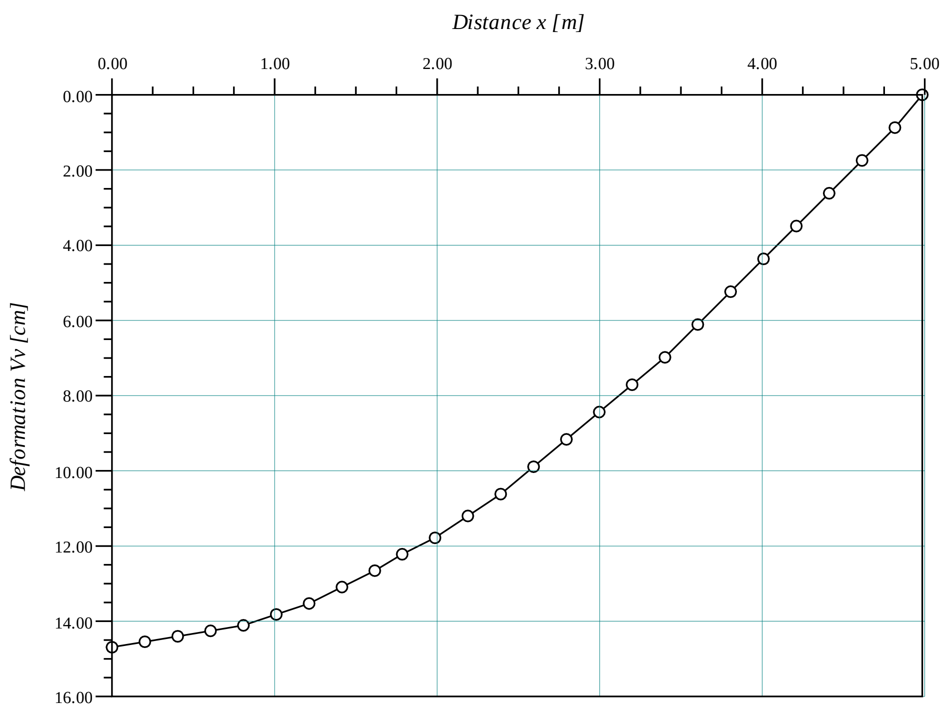

Vertical deformations
Section in shell base

GEOTEC Software Inc	
PO Box 14001 Richmond Road PO, Calgary AB, Canada T3E 7Y7	
Scale: 34	Project: Verification Examples
File: SimplySupportedPlate	Date: 11/01/2020
Page No.:	Title: Plate with simply supported edge under a uniform load

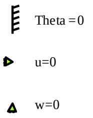

Analysis of rotational shell

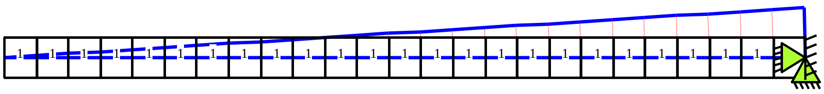

Boundary conditions

GEOTEC Software Inc

PO Box 14001 Richmond Road PO, Calgary AB, Canada T3E 7Y7

Scale 1:35	Title: Plate with clamped edge under a uniform load
File: ClampedSupportedPlate	Date: 11/01/2020
Page No.:	Project: Verification Examples

Analysis of rotational shell

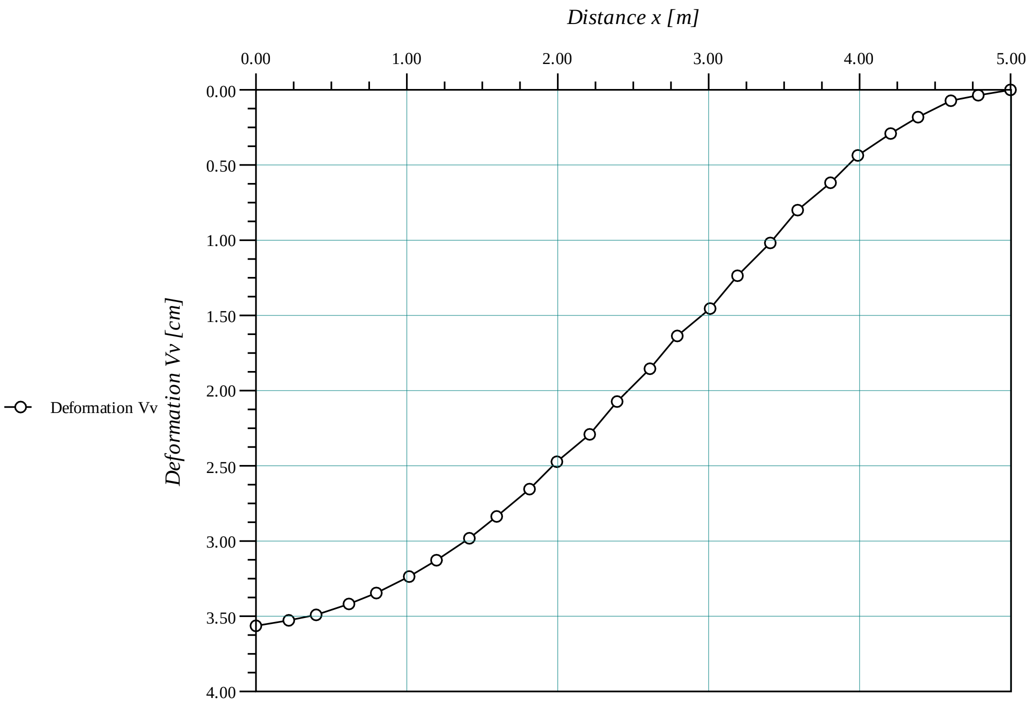

Vertical deformations
Section in shell base

GEOTEC Software Inc	
PO Box 14001 Richmond Road PO, Calgary AB, Canada T3E 7Y7	
Scale: 36	**Project: Verification Examples**
File: ClampedSupportedPlate	**Date: 11/01/2020**
Page No.:	**Title: Plate with clamped edge under a uniform load**

2.7 Example 5: Annular plate on *Winkler's* medium

2.7.1 Description of the problem

To verify the analysis of annular plates on *Winkler's* medium carried out by *ELPLA* using circular and annular elements, results of a simply supported annular plate on *Winkler's* medium obtained by *Karaşin et al.*, (2014) using a finite grid solution for circular plates on elastic foundations are compared with those obtained by *ELPLA*.

A simply supported annular plate subjected to a uniform load on *Winkler's* medium is chosen as shown in Figure 2.7. Load on the plate, plate radii, elastic properties of the soil and the plate are:

Inner radius of the plate	r_1	= 2.5	[m]
Outer radius of the plate	r_2	= 5	[m]
Thickness of the plate	t	= 0.25	[m]
Uniform load on the raft	p	= 200	[kN/m^2]
Modulus of sub grade reaction of the soil	k_s	= 10000	[kN/m^3]
Young's modulus of the plate material	E_c	= 2.7×10^7	[kN/m^2]
Poisson's ratio of the plate material	ν_c	= 0.2	[-]

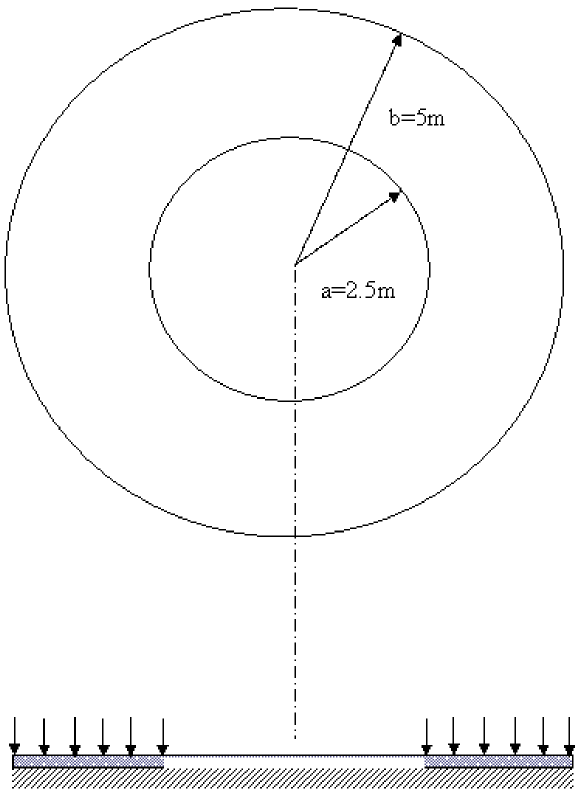

Figure 2.7 A simply supported annular plate subjected to a uniform load (after *Karaşin et al.*, (2014))

2.7.2 Analysis of the plate

The available method "Constant Modulus of Subgrade Reaction /2" in *ELPLA* is used here to determine the vertical displacement and moment of the plate on *Winkler's* medium. Figure 2.8 shows the annular plate with 10 annular regions and supports.

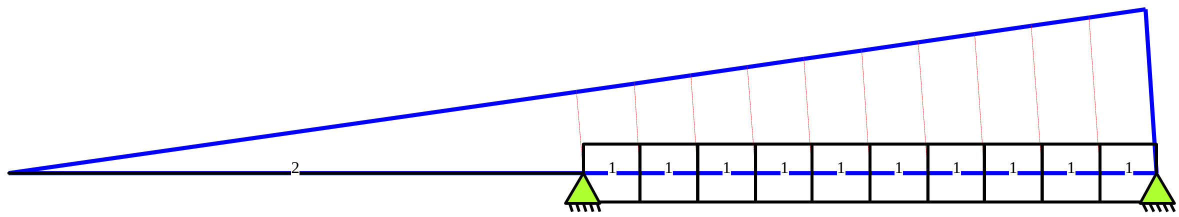

Figure 2.8 Annular plate with 10 annular regions and supports

2.7.3 Results and discussions

Karaşin et al., (2014) analyzed the annular plate using a finite grid solution for circular plates on elastic foundations and then compared their results with the FGM solution obtained by *Utku* and *Inceleme* (2000).

Table 2.2 and Table 2.3 show the comparison of the maximum moment and displacements obtained by *ELPLA* with those obtained by *Karaşin et al.*, (2014) and *Utku* and *Inceleme* (2000).

Table 2.2 Comparison of the maximum moment obtained by *ELPLA* with those obtained by *Karaşin et al.*, (2014) and *Utku* and *Inceleme* (2000)

	Karaşin et al., (2014)	*Utku* and *Inceleme* (2000)	*ELPLA*
Maximum moment *My* [kN.m/m]	134.5	140.5	136.0

Table 2.3 Displacements w [mm] under the middle of the annular plate obtained by *ELPLA* with those obtained by *Karaşin et al.*, (2014) and *Utku* and *Inceleme* (2000)

r [m]	*Karaşin et al.*, (2014)	*Utku* and *Inceleme* (2000)	*ELPLA*
2.75	0.81	0.85	0.80
3.00	1.51	1.59	1.49
3.25	2.04	2.16	2.01
3.50	2.35	2.49	2.32
3.75	2.43	2.58	2.40
4.00	2.28	2.43	2.25
4.25	1.92	2.05	1.90
4.5	1.39	1.49	1.37
4.75	0.73	0.78	0.72

It is obviously from the comparison that results of the simply supported annular plate subjected to a uniform load and resting on *Winkler's* medium obtained by *ELPLA* are nearly equal to those obtained by *Karaşin et al.*, (2014) and *Utku* and *Inceleme* (2000).

2.7.4 Results by *ELPLA*

Results of *ELPLA* are presented on the next pages. By comparison, one can see a good agreement with those obtained by other published solutions.

Method (2) (Analysis of rotational shell)
Variable Modulus of subgrade Reaction

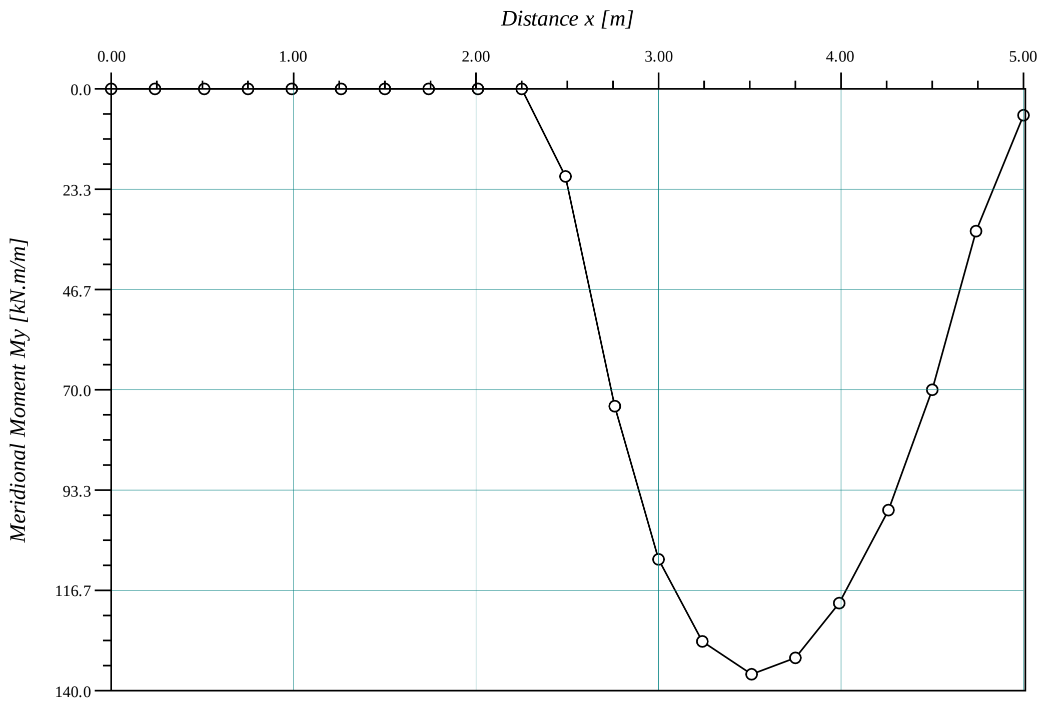

Meridional moments
Section in shell base

GEOTEC Software Inc PO Box 14001 Richmond Road PO, Calgary AB, Canada T3E 7Y7	
Scale: 30	**Project: Kara?in et al., (2014): A Finite Grid Solution for Circular Plates on Elastic Foundations**
File: Karasin	**Date: 11/01/2020**
Page No.:	**Title: Simple support annular plate on Winkler's medium**

Method (2) (Analysis of rotational shell)
Variable Modulus of subgrade Reaction

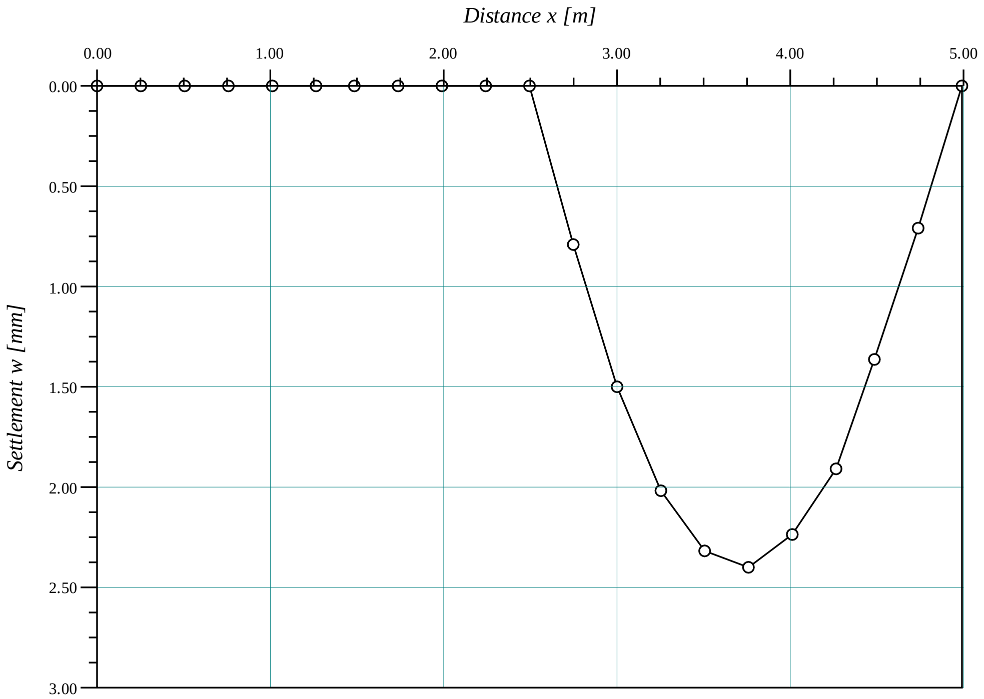

Base settlements
Section in shell base

GEOTEC Software Inc PO Box 14001 Richmond Road PO, Calgary AB, Canada T3E 7Y7	
Scale: 32	**Project: Kara?in et al., (2014): A Finite Grid Solution for Circular Plates on Elastic Foundations**
File: Karasin	**Date: 11/01/2020**
Page No.:	**Title: Simple support annular plate on Winkler's medium**

Method (2) (Analysis of rotational shell)
Variable Modulus of subgrade Reaction

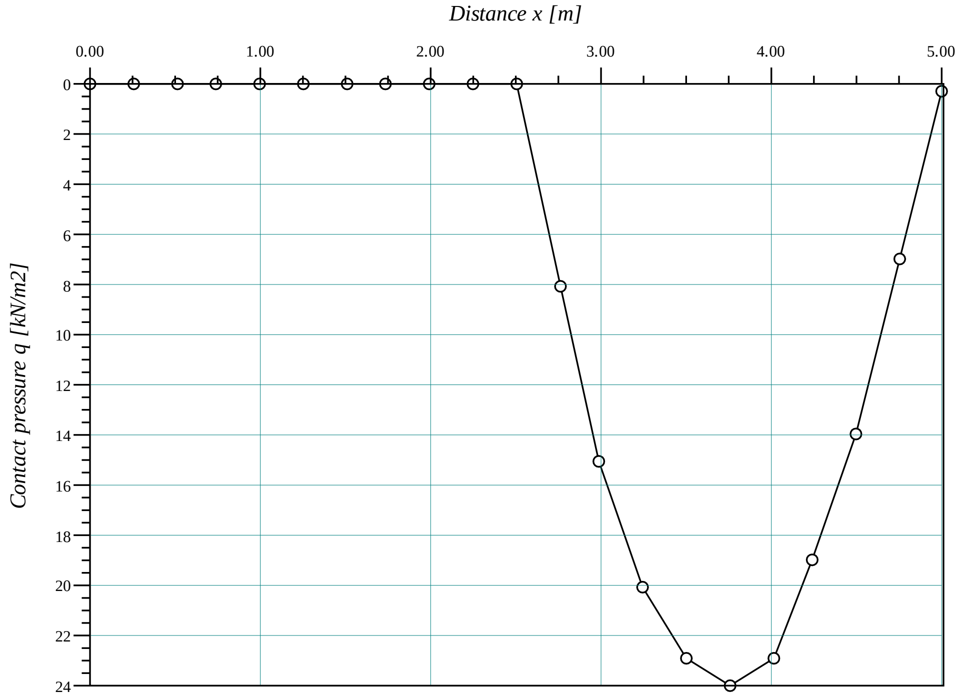

Base contact pressures
Section in shell base

GEOTEC Software Inc	
PO Box 14001 Richmond Road PO, Calgary AB, Canada T3E 7Y7	
Scale: 32	**Project: Kara?in et al., (2014): A Finite Grid Solution for Circular Plates on Elastic Foundations**
File: Karasin	**Date: 11/01/2020**
Page No.:	**Title: Simple support annular plate on Winkler's medium**

2.8 Example 6: Rigid circular raft on a deeply extended clay layer

2.8.1 Description of the problem

To verify the analysis of a rigid circular raft on a deeply extended clay layer calculated by *ELPLA* using circular and annular elements, contact pressure of a rigid circular raft obtained by the solutions of *Borowicka* (1939) and the settlement at the characteristic point according to *Graßhoff* (1955) are compared with those obtained by *ELPLA*.

A circular raft of a radius a = 5.0 [m] on a deeply extended clay layer is chosen and subdivided into 25 annular regions as shown in Figure 2.9. The raft is subjected to an average uniform load of p = 100 [kN/m^2].

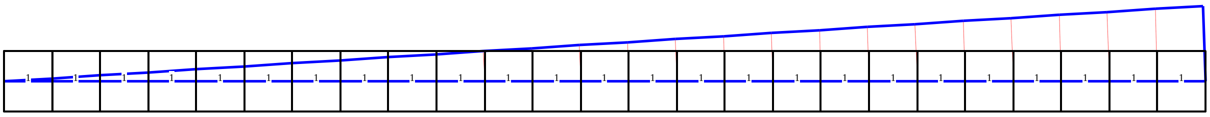

Figure 2.9 Rigid circular raft with dimension and annular regions

2.8.2 Clay properties

The clay has the following properties:

Compression index	C_c	= 0.07	[-]
Initial void ratio	e_o	= 0.85	[-]
Unit weight of the clay	γ'	= 8.69	[kN/m^3]

2.8.3 Analysis of the raft

The analytical contact pressure distribution under the rigid circular raft is derived with the assumption of a semi-infinite soil layer. According to *Borowicka* (1939), the contact pressure q [kN/m^2] under a rigid circular raft on isotropic elastic half-space medium may be evaluated by

$$q = \frac{P\,r}{2\sqrt{r^2 - e^2}} \qquad (2)$$

where:

r Raft radius [m]
p Load intensity on the raft [kN/m^2]
e distance from the center [m]

The definition of the characteristic point according to *Graßhoff* (1955) can be used to verify the numerical solutions. The characteristic point is defined as that point of a surface area loaded by a uniformly distributed pressure, where the settlement s_o due to that pressure is identical with the displacement w_o of a rigid raft of the same shape and loading. For a circular raft, the characteristic point lies at distance a_c =0.845 a from the center. Therefore, the analysis is carried out also for a flexible raft, where the contact stress is equal to the applied stress on the soil.

2.8.4 Results and discussions

Figure 2.10 shows the consolidation settlement at the middle of the raft. Table 2.4 compares the consolidation settlements at the characteristic point for the rigid raft with taht for the flexible raft. It can be clearly observed from Figure 2.10 and from Table 2.4 that the settlements at characteristic point for the flexible raft are nearly equal to that for the rigid raft with difference 4%.

Figure 2.11 shows the comparison of the contact pressure ratio *q/p* [-] at the at the middle of the raft. It can be found from the figures that the results of the circular rigid raft obtained by the *ELPLA* are nearly equal to that obtained by semi-analytical procedure.

Table 2.4 Consolidation settlements *s* [cm] at the characteristic point

	rigid raft [cm]	Flexible raft at characteristic point [cm]
Settlement	17.51	16.77

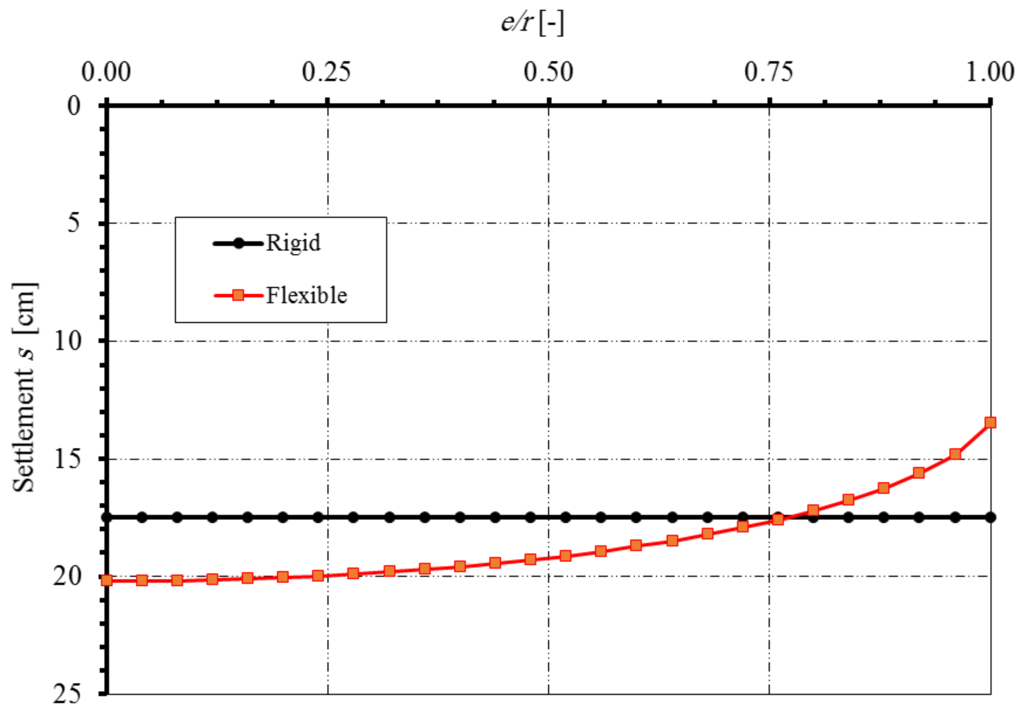

Figure 2.10 Consolidation settlement *s* [cm] at the middle of the raft

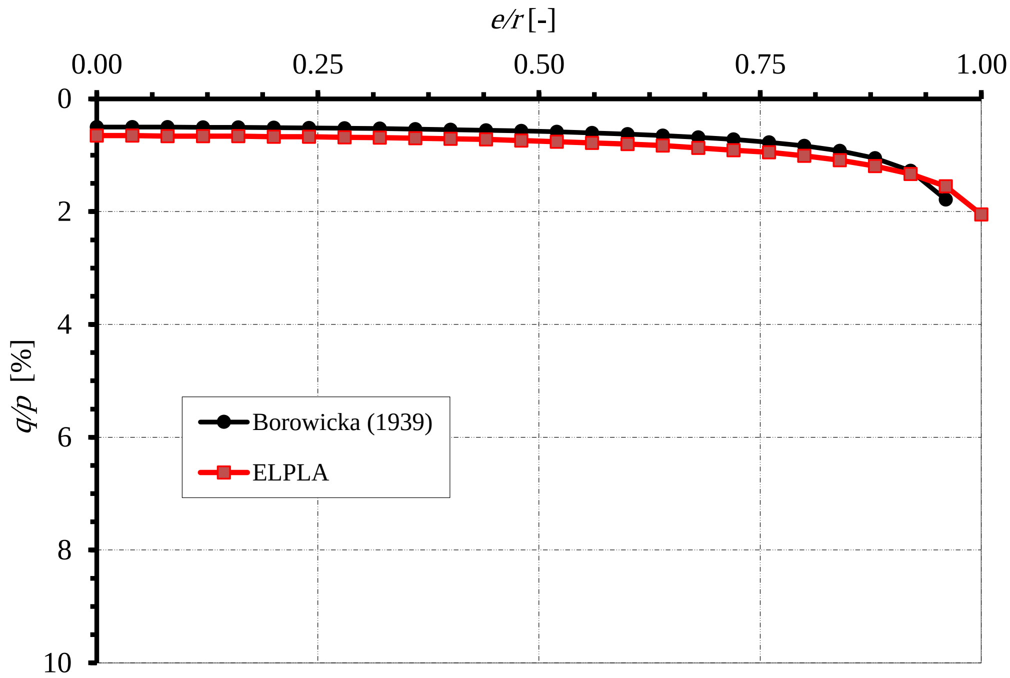

Figure 2.11 Contact pressure ratio *q/p* [-] at the middle of the raft

2.8.5 Rigid consolidation by *ELPLA*

The input data and results of *ELPLA* are presented on the next pages.

Method (8) (Half Space model)
Modulus of Compressibility for Rigid Raft

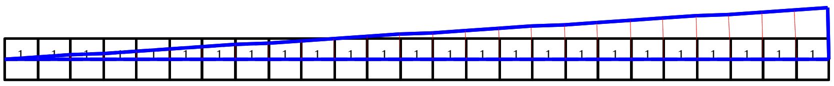

Raft with annular elments

GEOTEC Software Inc
PO Box 14001 Richmond Road PO, Calgary AB, Canada T3E 7Y7

Scale 1:35	Title: Rigid circular raft on a deeply extended clay layer
File: RigidRaft	Date: 13/01/2020
Page No.:	Project: Verification Examples

Method (8) (Analysis of rotational shell)
Modulus of Compressibility for Rigid Raft (Half Space model)

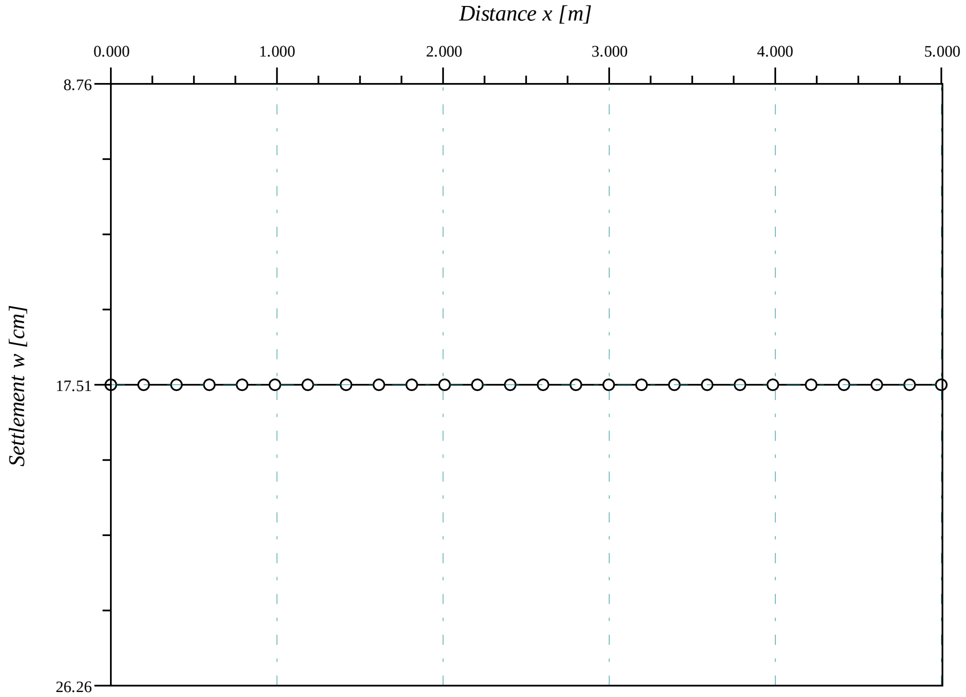

Base settlements
Section in shell base

GEOTEC Software Inc	
PO Box 14001 Richmond Road PO, Calgary AB, Canada T3E 7Y7	
Scale: 33	**Project: Verification Examples**
File: RigidRaft	**Date: 13/01/2020**
Page No.:	**Title: Rigid circular raft on a deeply extended clay layer**

Method (8) (Analysis of rotational shell)
Modulus of Compressibility for Rigid Raft (Half Space model)

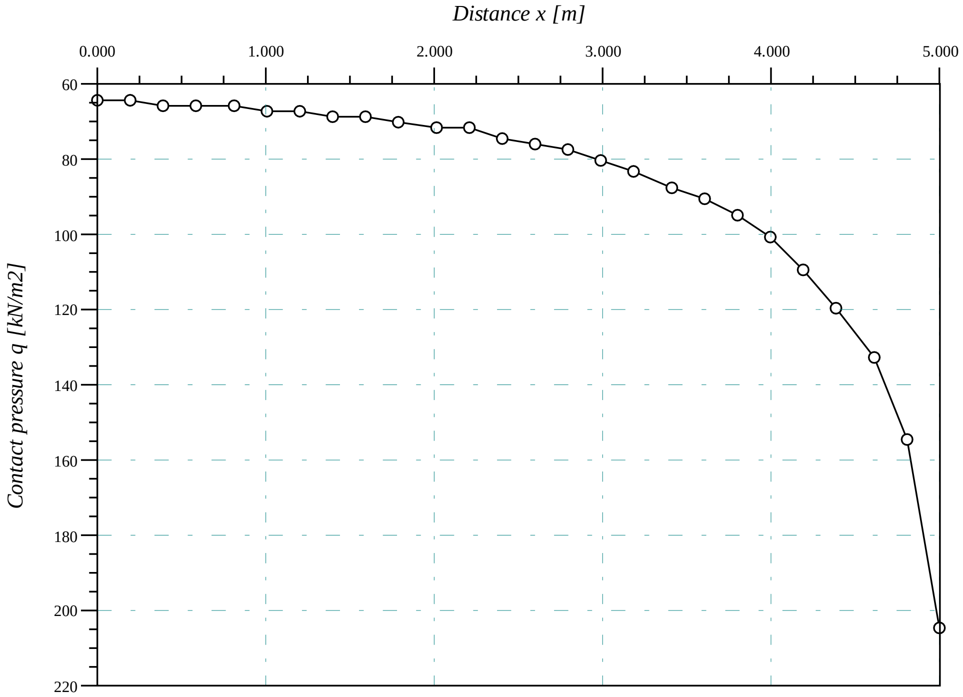

Base contact pressures
Section in shell base

GEOTEC Software Inc PO Box 14001 Richmond Road PO, Calgary AB, Canada T3E 7Y7	
Scale: 32	**Project: Verification Examples**
File: RigidRaft	**Date: 13/01/2020**
Page No.:	**Title: Rigid circular raft on a deeply extended clay layer**

Method (9) (Analysis of rotational shell)
Flexible Foundation (Half Space model)

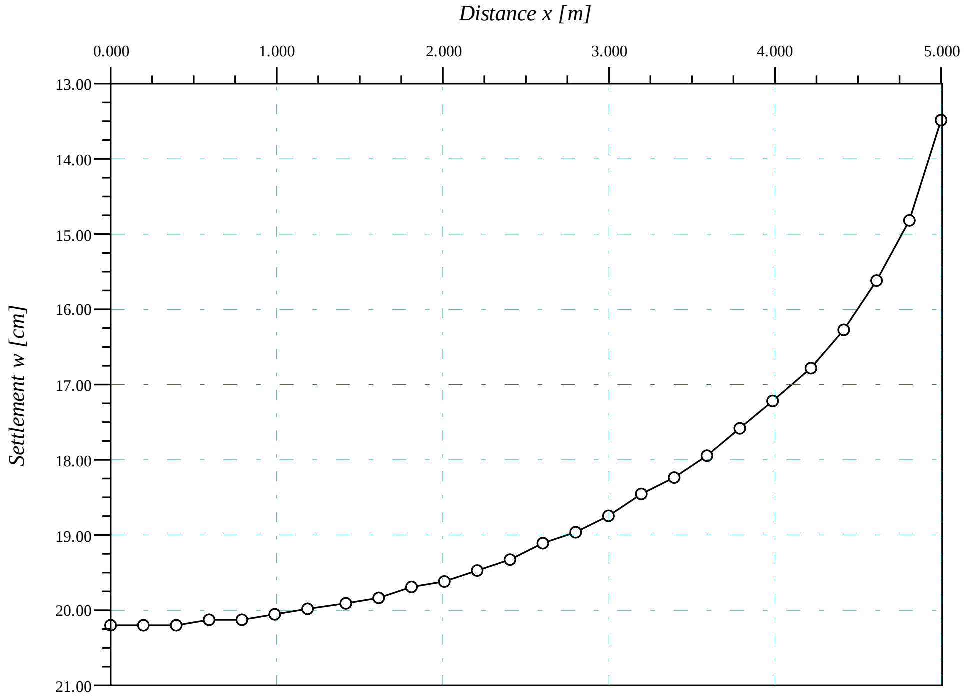

Base settlements
Section in shell base

GEOTEC Software Inc PO Box 14001 Richmond Road PO, Calgary AB, Canada T3E 7Y7	
Scale: 33	Project: Verification Examples
File: RigidRaft	Date: 13/01/2020
Page No.:	Title: Rigid circular raft on a deeply extended clay layer

2.9 Example 7: Rigid circular raft on an isotropic elastic half-space medium

2.9.1 Description of the problem

To verify the settlement of a rigid circular raft resting on an isotropic elastic half-space medium calculated by *ELPLA* using circular and annular elements, results of a rigid circular raft obtained by other analytical solutions from *Borowicka* (1939) and numerical solution from *Selvadurai* (1979) are compared with those obtained by *ELPLA*.

According to *Borowicka* (1939), the vertical displacement w [m] of a rigid circular raft on isotropic elastic half-space medium may be evaluated by

$$w = \frac{4(1-\nu_s^{\,2})P\,r}{\pi\;E_s}\,I$$

where:

ν_s	*Poisson's* ratio of the soil [-]
E_s	*Young's* modulus of the soil [kN/m^2]
r	Raft radius [m]
p	Load intensity on the raft [kN/m^2]
I	Displacement factor [-]

while the contact pressure distribution q [kN/m^2] under the raft at a distance e [m] from the center may be evaluated by

$$q = \frac{P\,r}{2\sqrt{r^2 - e^2}}$$

A circular raft on isotropic elastic half-space soil medium is chosen and subdivided into 10 equal annular regions. Load on the raft, raft radius and the elastic properties of the soil are chosen to make the first term from Eq. 1 equal to 0.01, hence:

Raft radius	r	= 10	[m]
Uniform load on the raft	p	= 100	[kN/m^2]
Young's modulus of the soil	E_s	= 119366	[kN/m^2]
Poisson's ratio of the soil	ν_s	= 0.25	[-]

2.9.2 Analysis of the raft

The available method "Rigid raft 8" in *ELPLA* is used here to determine the vertical displacement of the raft on isotropic elastic half-space medium. Figure 2.12 shows a radial strip of the raft with annular regions.

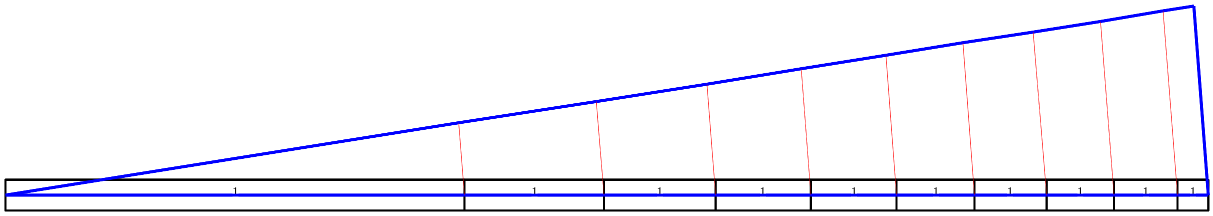

Figure 2.12 A radial strip of the rigid raft with 10 annular regions

2.9.3 Results and discussions

Table 2.5 shows the comparison of the displacement factor *I* obtained by *ELPLA* with those obtained by *Borowicka* (1939) and *Selvadurai* (1979). Besides, Figure 2.13 and Table 2.6 show the comparison of the contact pressure ratio *q/p* [-] at the middle section of the raft obtained by *ELPLA* with those obtained by *Borowicka* (1939) and *Selvadurai* (1979).

It is obviously from the comparison that results of the circular rigid raft obtained by *ELPLA* are nearly equal to those obtained by *Borowicka* (1939) and *Selvadurai* (1979). It is evident that the numerical analysis for both *ELPLA* and *Selvadurai* (1979) gives contact pressure nearly equal to that of analytical analysis for all locations except near the boundary of the rigid raft.

Table 2.5 Comparison of the displacement factor *I* obtained by *ELPLA* with those obtained by *Borowicka* (1939) and *Selvadurai* (1979)

	Borowicka (1939)	*Selvadurai* (1979)	*ELPLA*
Central displacement *I* [-]	1.2337	1.2451	1.2045

2.9.4 Settlement by *ELPLA*

The input data and results of *ELPLA* are presented on the next pages. By comparison, one can see a good agreement with those obtained by other published solutions.

Table 2.6 Contact pressure ratio *q/p* [-] under the middle of the circular rigid raft obtained by *ELPLA* with those obtained by *Borowicka* (1939) and *Selvadurai* (1979)

r/e	*Borowicka* (1939)	*Selvadurai* (1979)	*ELPLA*
1	-	-	10.5666
0.9743	2.2214	3.0264	1.0231
0.9216	1.2882	1.3089	1.2614
0.8654	0.9978	1.0407	0.9265
0.8056	0.8440	0.8719	0.8011
0.7409	0.7445	0.7660	0.7125
0.6698	0.6733	0.6909	0.6483
0.5901	0.6193	0.6343	0.6000
0.4977	0.5765	0.5896	0.5607
0.3817	0.5409	0.5559	0.5278
0	0.5000	0.5154	0.5278

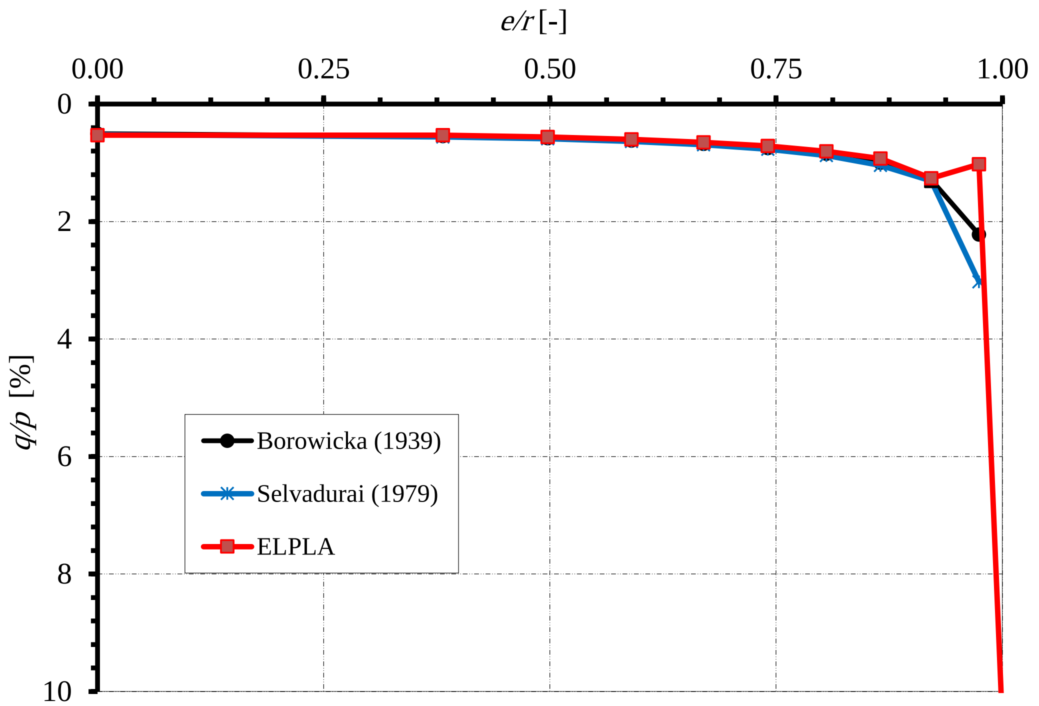

Figure 2.13 Contact pressure ratio *q/p* [-] under the middle of the circular rigid raft

Method (8) (Half Space model)
Modulus of Compressibility for Rigid Raft

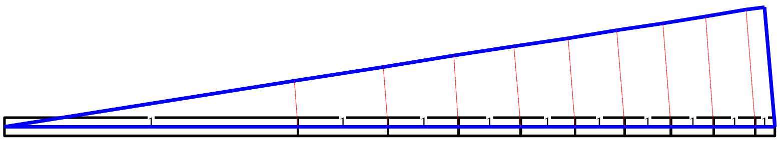

Raft with dimensions and 10 annular regions

GEOTEC Software Inc
PO Box 14001 Richmond Road PO, Calgary AB, Canada T3E 7Y7

Scale 1:75	**Title: Rigid circular raft on Isotropic elastic half-space medium**
File: Selvadurai	**Date: 05/01/2020**
Page No.:	**Project: Selvadurai (1979): Elastic Analysis of Soil Foundation Interaction.**

Method (8) (Analysis of rotational shell)
Modulus of Compressibility for Rigid Raft (Half Space model)

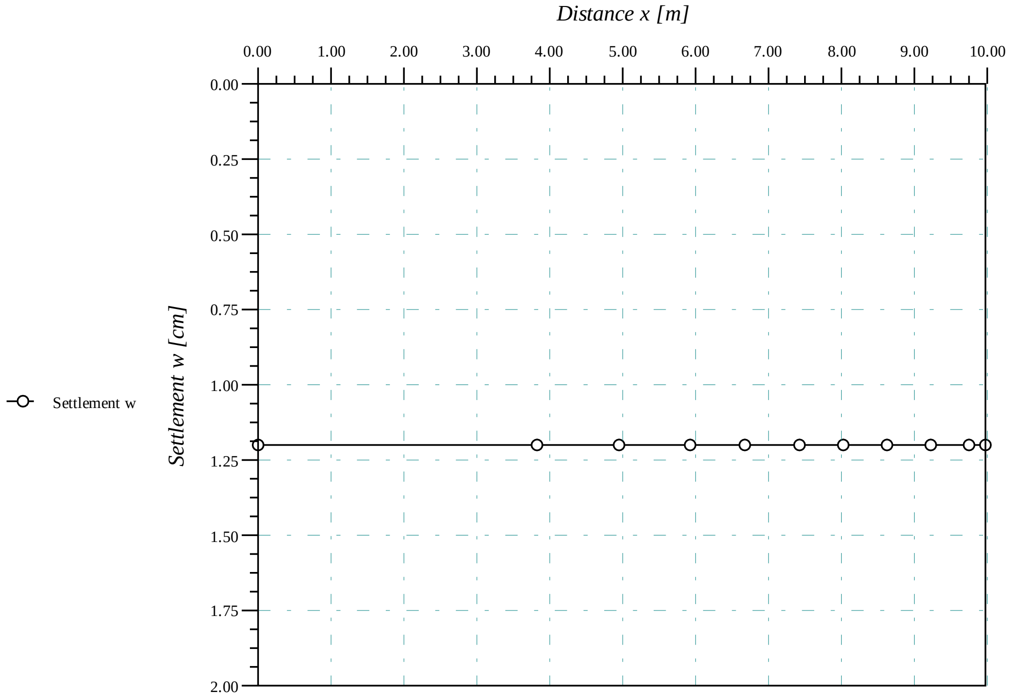

Base settlements
Section in shell base

GEOTEC Software Inc	
PO Box 14001 Richmond Road PO, Calgary AB, Canada T3E 7Y7	
Scale: 75	**Project: Selvadurai (1979): Elastic Analysis of Soil Foundation Interaction.**
File: Selvadurai	**Date: 05/01/2020**
Page No.:	**Title: Rigid circular raft on Isotropic elastic half-space medium**

Method (8) (Analysis of rotational shell)
Modulus of Compressibility for Rigid Raft (Half Space model)

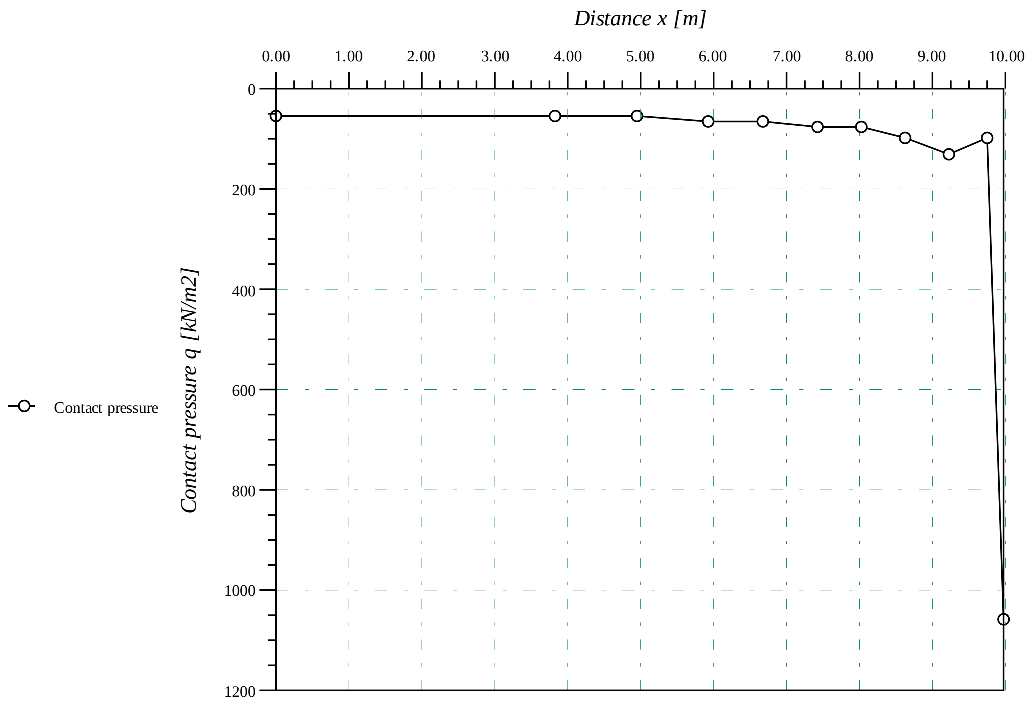

Base contact pressures
Section in shell base

GEOTEC Software Inc PO Box 14001 Richmond Road PO, Calgary AB, Canada T3E 7Y7	
Scale: 75	**Project: Selvadurai (1979): Elastic Analysis of Soil Foundation Interaction.**
File: Selvadurai	**Date: 05/01/2020**
Page No.:	**Title: Rigid circular raft on Isotropic elastic half-space medium**

2.10 Example 8: Tank with fixed base

2.10.1 Description of the problem

A closed form solution for axi-symmetrically circular cylindrical tank is available in the reference *Bakhoum* (1992). To verify the finite element analysis of shell structures and to test the limitation of mesh size, the internal forces, horizontal displacement and meridional rotation calculated analytically by the available closed form solution are compared with those obtained by the finite element analysis of *ELPLA* using circular cylindrical shell elements.

A circular cylindrical tank of a radius of a = 7 [m] and a height of H = 5 [m] is considered as shown in Figure 2.14. Thickness of the tank wall is t = 0.25 [m]. The tank is filled with water. The lower edge of the tank is clamped. Figure 2.14 shows the circular cylindrical tank with dimensions, while the tank material and unit weight of the water are listed in Table 2.7.

Table 2.7 Tank material and water unit weight

Modulus of Elasticity of the tank material	E_c	= 2×10^7 [kN/m^2]
Poisson's ratio of the tank material	ν_c	= 0.15 [-]
Unit weight of the water	γ_w	= 10 [kN/m^3]

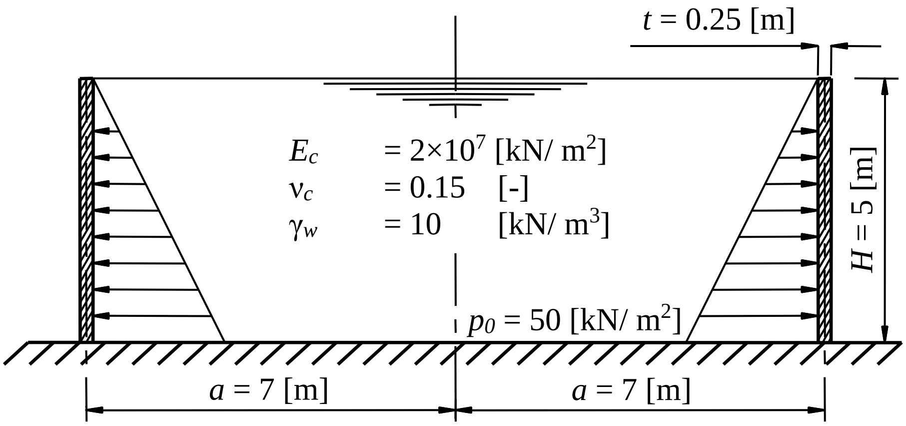

Figure 2.14 Cylindrical circular tank with dimensions

2.10.2 Numerical Analysis

To examine the accuracy of the numerical analysis of circular cylindrical shell tank using the finite element method, the meridional moment M_y at the tank base is verified using different mesh sizes. As shown in Figure 2.15 the height of the tank is divided into 5 equal segments. In each segment, element size and number of elements are varied for different cases. Chosen of total elements in each case are 5, 10, 20, 25, 50 and 80, which give element sizes of 100, 50, 25, 10, and 6.25 [cm].

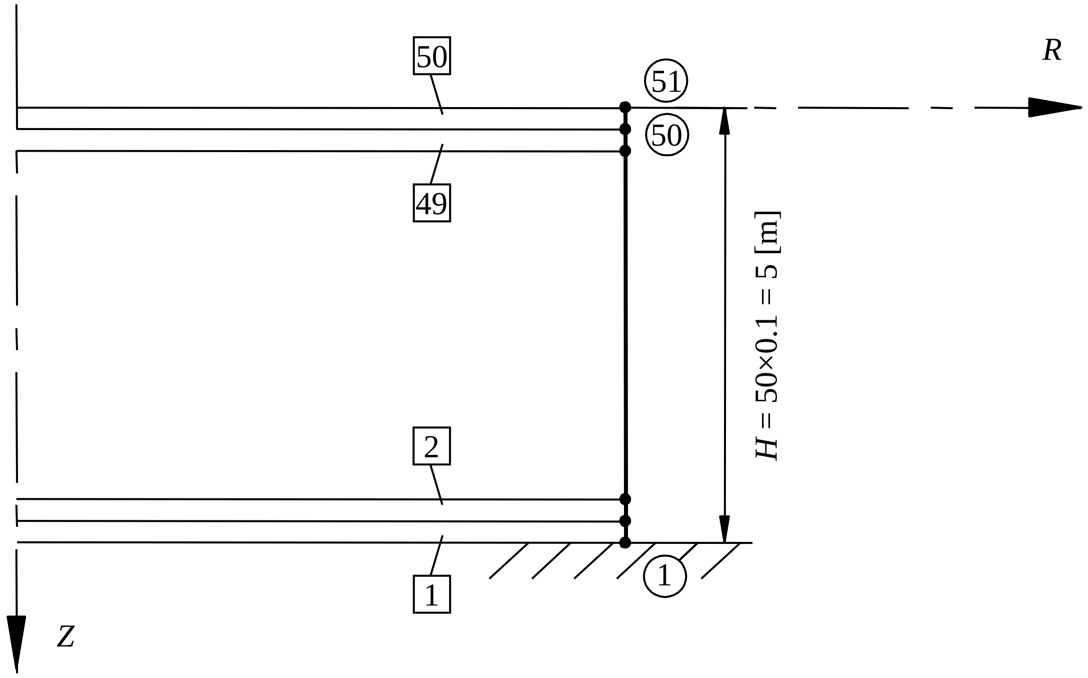

Figure 2.15 Finite element mesh of the tank

2.10.3 Results and discussion

Results of numerical analysis along the wall height are compared with those of the closed form solution. Figure 2.16 shows the meridional moment M_y [kN.m/m], Figure 2.17 shows the radial force N_r [kN/ m], Figure 2.18 shows the horizontal displacement v_h and Figure 2.19 shows the meridional rotation v_m with tank height. The analysis is carried out with total elements along the wall height equal to 50, which gives an element size of 10 [cm]. These figures show that verification results of the available finite element analysis are in an excellent agreement with those of the analytical solution of *Bakhoum* (1992). Table 2.8 show a comparison between maximum internal forces obtained from analytical solution and those obtained from *ELPLA* using circular cylindrical shell elements. The table shows that the error in the maximum values of radial force and meridional rotation is about 0.5%, while that of the horizontal displacement is 0.74%. The error in the maximum meridional moment is about 7%.

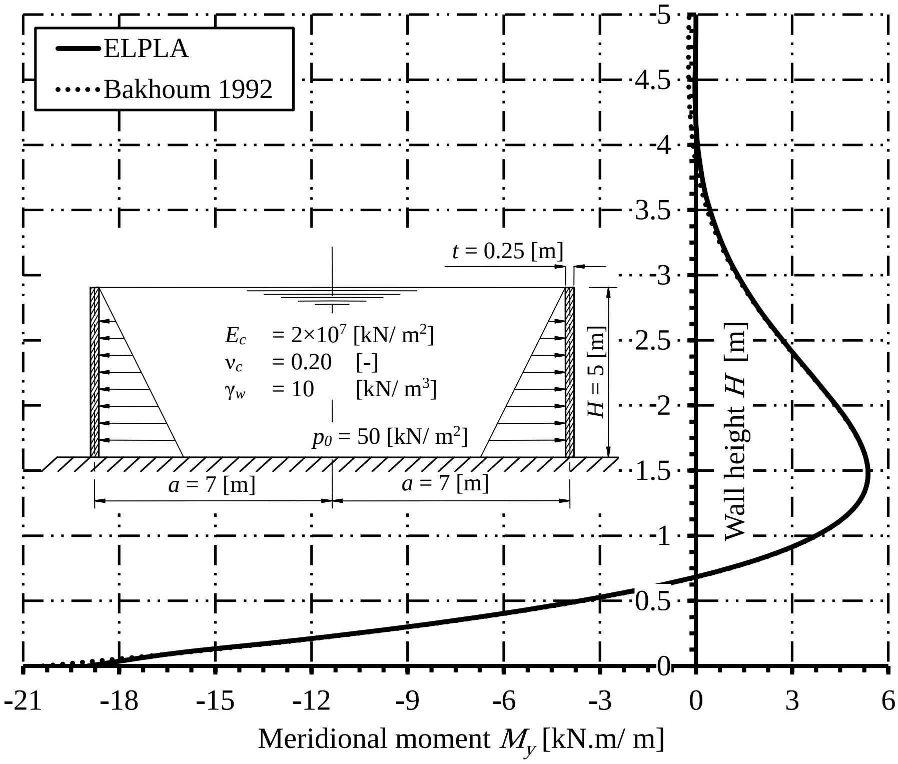

Figure 2.16 Meridional moment M_y [kN.m/ m] with tank height.

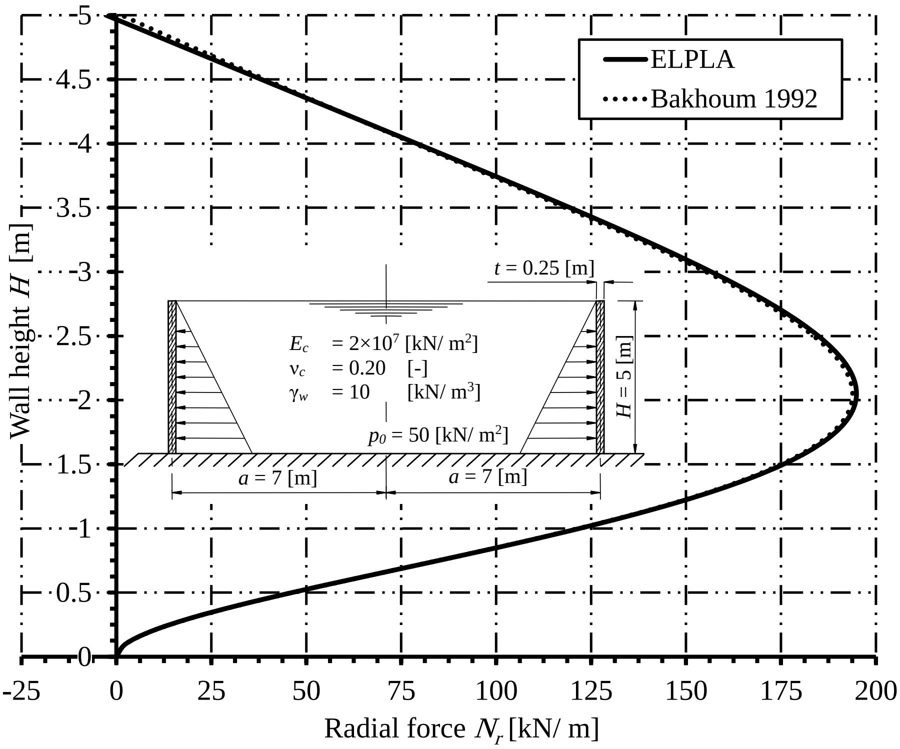

Figure 2.17 Radial force N_r [kN/ m] with tank height.

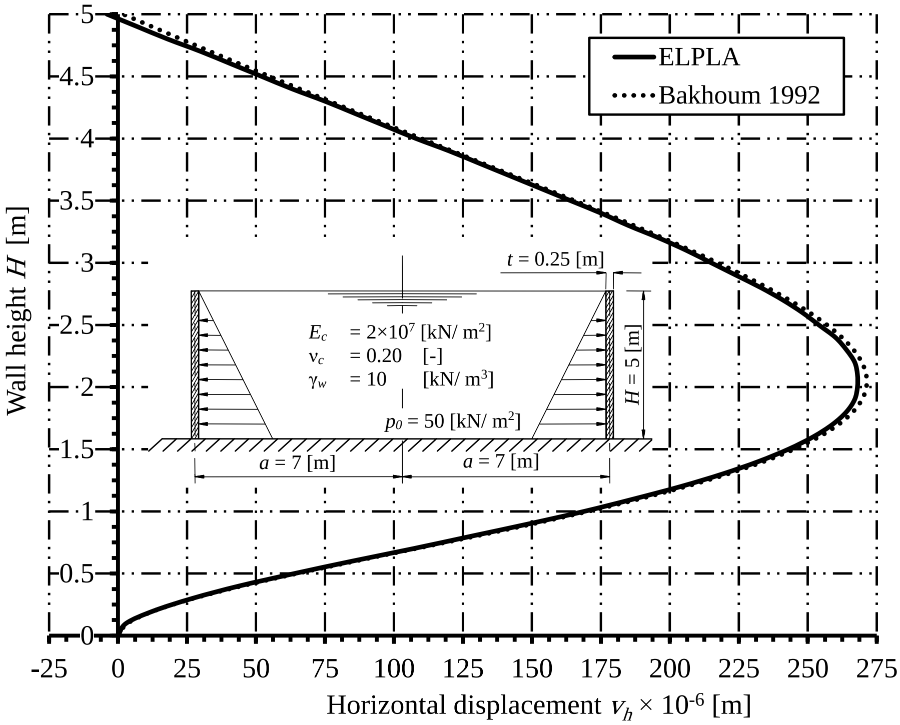

Figure 2.18 Horizontal displacement v_h with tank height.

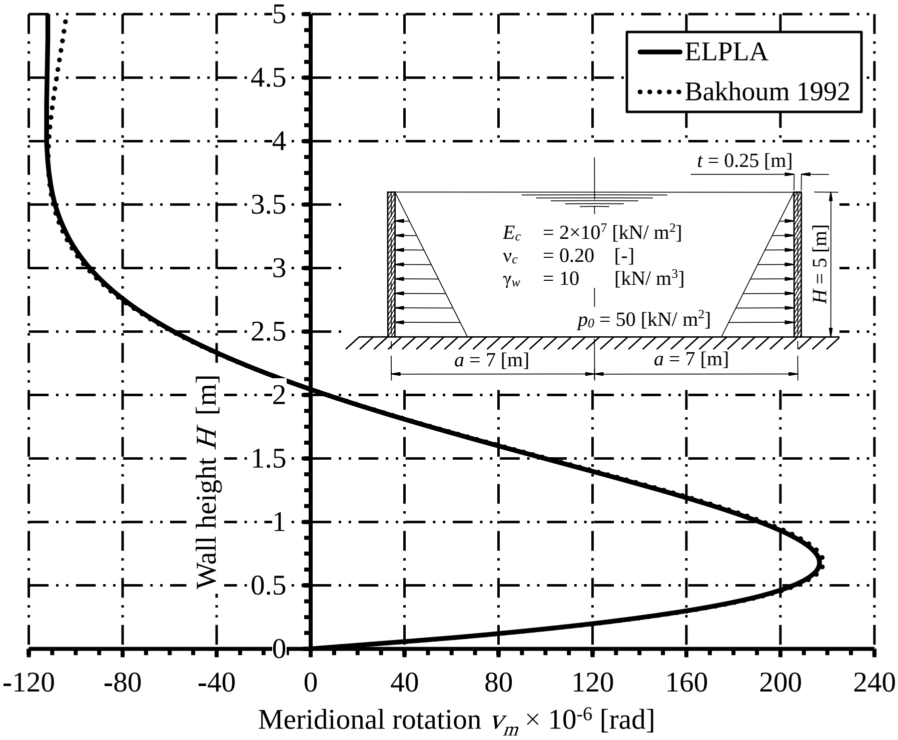

Figure 2.19 Meridional rotation v_m with tank height.

Table 2.8 Comparison between maximum internal forces and deformations obtained from analytical solution and those obtained from *ELPLA* using circular cylindrical shell elements

Result	Type of analysis		Difference
	Bakhoum (1992)	*ELPLA*	
Maximum positive meridional moment M_y^+	M_y^+ [kN.m/ m]	M_y^+ [kN.m/ m]	ΔM_y^+ [%]
	5.37	5.37	0.00
Maximum negative meridional moment M_y^-	M_y^- [kN.m/ m]	M_y^- [kN.m/ m]	ΔM_y^- [%]
	-20.38	-18.97	6.92
Maximum radial force N_r	N_r [kN/ m]	N_r [kN/ m]	ΔN_r [%]
	193.74	194.74	0.52
Maximum Horizontal displacement v_h	v_h [mm]	v_h [mm]	Δv_h [%]
	0.271	0.268	1.107
Maximum meridional rotation v_m	v_m [rad]	v_m [rad]	Δv_m [%]
	2.18106×10^{-4}	2.165×10^{-4}	0.74

2.10.4 Conversion of the solution

Figure 2.20 shows the convergence accuracy of the circular cylindrical shell element with different No. of elements. The figure show that element with size of about 25 [cm] gives a good result with an error less than 20 %, while element with size of about 10 [cm] gives a good result with an error less than 10 % compared with the analytical solution. This conclusion concerning element size will be considered in all analyses of shell structures in these theses.

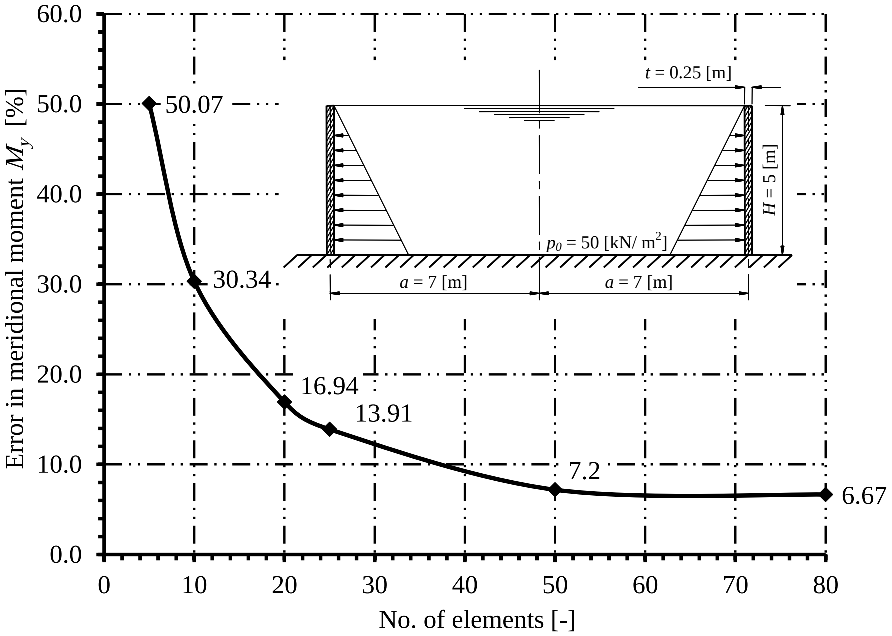

Figure 2.20 Convergence accuracy of the circular cylindrical shell element

2.11 Example 9: Tank with hinged base

2.11.1 Description of the problem

A method based on analytical solutions of the differential equation that governs the behavior of the wall of a cylindrical tank is available in the reference *Godbout et al.* (2003). To verify the finite element analysis of shell structures, the internal forces obtained by this method are compared with those obtained by *ELPLA* using circular cylindrical shell elements.

A circular cylindrical tank of a radius of a = 15 [m] and a height of H = 3.7 [m] is considered as shown in Figure 2.14Figure 2.21. Thickness of the tank wall is t = 0.2 [m]. The lower edge of the tank is hinged. The tank material has the following properties:

Modulus of Elasticity of the tank material	E_c	= 3×10⁷ [kN/m²]
Poisson's ratio of the tank material	ν_c	= 0.17 [-]

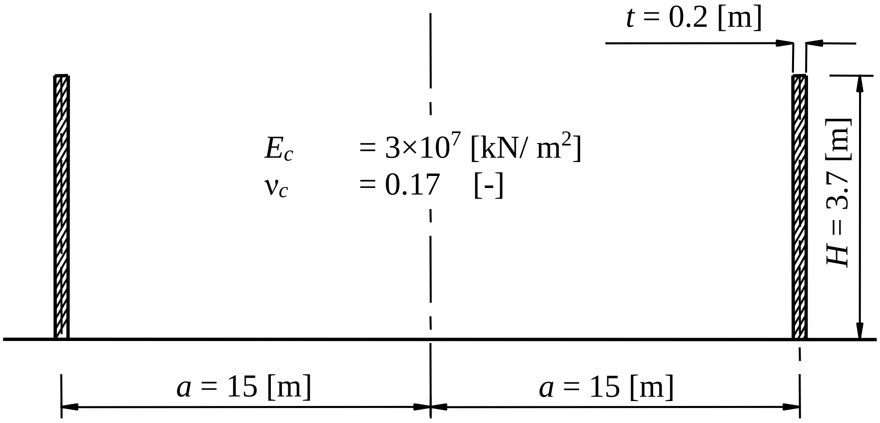

Figure 2.21 Cylindrical circular tank with dimensions

2.11.2 Numerical Analysis

In the analysis, the height of the tank is divided into 14 segments (12×0.25 [m]+2×0.35 [m]) as shown in 1.

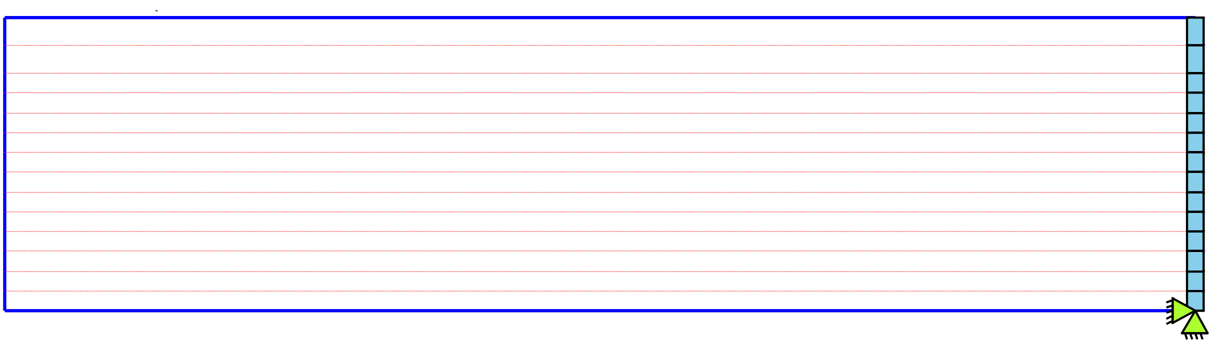

Figure 2.22 Finite element mesh of the tank with boundary conditions

Meridional moment M_y and radial force N_r are determined for the following cases:

1. Fully filled tank with water, Figure 2.23. Unit weight of the water γ_w = 10 [kN/m^3]

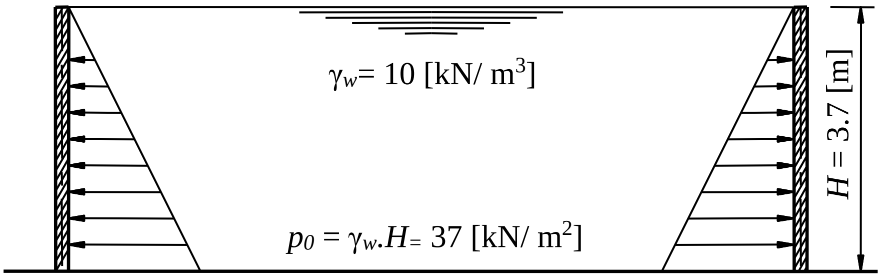

Figure 2.23 Fully filled tank with water

2. Tank with a ground level of Hs=2 [m] above the base, Figure 2.24. The active earth press is $ks.\gamma_s$ = 5.7 [kN/m^3]

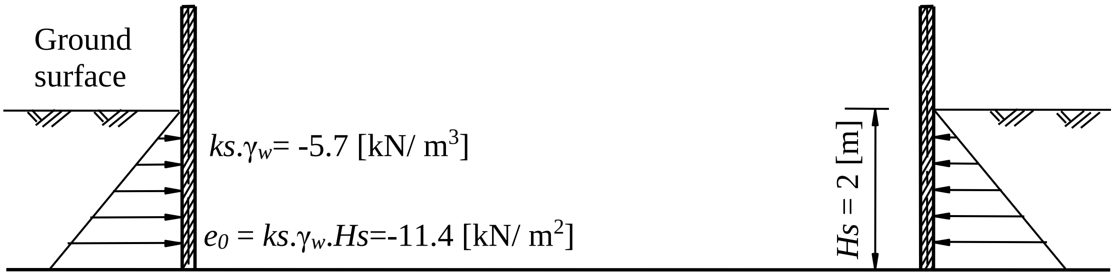

Figure 2.24 Tank with a ground level of Hs=2 [m] above the base

3. Tank under a partially uniform load on the wall q= -5 [kN/m^2], Figure 2.25. The load has a height of Hs=2 [m] from the base.

Figure 2.25 Tank under a partially uniform load on the wall

2.11.3 Results and discussion

Results of *ELPLA* using the finite element analysis along the wall height are compared with those obtained by *Godbout et al.* (2003). Results are plotted in Figure 2.26 to Figure 2.31. These figures show that results of *ELPLA* are in a good agreement with those of *Godbout et al.* (2003).

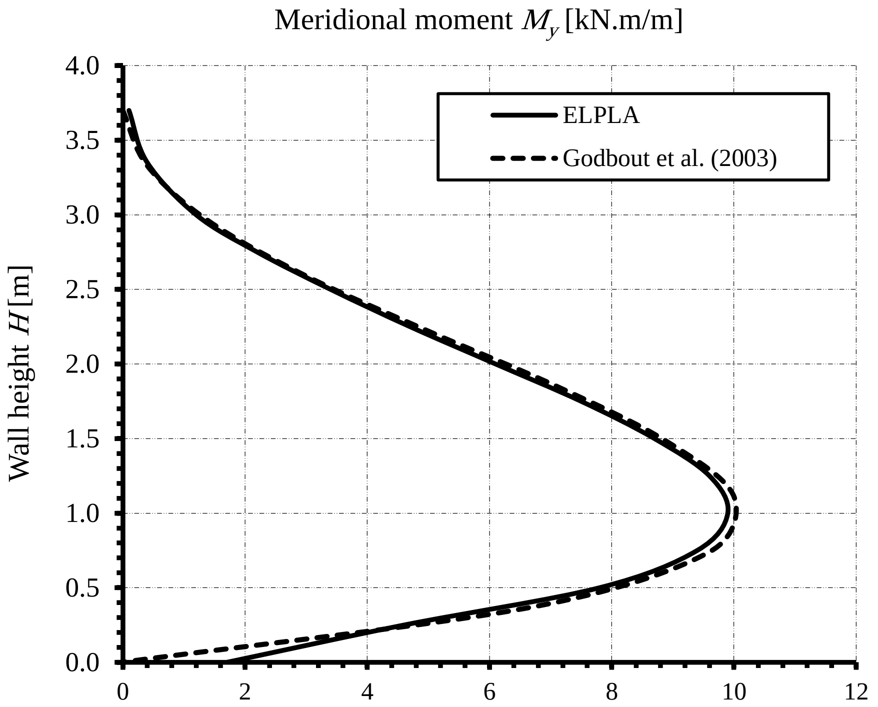

Figure 2.26 Meridional moment M_y [kN.m/ m] with wall height. Case 1

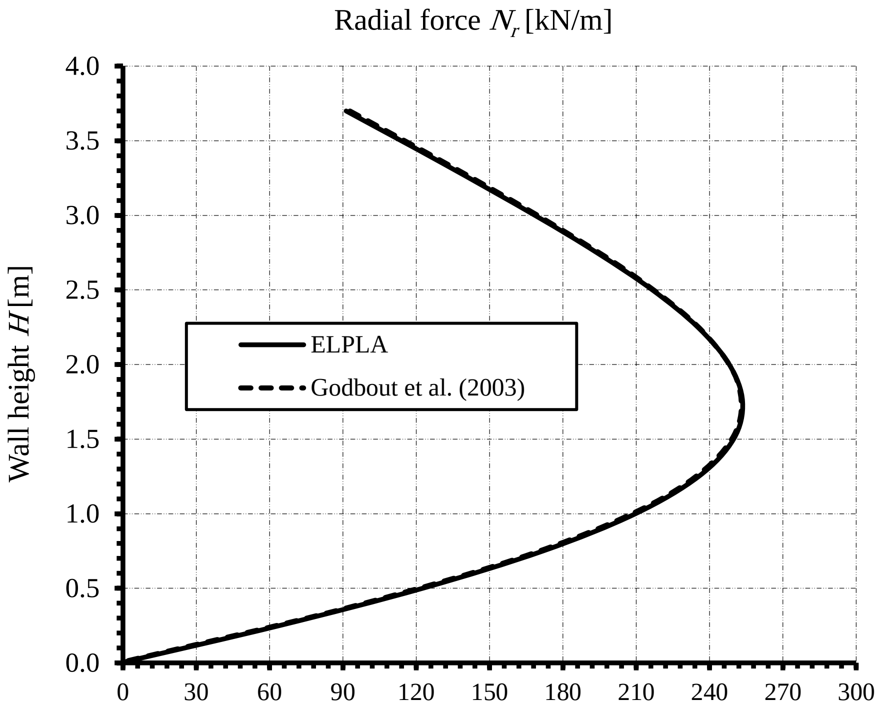

Figure 2.27 Radial force N_r [kN/ m] with wall height. Case 1

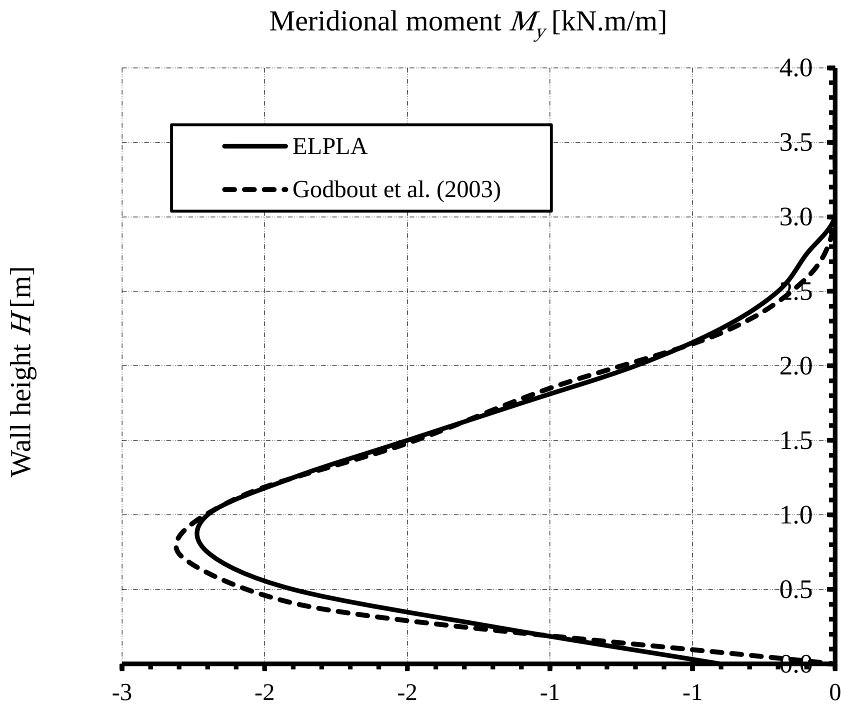

Figure 2.28 Meridional moment M_y [kN.m/ m] with wall height. Case 2

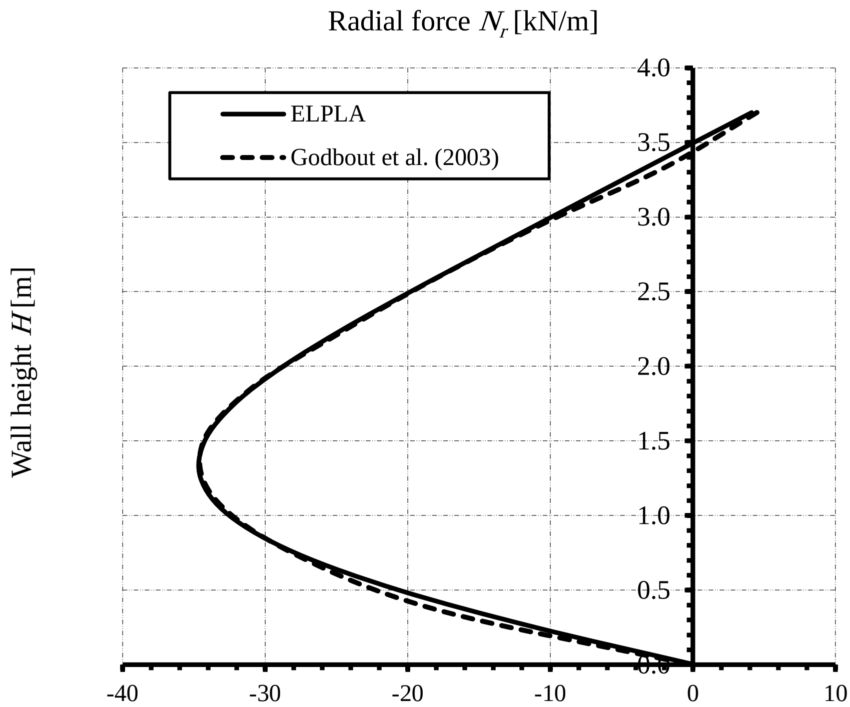

Figure 2.29 Radial force N_r [kN/ m] with wall height. Case 2

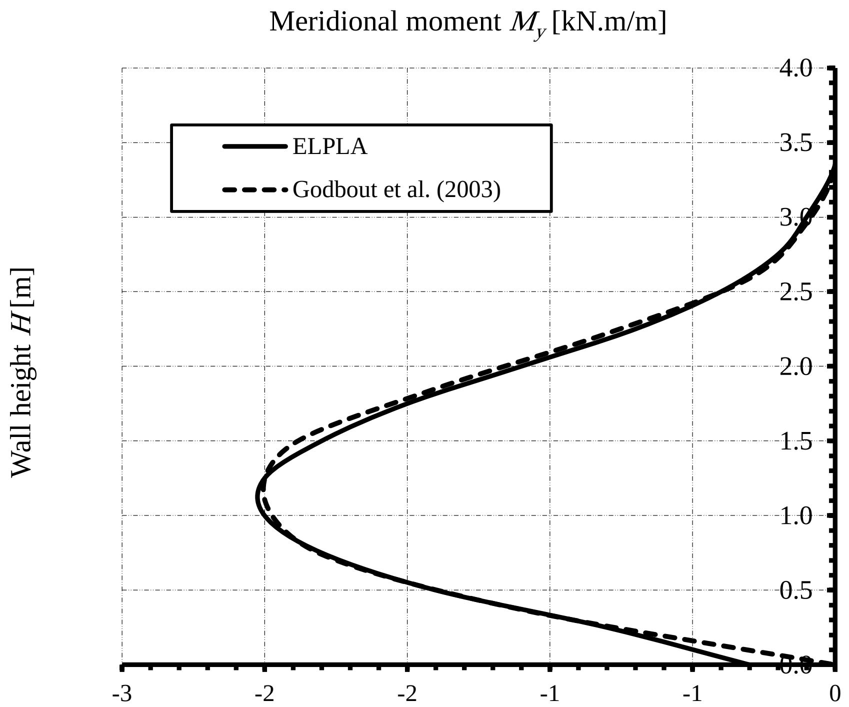

Figure 2.30 Meridional moment M_y [kN.m/ m] with wall height. Case 3

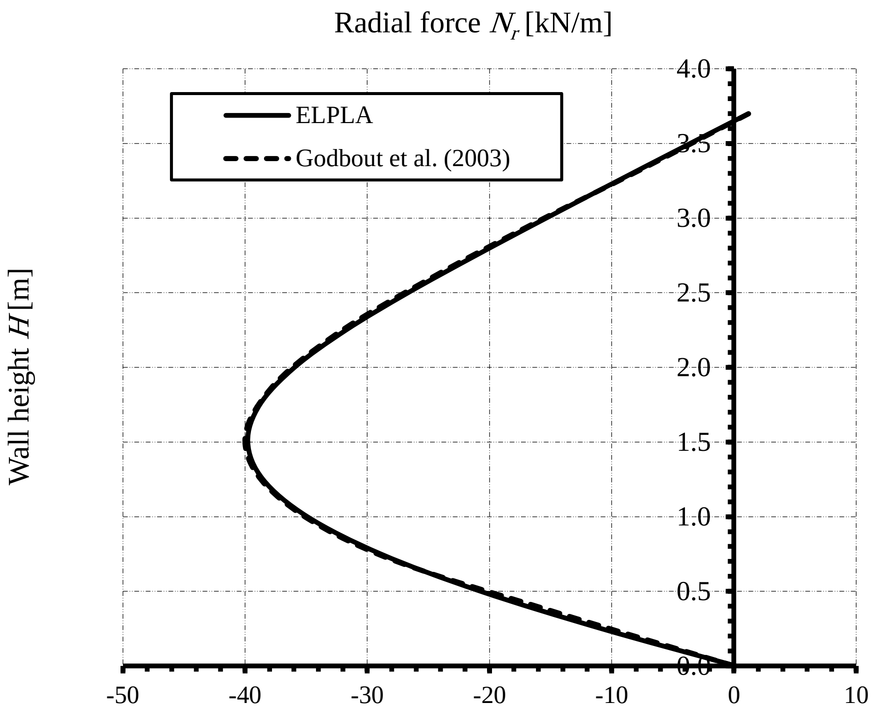

Figure 2.31 Radial force N_r [kN/ m] with wall height. Case 3

2.12 Example 10: Ring wall with variable wall thickness

2.12.1 Description of the problem

An example for cylindrical shells with variable wall thickness using the finite difference method is available in the reference *Naïmi* (1957). To verify the finite element analysis of shell structures, the internal forces and horizontal displacement calculated numerically by the finite difference method are compared with those obtained by *ELPLA* using circular cylindrical shell elements.

A ring wall of a radius a = 100 [m] and a height H = 100.1 [m] is considered as shown in Figure 2.32. The wall of the ring has a variable thickness, at the base the thickness is h_{11} = 13.3 [m], while at the top the thickness is h_0 = 4 [m], thickness in between h [m] can be obtained from the following equation:

$$h = \frac{4e^{1.2}}{100}x$$

where x is the distance from the base in [m].

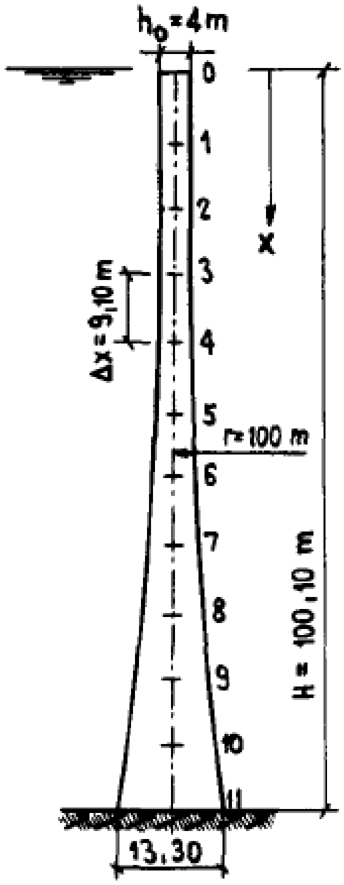

Figure 2.32 Ring wall with dimensions (after *Naïmi* (1957))

The ring wall is exposed to a hydrostatic water pressure and is fixed at the base. The wall material and unit weight of the water are listed in Table 2.9.

Table 2.9 Wall material and water unit weight

Modulus of Elasticity of the tank material	E_c	$= 2.1\times10^7$	[kN/m^2]
Poisson's ratio of the tank material	ν_c	= 0	[-]
Unit weight of the water	γ_w	= 10	[kN/m^3]

2.12.2 Analysis of the ring wall

In the analysis, the total height of the wall is divided into 11 segments with a constant length; each is (Figure 2.33):

$$\Delta x = \frac{100.10}{11} = 9.10\ [m]$$

Figure 2.33 Finite element mesh of the ring wall with wall thickness

2.12.3 Results and discussion

Results of *ELPLA* using the finite element analysis along the wall height are compared with those obtained from the finite difference analysis by *Naïmi* (1957). Figure 2.34 shows the meridional moment M_y, Figure 2.35 shows the radial force N_r and Figure 2.36 shows the horizontal displacement V_h. These figures show that verification results of the available finite element analysis are in an good agreement with those of the finite difference analysis of *Naïmi* (1957).

2.12.4 Results by *ELPLA*

The input data and results of *ELPLA* are presented on the next pages.

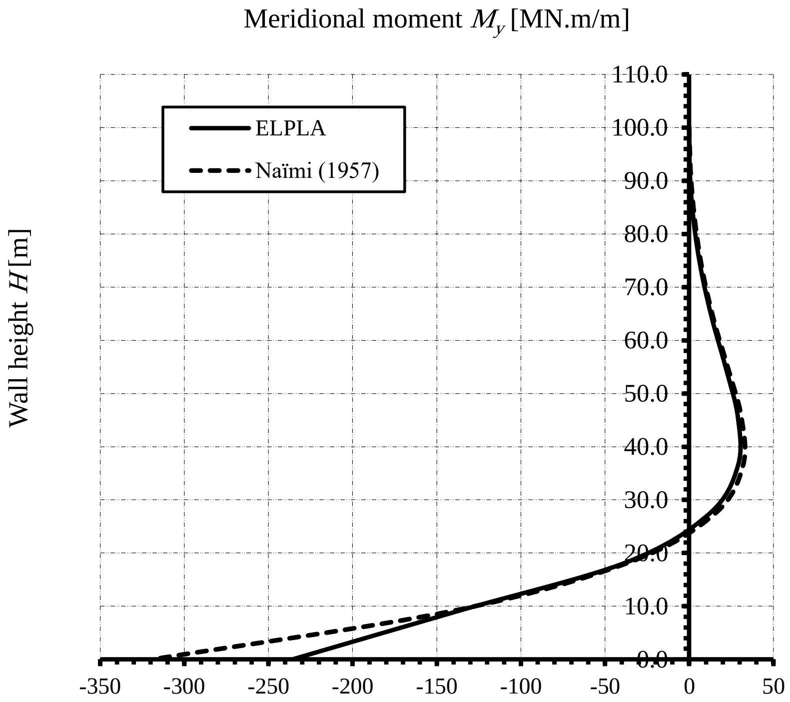

Figure 2.34 Meridional moment M_y [MN.m/ m] with ring height.

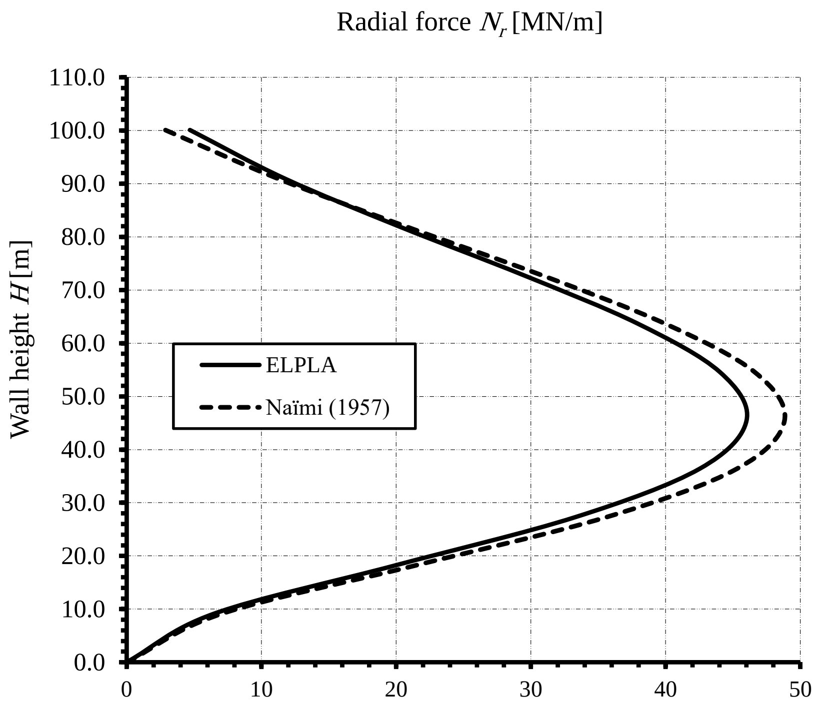

Figure 2.35 Radial force N_r [MN/ m] with ring height.

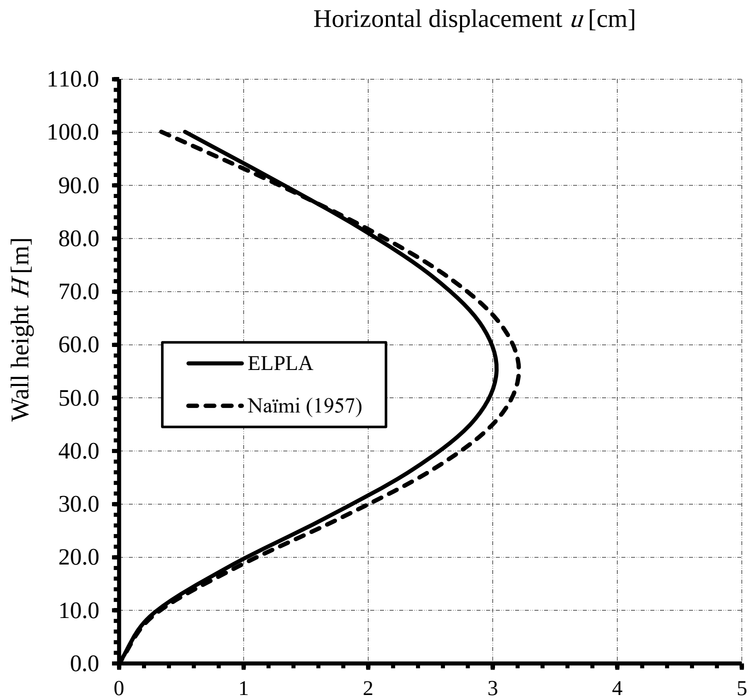

Figure 2.36 Horizontal displacement V_x [cm] with tank height.

Analysis of rotational shell

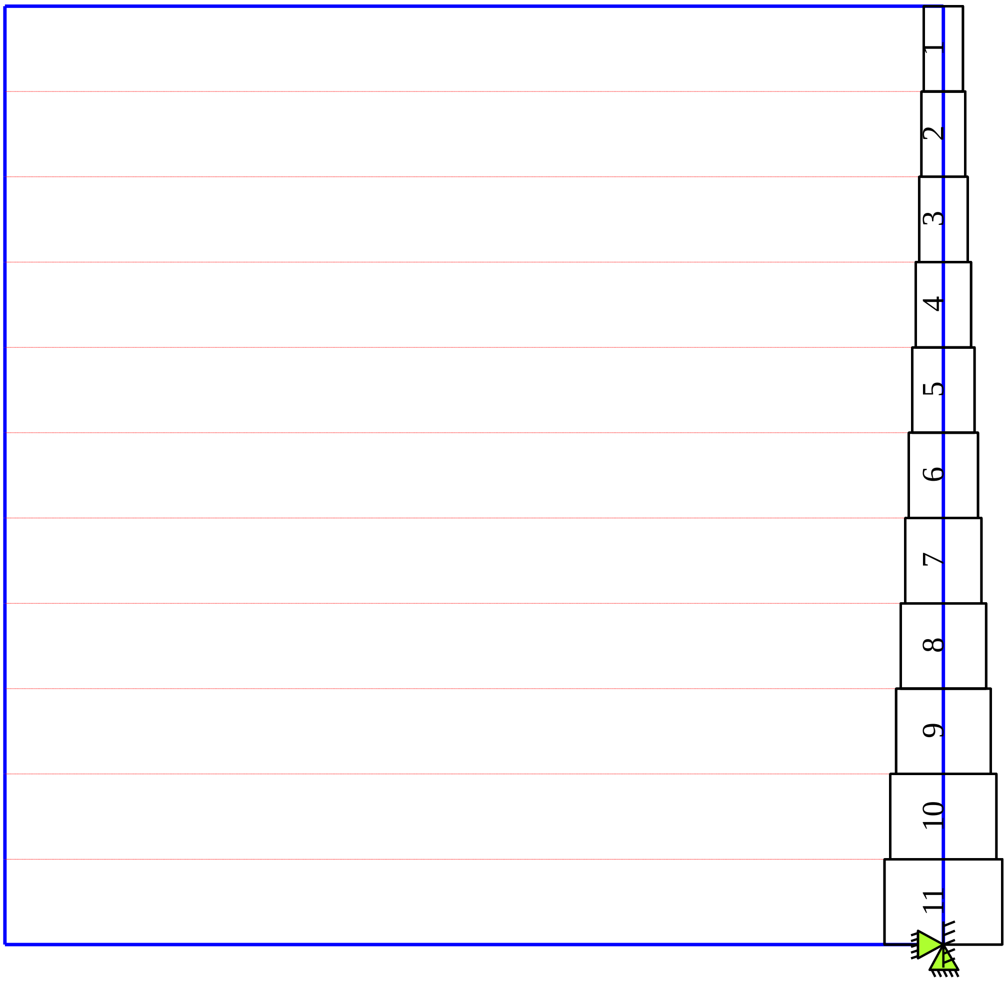

Boundary conditions

GEOTEC Software Inc PO Box 14001 Richmond Road PO, Calgary AB, Canada T3E 7Y7	
Scale 1:615	Title: Berechnung einer Ringmauer
File: Houchmand	Date: 18/11/2019
Page No.:	Project: Houchmand (1957): Beitraege zur Anwendung der Schalentheorie bei Bogenstaumauern.

Analysis of rotational shell

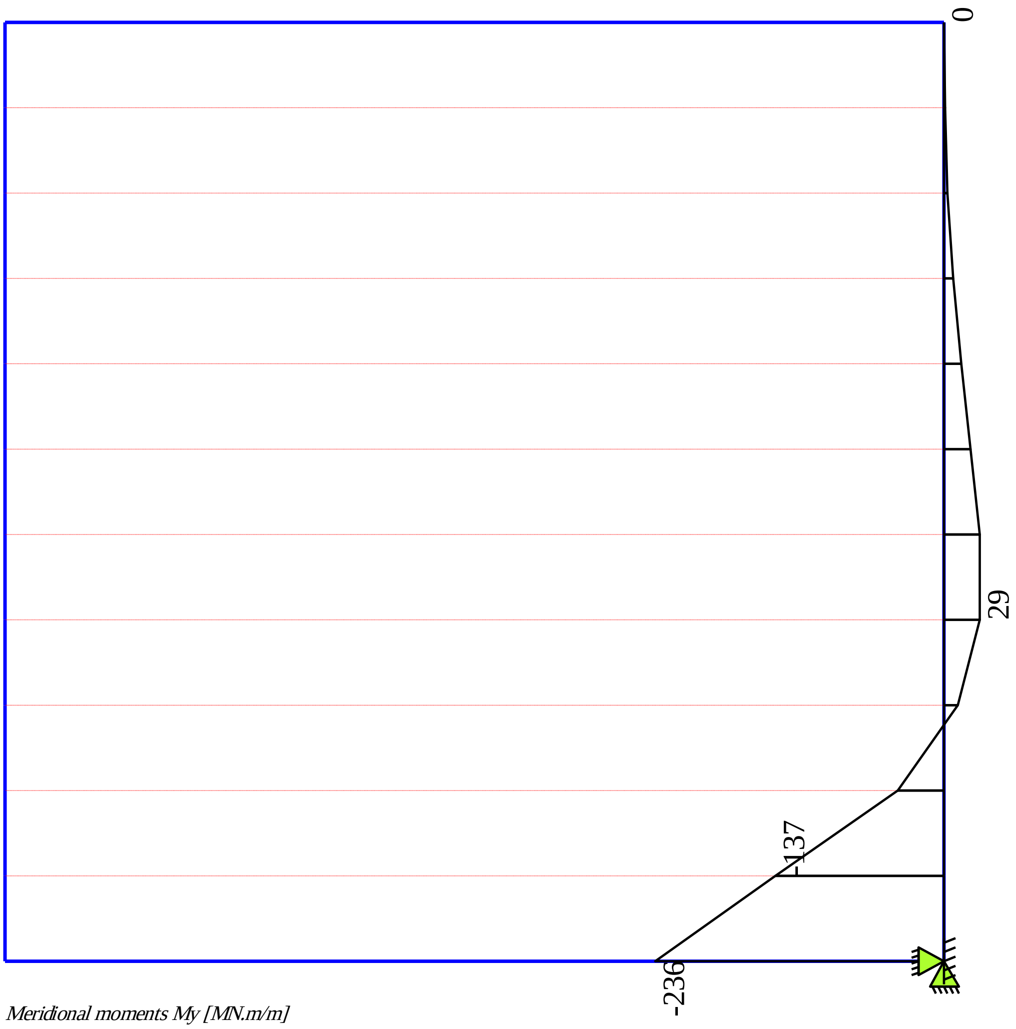

Meridional moments My [MN.m/m]
Max. My = 29 at node 10, Min. My = -236 at node 2

GEOTEC Software Inc
PO Box 14001 Richmond Road PO, Calgary AB, Canada T3E 7Y7

Scale 1:615	Title: Berechnung einer Ringmauer
File: Houchmand	Date: 18/11/2019
Page No.:	Project: Houchmand (1957): Beitraege zur Anwendung der Schalentheorie bei Bogenstaumauern.

Analysis of rotational shell

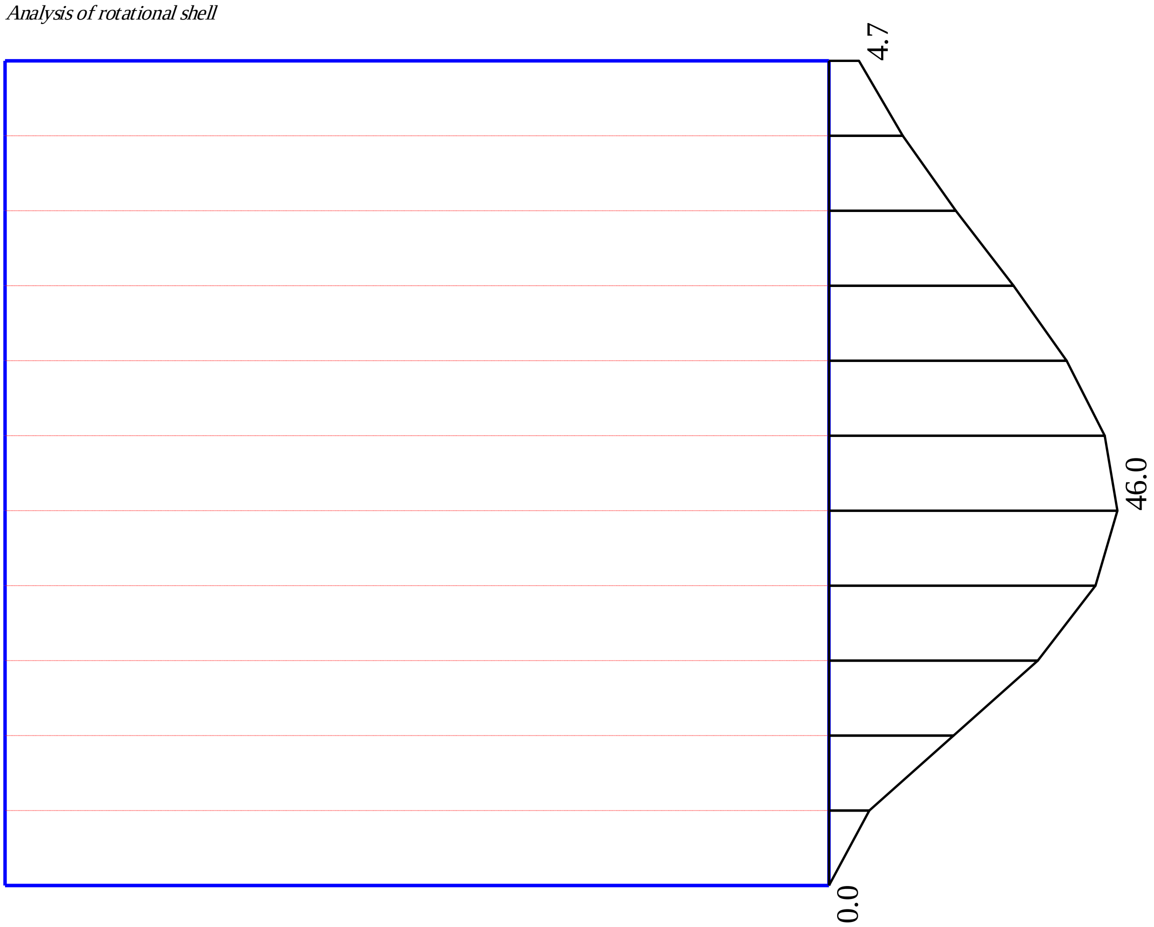

Radial forces Nr [MN/m]
Max. Nr = 46.0 at node 12, Min. Nr = 0.0 at node 2

GEOTEC Software Inc
PO Box 14001 Richmond Road PO, Calgary AB, Canada T3E 7Y7

Scale 1:700	Title: Berechnung einer Ringmauer
File: Houchmand	Date: 18/11/2019
Page No.:	Project: Houchmand (1957): Beitraege zur Anwendung der Schalentheorie bei Bogenstaumauern.

Analysis of rotational shell

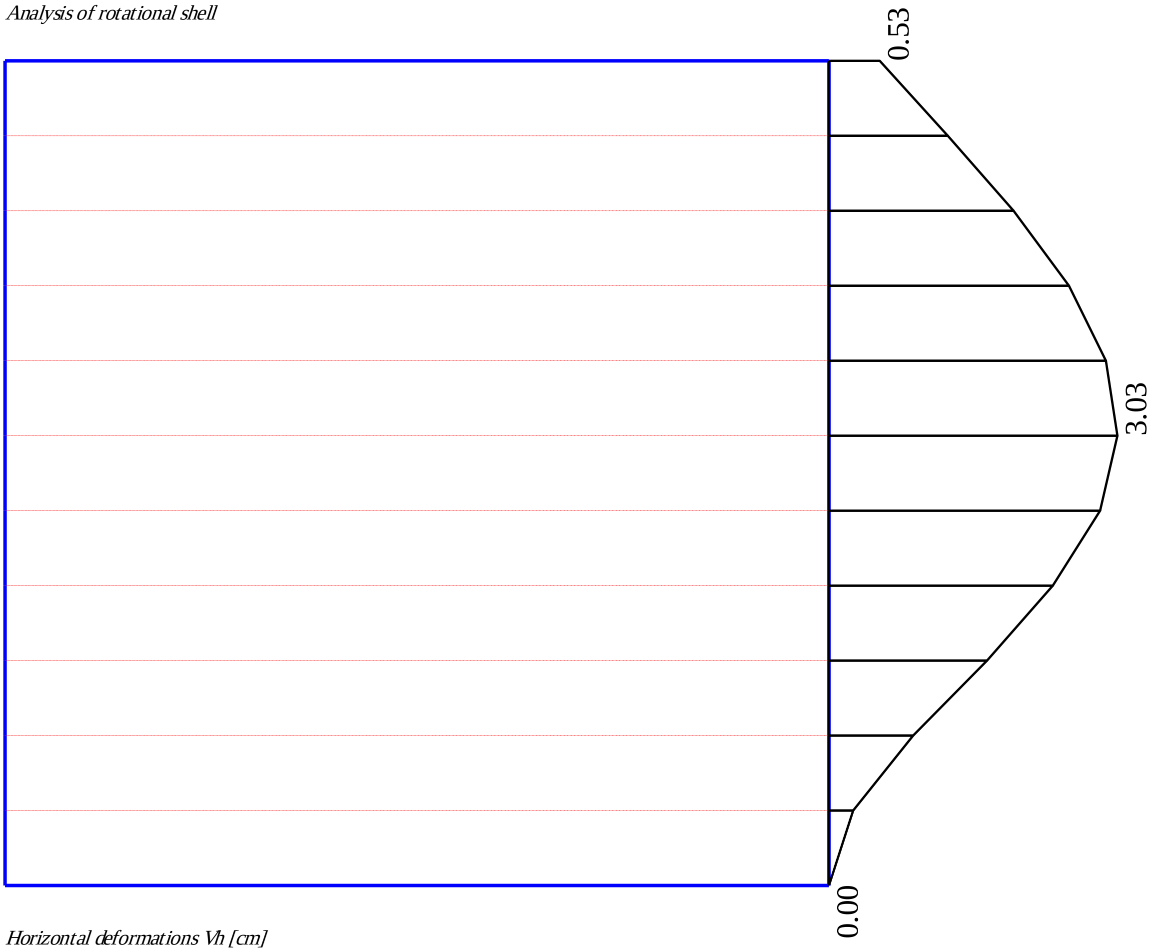

Horizontal deformations Vh [cm]
Max. Vh = 3.03 at node 14, Min. Vh = 0.00 at node 2

GEOTEC Software Inc PO Box 14001 Richmond Road PO, Calgary AB, Canada T3E 7Y7	
Scale 1:700	Title: Berechnung einer Ringmauer
File: Houchmand	Date: 18/11/2019
Page No.:	Project: Houchmand (1957): Beitraege zur Anwendung der Schalentheorie bei Bogenstaumauern.

2.13 Example 11: Tank covered with a spherical dome

2.13.1 Description of the problem

Numerical analysis for axi-symmetrically circular cylindrical tank covered with a spherical dome is presented by *Melerski* (2006) using a hybrid of displacement techniques based on finite element method. To verify analysis of cylindrical tank covered with a spherical dome, the internal forces calculated by *Melerski* (2006) are compared with those obtained by *ELPLA* using circular cylindrical shell elements.

Figure 2.37 shows half of an axial section of a large-diameter reinforced concrete circular cylindrical tank covered with a dome roof. The wall connection with the roof is monolithic, while the end of the wall is fixed at the base. Details concerning the geometry of the structure are as shown in Figure 2.37. The elastic properties of the tank material are shown in Table 2.10. Only the self-weight is considered in this analysis.

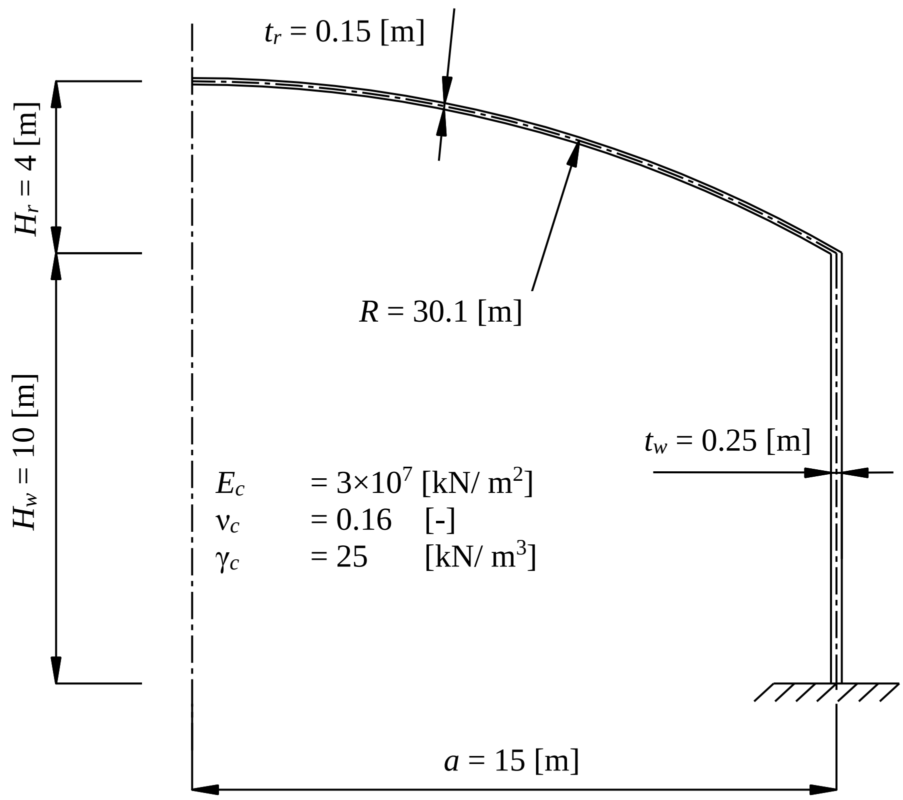

Figure 2.37 Radial section through the tank

Table 2.10 Tank material

Modulus of Elasticity of the tank material	E_c	$= 3\times10^7$	[kN/ m^2]
Poisson's ratio of the tank material	ν_c	= 0.16	[-]
Unit weight of the tank material	γ_c	= 25	[kN/ m^3]

2.13.2 Numerical Analysis

In order to illustrate the comparison between the analysis of *Melerski* (2006) and that of *ELPLA*, the height of the wall is divided into 50 equal elements, each of 0.20 [m], while the roof shell (dome) is divided into 40 equal arcs each of 0.75 [°] as shown in Figure 2.38.

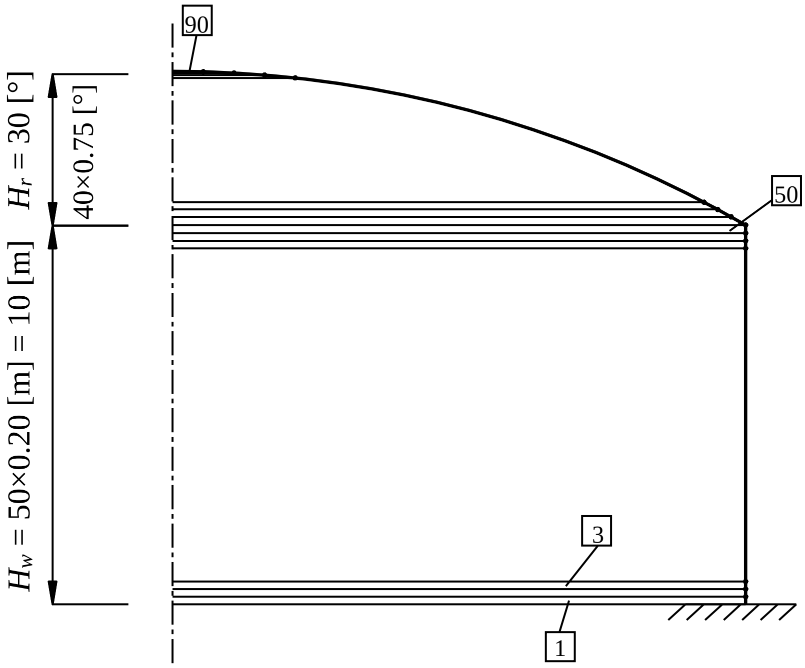

Figure 2.38 Finite element mesh of the tank

2.13.3 Results and discussions

The analysis of the considered tank is carried out by *ELPLA*, where the circular cylindrical wall and the spherical roof were simulated with a thin circular cylindrical shell element using the finite element method. *Melerski* (2006) analyzed the same tank by a finite element using a hybrid of displacement techniques.

Results of numerical analysis in the roof are compared with those of *Melerski* (2006). Figure 2.39 shows the tangential moment M_t [kN.m/m], Figure 2.40 shows the meridional moment M_y [kN.m/m], Figure 2.41 shows the radial force N_r [kN/ m], Figure 2.42 shows the meridional force N_y [kN/ m], Figure 2.43 shows the horizontal displacement v_h [mm] and Figure 2.44 shows the vertical displacement v_v [mm]. These figures show that results of the available finite element analysis using circular cylindrical shell elements are in a good agreement with those of the numerical solution of *Melerski* (2006) by a finite element using a hybrid of displacement techniques. Table 2.11 shows a comparison between maximum internal forces obtained from the solution of *Melerski* (2006) and those obtained from *ELPLA*. The table shows that the error in the maximum values of tangential and meridional moments are 7.63%. The radial forces are more accurate with error of 1.39%, while that of the meridional forces are 1.67%. The horizontal displacements are in excellent accuracy with zero error, while the vertical displacements are less accurate with error of 6.40%.

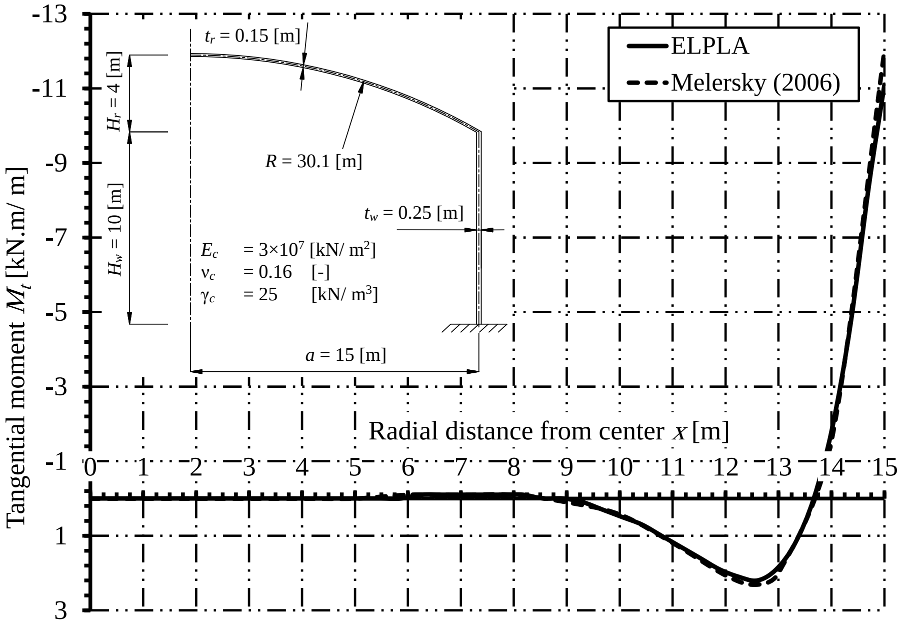

Figure 2.39 Tangential moment M_t in the roof

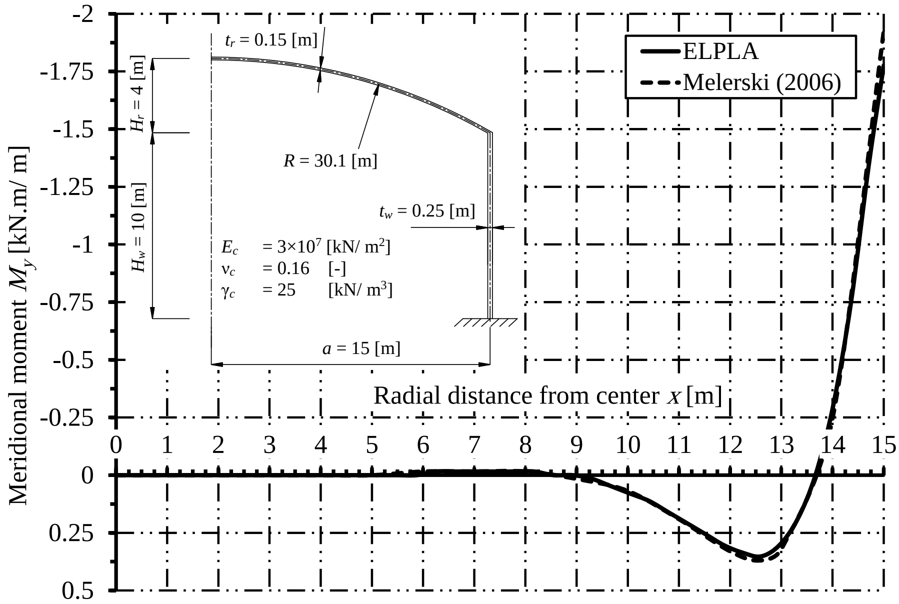

Figure 2.40 Meridional moment M_y in the roof

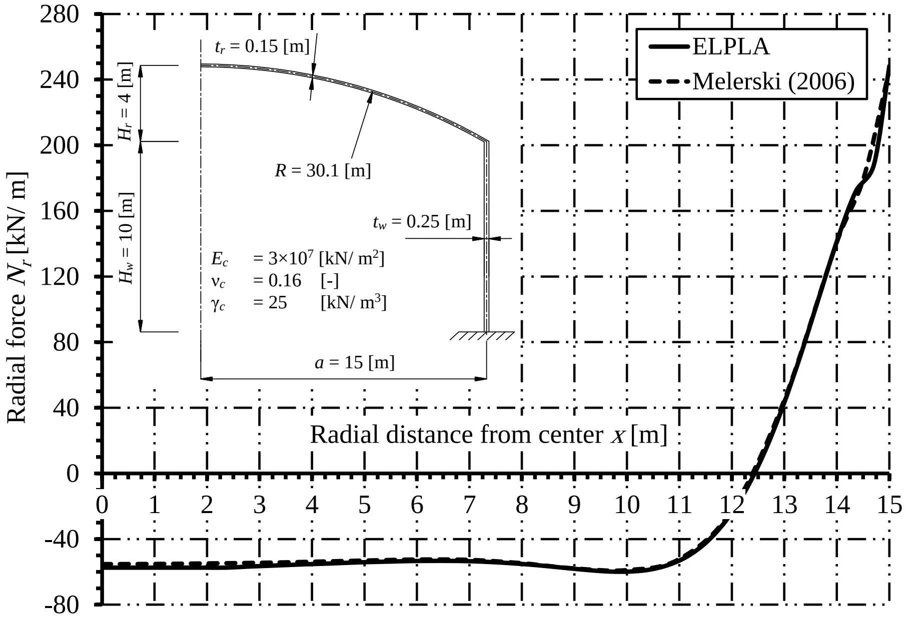

Figure 2.41 Radial force N_r in the roof

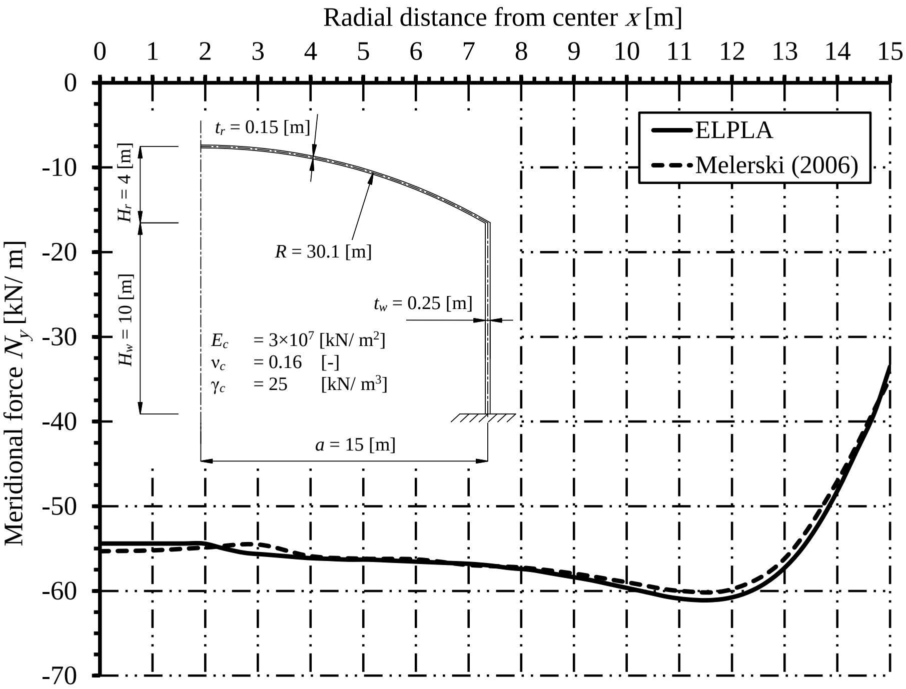

Figure 2.42 Meridional force N_y in the roof

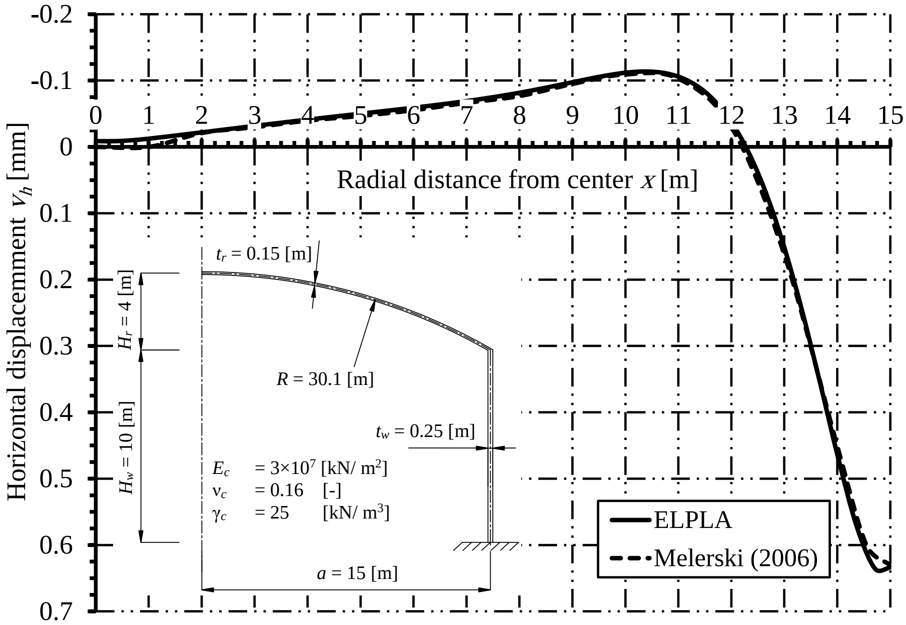

Figure 2.43 Horizontal displacement v_h in the roof

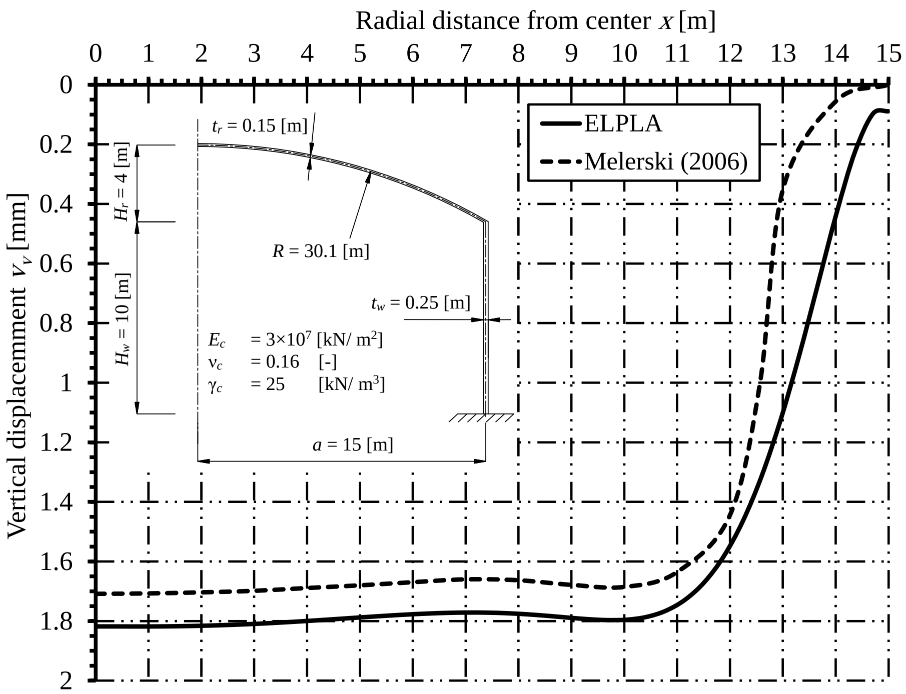

Figure 2.44 Vertical Displacement v_v in the roof

Table 2.11 Comparison between maximum internal forces obtained from *Melerski* (2006) solution by a finite element using a hybrid of displacement techniques and those obtained from *ELPLA* using circular cylindrical shell elements

Result	Type of analysis		Difference
	Melerski (2006)	*ELPLA*	
Maximum positive tangential moment M_t^+	M_t^+ [kN.m/ m]	M_t^+ [kN.m/ m]	ΔM_t^+ [%]
	2.31	2.20	4.76
Maximum negative tangential moment M_t^-	M_t^- [kN.m/ m]	M_t^- [kN.m/ m]	ΔM_t^- [%]
	-12.02	-11.10	7.63
Maximum positive radial force N_r^+	N_r^+ [kN/ m]	N_r^+ [kN/ m]	ΔN_r^+ [%]
	246	248.20	0.89
Maximum negative radial force N_r^-	N_r^- [kN/ m]	N_r^- [kN/ m]	ΔN_r^- [%]
	-58.98	-59.80	1.39
Maximum meridional force N_y	N_y [kN/ m]	N_y [kN/ m]	ΔN_y [%]
	-60	-61.10	1.83
Maximum positive horizontal displacement v_h^+	v_h^+ [kN/ m]	v_h^+ [kN/ m]	Δv_h^+ [%]
	0.63	0.63	0
Maximum negative horizontal displacement v_h^-	v_h^- [mm]	v_h^- [mm]	Δv_h^- [%]
	-0.11	-0.11	0
Maximum vertical displacement v_v	v_v [mm]	v_v [mm]	Δv_v [%]
	1.71	1.82	6.40

2.14 Example 12: Tank resting on *Winkler's* medium

2.14.1 Description of the problem

Numerical and analytical analysis for axi-symmetrically circular cylindrical tank resting on elastic foundation using *Winkler's* model is presented by *Vichare/ Inamdar* (2010). To verify analysis of circular cylindrical tank resting on *Winkler's* medium, the internal forces calculated numerically and analytically by *Vichare/ Inamdar* (2010) at different cases of modulus of subgrade reaction are compared with those obtained by *ELPLA*.

A circular cylindrical tank of an inner diameter of d = 13 [m] and a height of H = 3.5 [m] is considered as shown in Figure 2.45. Thickness of the tank wall is t = 0.175 [m]. The tank is filled with water. The soil under the base of the tank is represented by isolated springs of stiffness k_s, which represent modulus of subgrade reaction. The tank material, unit weight of the water and the modulus of subgrade reaction are listed in Table 2.12.

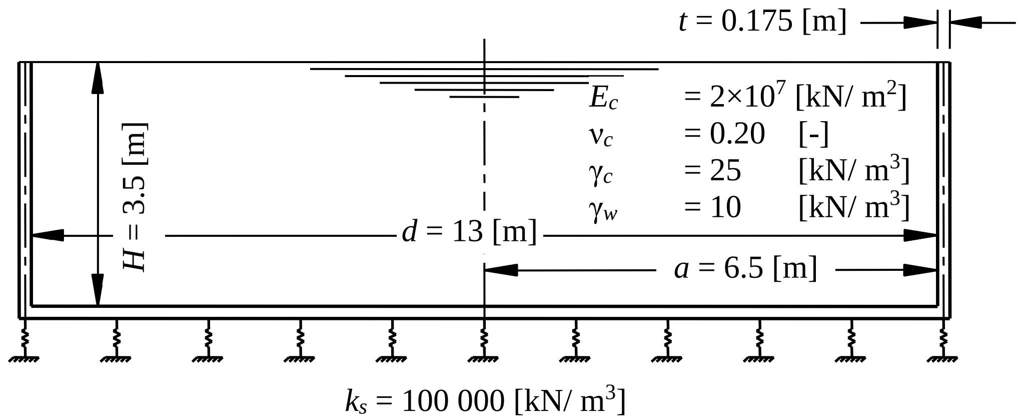

Figure 2.45 Circular cylindrical tank on isolated springs with dimensions

Table 2.12 Tank material, water unit weight and modulus of subgrade reaction

Modulus of Elasticity of the tank material	E_c	= 2×10^7	[kN/ m^2]
Poisson's ratio of the tank material	ν_c	= 0.2	[-]
Unit weight of the tank material	γ_c	= 25	[kN/ m^3]
Unit weight of the water	γ_w	= 10	[kN/ m^3]
Modulus of subgrade reaction	k_s	= 100 000	[kN/ m^3]

2.14.2 Numerical Analysis

In order to illustrate the comparison between analytical and numerical analysis of *Vichare/ Inamdar* (2010) and that of *ELPLA* 9.4, the height of the tank is divided into 35 equal elements, each of 0.10 [m], as shown in Figure 2.46. The base of the tank is divided into 50 equal elements, each of 0.13 [m].

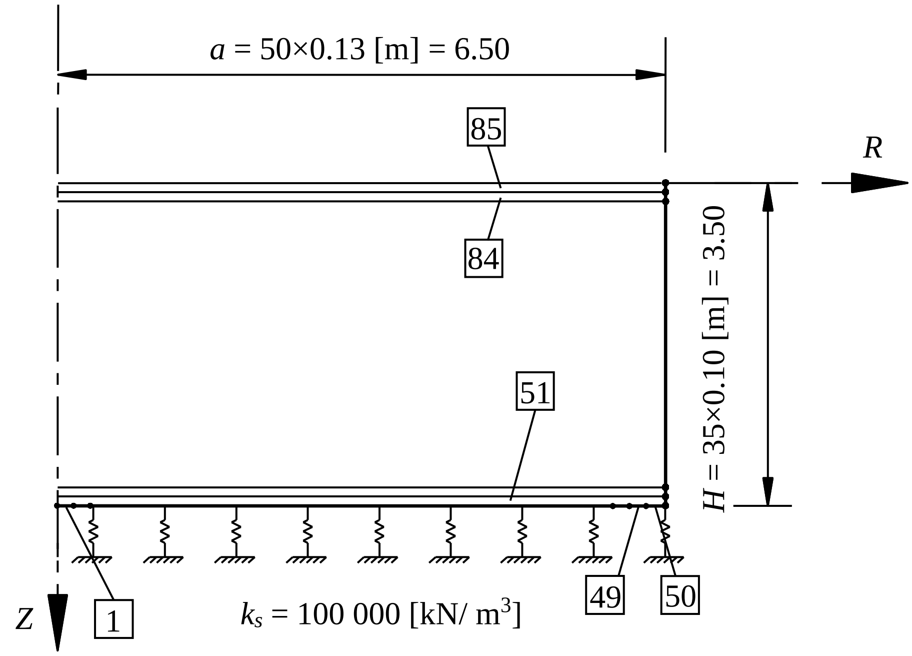

Figure 2.46 Finite element mesh of the tank

2.14.3 Results and discussions

The analysis of the considered tank is carried out numerically by *ELPLA*, where the tank wall and the base were simulated with a thin circular cylindrical shell element using finite element method. *Vichare*/ *Inamdar* (2010) analyzed the same tank first numerically by *ABAQUS* 6.8 using three-dimensional finite element model, then analytically using equations of *Timoshenko*/ *Krieger* (1959).

Figure 2.47, Figure 2.48 and Figure 2.49 show a comparison between results of the above analyses for meridional moment M_y along the wall height, radial force N_r along the wall height and the meridional moment across the base M_{base} respectively. In these analyses, the modulus of subgrade reaction is chosen to be k_s = 100 000 [kN/m^3].

Table 2.13 shows a comparison between maximum internal forces obtained from analytical solution and those obtained from *ELPLA*, while Table 2.14 shows a comparison between maximum internal forces obtained from *ABAQUS* 6.8 and those obtained from *ELPLA*. From these figures and tables, it can be concluded for the considered tank and soil that the difference in values is not more than 5 % which illustrates a good accuracy for the program used in this research.

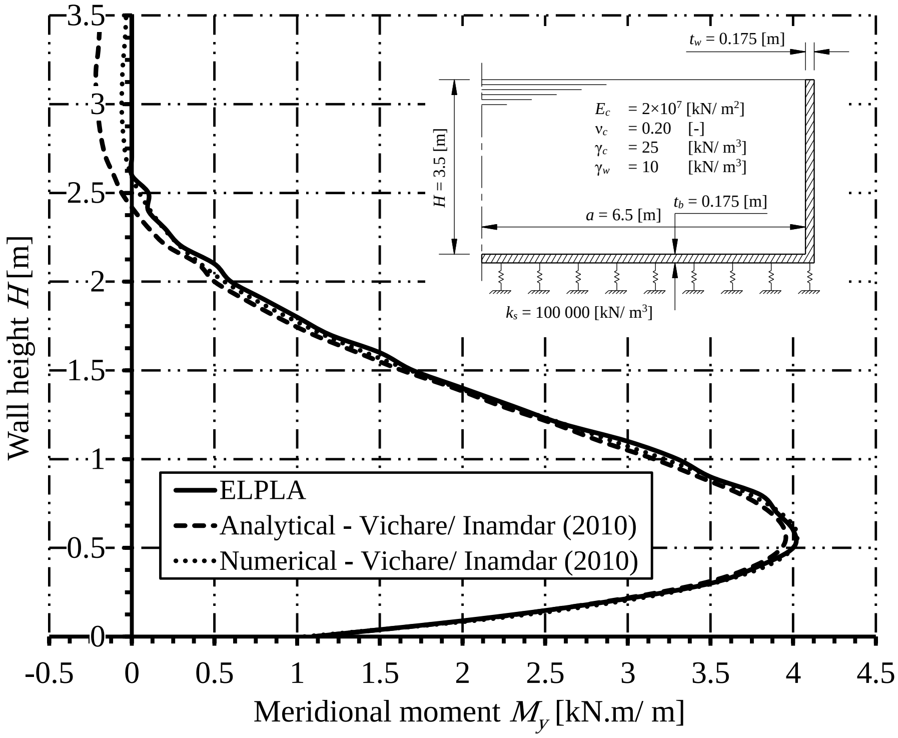

Figure 2.47 Meridional moment M_s along the wall height

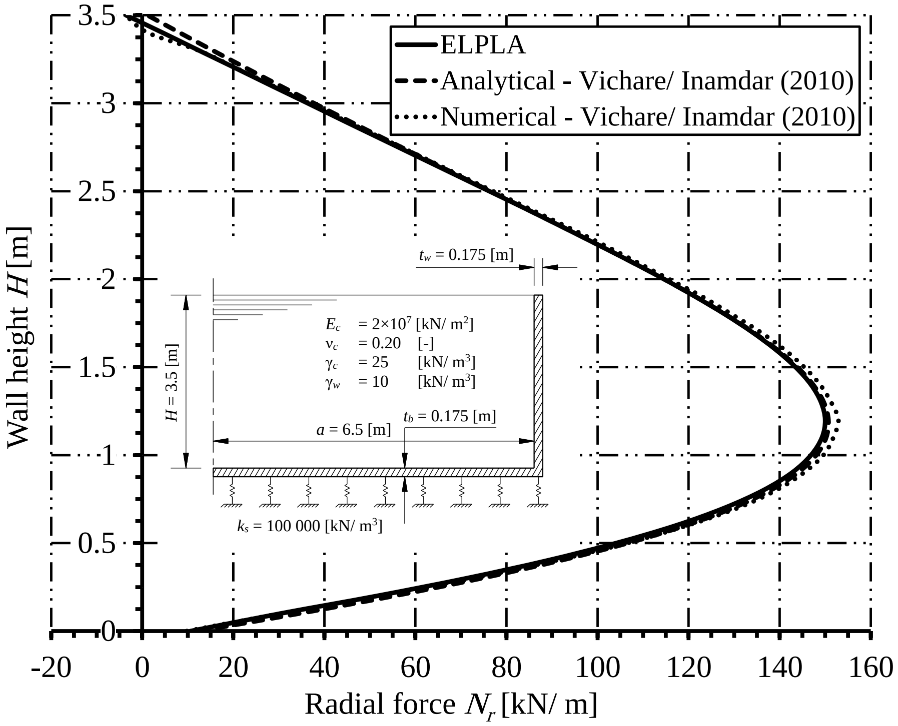

Figure 2.48 Radial force N_r along the wall height

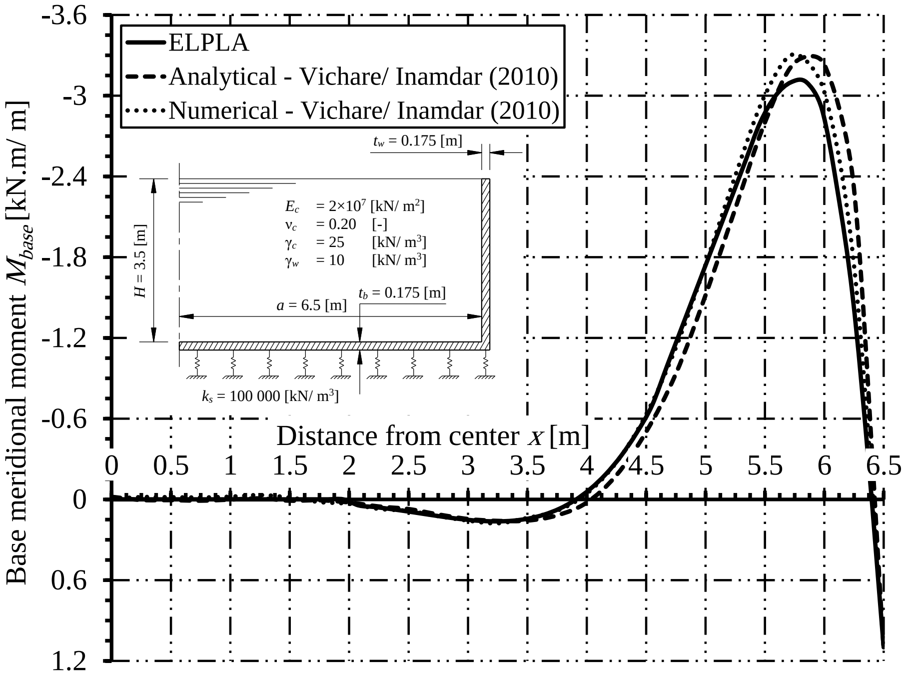

Figure 2.49 Base meridional moment across the raft M_{base}

Table 2.13 Comparison between maximum internal forces obtained from analytical solution and those obtained from *ELPLA*

Result	Type of analysis		Difference
	Analytical	*ELPLA*	
Maximum meridional moment on the wall M_y	M_y [kN.m/ m]	M_y [kN.m/ m]	ΔM_y [%]
	3.95	3.90	1.27
Maximum radial force on the wall N_r	N_r [kN/ m]	N_r [kN/ m]	ΔN_r [%]
	150.73	146.7	2.67
Maximum meridional moment on the base M_{base}	M_{base} [kN.m/ m]	M_{base} [kN.m/ m]	ΔM_{base} [%]
	-3.25	-3.1	4.62

Table 2.14 Comparison between maximum internal forces obtained from *ABAQUS* 6.8 and those obtained from *ELPLA*

Result	Type of analysis		Difference
	ABAQUS 6.8	*ELPLA*	
Maximum meridional moment on the wall M_y	M_y [kN.m/ m]	M_y [kN.m/ m]	ΔM_y [%]
	4.02	3.9	2.99
Maximum radial force on the wall N_r	N_r [kN/ m]	N_r [kN/ m]	ΔN_r [%]
	152.91	146.7	4.06
Maximum meridional moment on the base M_{base}	M_{base} [kN.m/ m]	M_{base} [kN.m/ m]	ΔM_{base} [%]
	-3.31	-3.1	0.21

2.14.4 Conversion of the solution

To show the accuracy of the results of *ELPLA* for different moduli of subgrade reactions, the considered tank is analyzed again for different values of modulus of subgrade reaction k_s ranges from 20 [MN/m^3] to 200 [MN/m^3].

For this range of k_s values, Figure 2.50 shows the maximum meridional moment M_y in the wall, Figure 2.51 shows the maximum radial force in the wall and Figure 2.52 shows the maximum meridional moment in the base.

It is observed that with increasing k_s value, the maximum meridional moment and radial force decrease. For the base, it is observed that the variation of base moment with stiffness is marginal. A little difference in base moment occurred at stiff soil.

In general, the above comparison shows that the results of analyzing circular cylindrical tank on elastic foundation using *Winkler's* model are in a good agreement with those obtained analytically or numerically using three-dimensional finite element model.

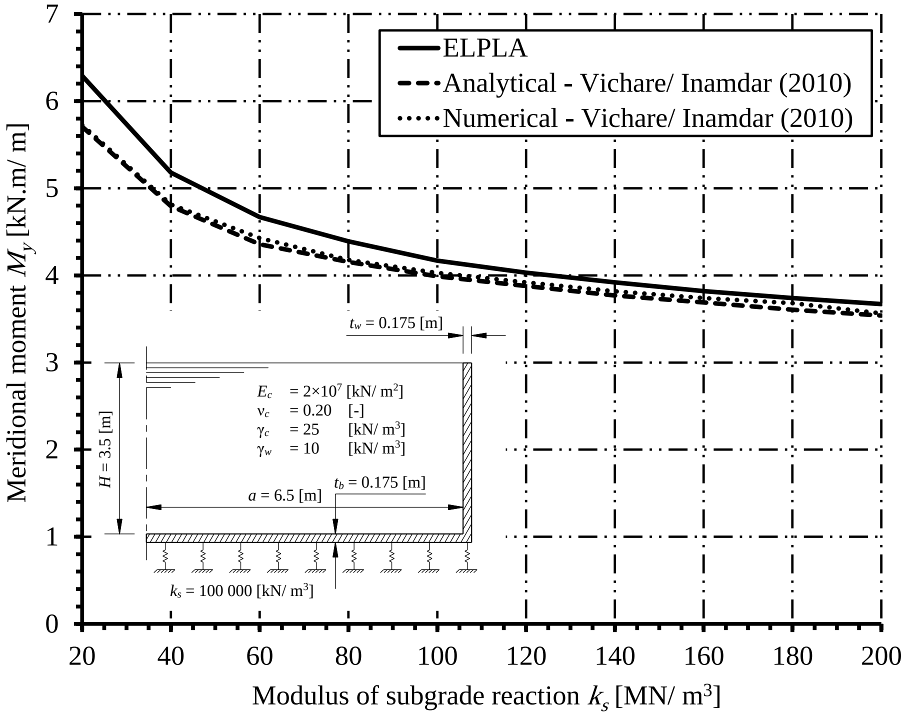

Figure 2.50 Maximum meridional moment M_y along the wall with varying k_s

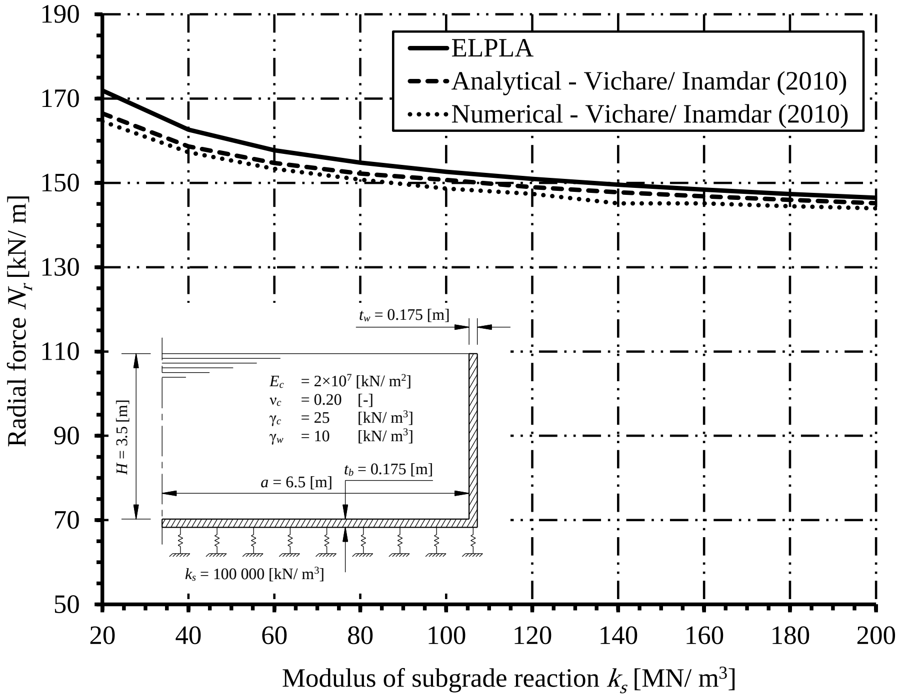

Figure 2.51 Maximum radial force N_r along the wall with varying k_s

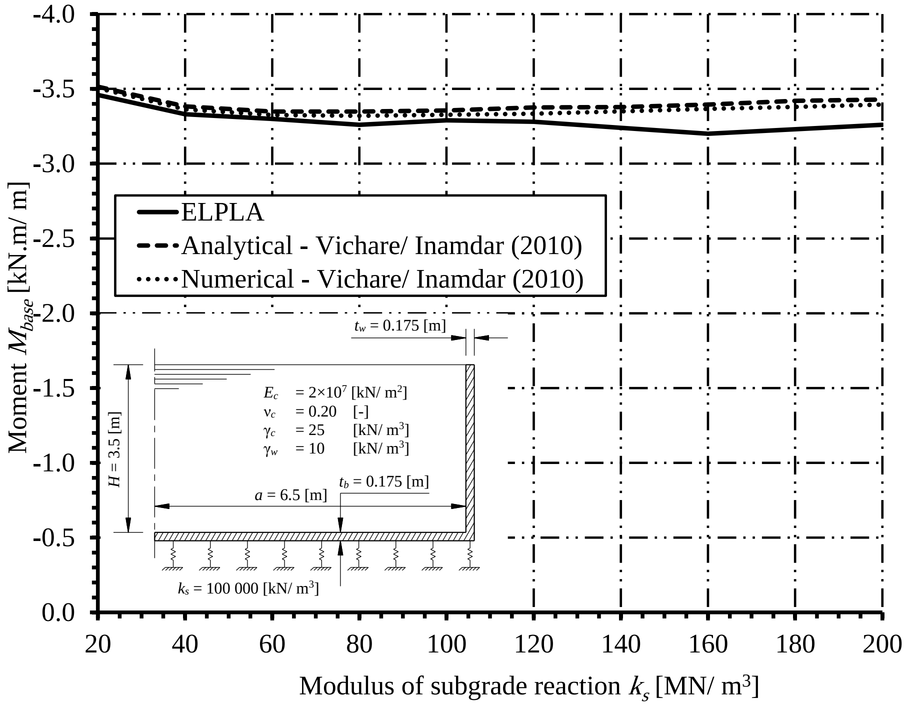

Figure 2.52 Maximum meridional moment M_{base} across the base raft with varying k_s

2.15 Example 13: Tank with conical base resting on *Winkler's* medium

2.15.1 Description of the problem

Numerical and analytical analysis for axi-symmetrically circular cylindrical tank with conical base resting on elastic foundation using *Winkler's* model is presented by *EL Mezaini* (2006). To verify analysis of circular cylindrical tank with conical base resting on *Winkler's* medium, the internal forces calculated analytically by *EL Mezaini* (2006) are compared with those obtained by *ELPLA* using circular cylindrical shell elements.

A circular cylindrical tank of an inner diameter of d = 15 [m] and a height of H = 6 [m] is considered as shown in Figure 2.53 . Thickness of the tank wall is t = 0.5 [m]. The tank is filled with water. The soil under the base of the tank is represented by isolated springs of stiffness k_s, which represent modulus of subgrade reaction. Figure 5.25 shows the tank with dimensions, while the tank material, unit weight of the water and the modulus of subgrade reaction are listed in Table 2.15.

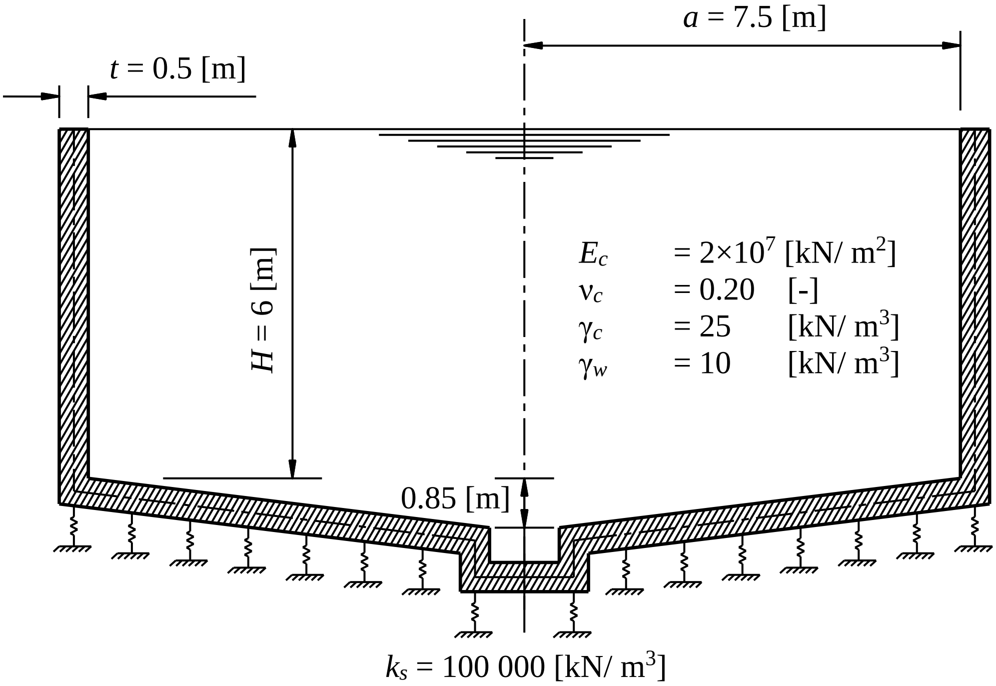

Figure 2.53 Circular cylindrical tank on isolated springs with dimensions

Table 2.15 Tank material, water unit weight and modulus of subgrade reaction

Modulus of Elasticity of the tank material	E_c	= 2×10^7	[kN/ m^2]
Poisson's ratio of the tank material	ν_c	= 0.2	[-]
Unit weight of the tank material	γ_c	= 25	[kN/ m^3]
Unit weight of the water	γ_w	= 10	[kN/ m^3]
Modulus of subgrade reaction	k_s	= 100 000	[kN/ m^3]

2.15.2 Numerical Analysis

In order to illustrate the comparison between numerical analysis of *EL Mezaini* (2006) and that of *ELPLA*, the height of the tank is divided into 20 equal elements, each of 0.30 [m], as shown in Figure 2.54 . The conical base of the tank is divided into 14 equal elements, each of 0.49 [m].

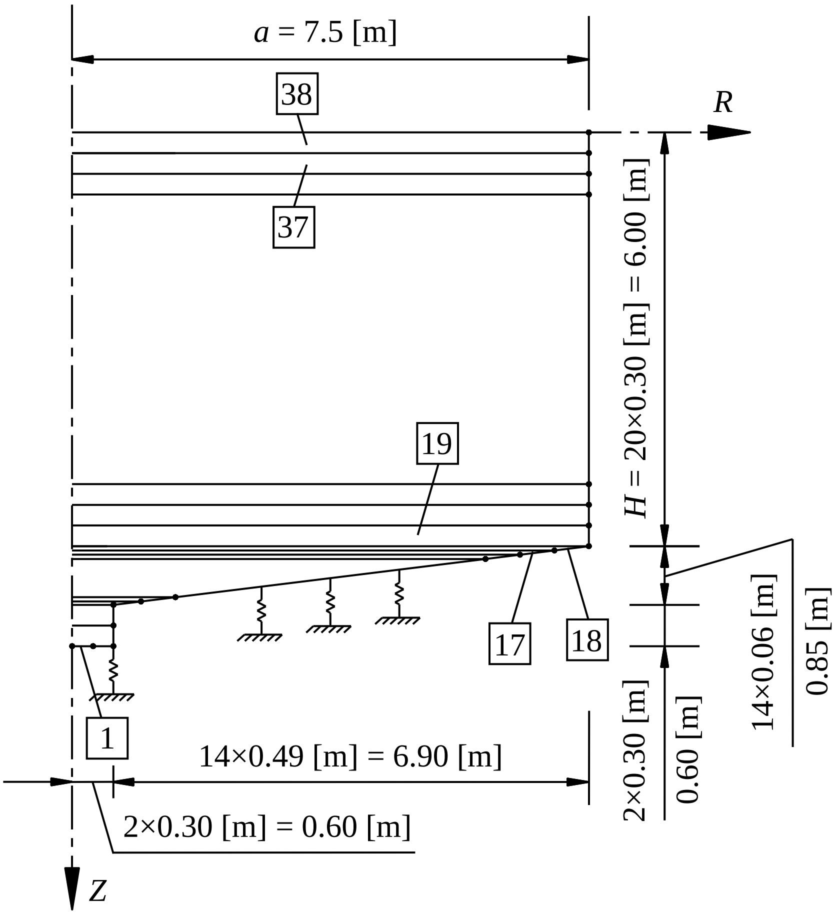

Figure 2.54 Finite element mesh of the tank

2.15.3 Results and discussions

The analysis of the considered tank is carried out numerically by *ELPLA*, where the circular cylindrical tank and the conical base were simulated with a thin circular cylindrical shell element using finite element method. *EL Mezaini* (2006) analyzed the same tank numerically by *SAP* 2000 [54] using three-dimensional finite element model.

Table 2.16 shows a comparison between maximum internal forces obtained from *SAP* 2000 and those obtained from *ELPLA*.

Figure 2.55, Figure 2.56 and Figure 2.57 show a comparison between results of the above analyses for meridional moment M_y along the wall height, radial force N_r along the wall height, the moment across the base raft M_{base} and the base settlement s_{base} respectively. In these analyses, the modulus of subgrade reaction is chosen to be k_s = 100 000 [kN/m].

From these figures and tables, it can be concluded for the considered tank and soil that the difference in values is not more than 7% and that illustrates a good accuracy for the program used in this research.

Table 2.16 Comparison between maximum internal forces obtained from *SAP* 2000 and those obtained from *ELPLA*

Result	Type of analysis		Difference
	SAP 2000	*ELPLA*	
Maximum meridional moment on the wall M_y	M_y [kN.m/ m]	M_y [kN.m/ m]	ΔM_y [%]
	24.30	23.80	2.06
Maximum radial force on the wall N_r	N_r [kN/ m]	N_r [kN/ m]	ΔN_r [%]
	308.05	308.40	0.11
Maximum meridional moment on the base M_{base}	M_{base} [kN.m/ m]	M_{base} [kN.m/ m]	ΔM_{base} [%]
	-15.40	-14.90	3.25
Meridional moment at the edge of the base M_{base}	M_{base} [kN.m/ m]	M_{base} [kN.m/ m]	ΔM_{base} [%]
	15.70	15.80	0.64
Settlement at the center s_{center}	s_{center} [mm]	s_{center} [mm]	Δs_{center} [%]
	0.682	0.730	7.04
Settlement at the edge s_{edge}	s_{edge} [mm]	s_{edge} [mm]	Δs_{edge} [%]
	1.148	1.196	4.18

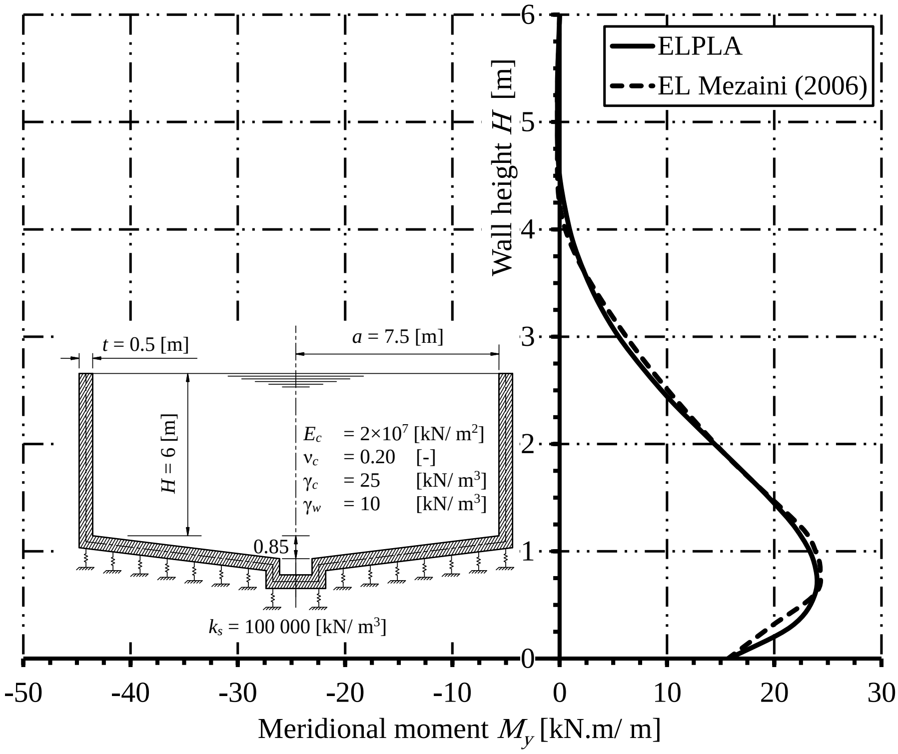

Figure 2.55 Meridional moment M_y along the wall height

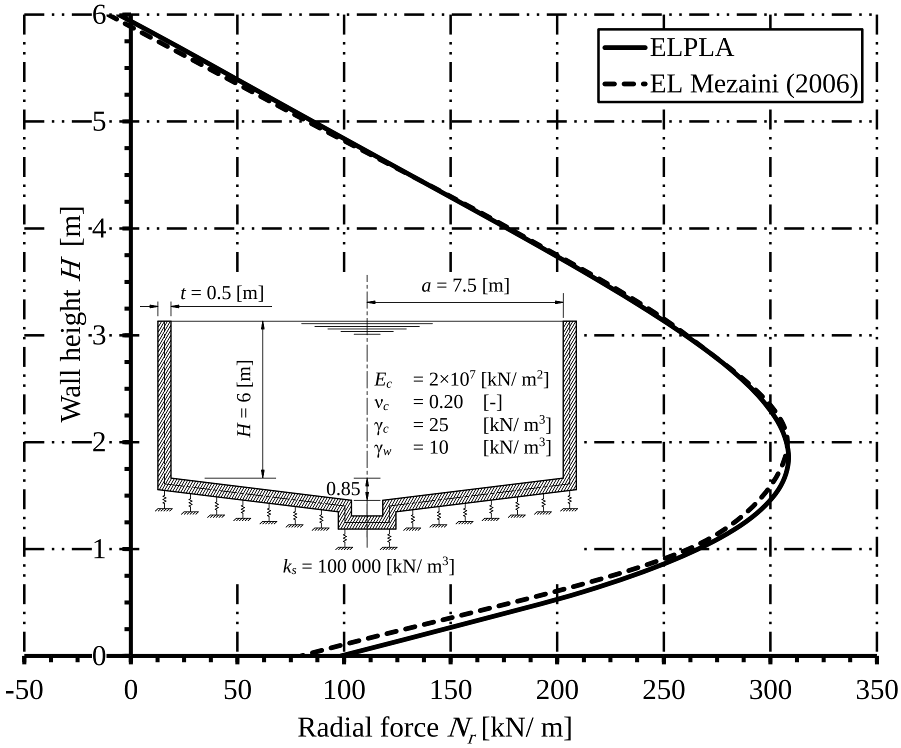

Figure 2.56 Radial force N_r along the wall height

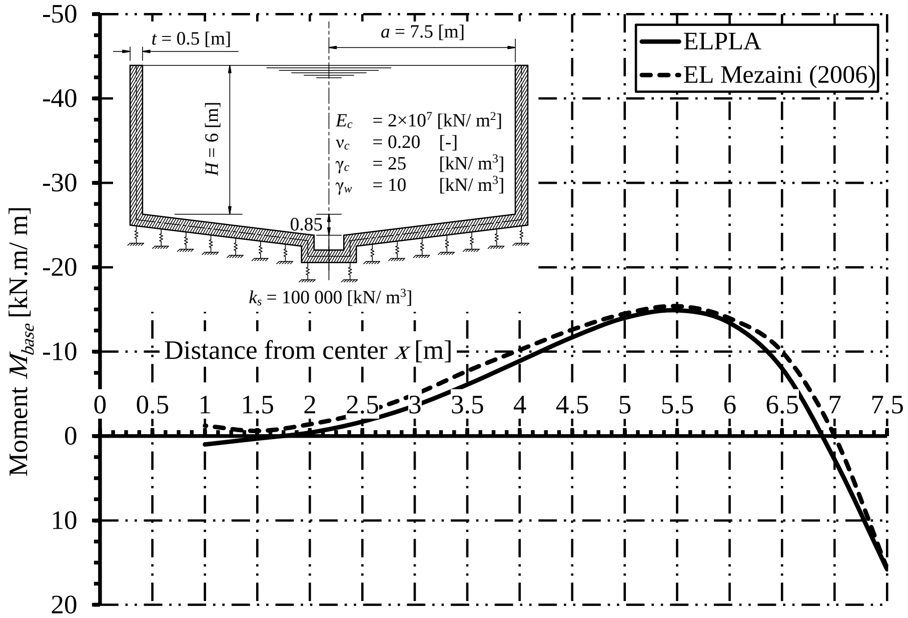

Figure 2.57 Meridional moment across the conical base M_{base}

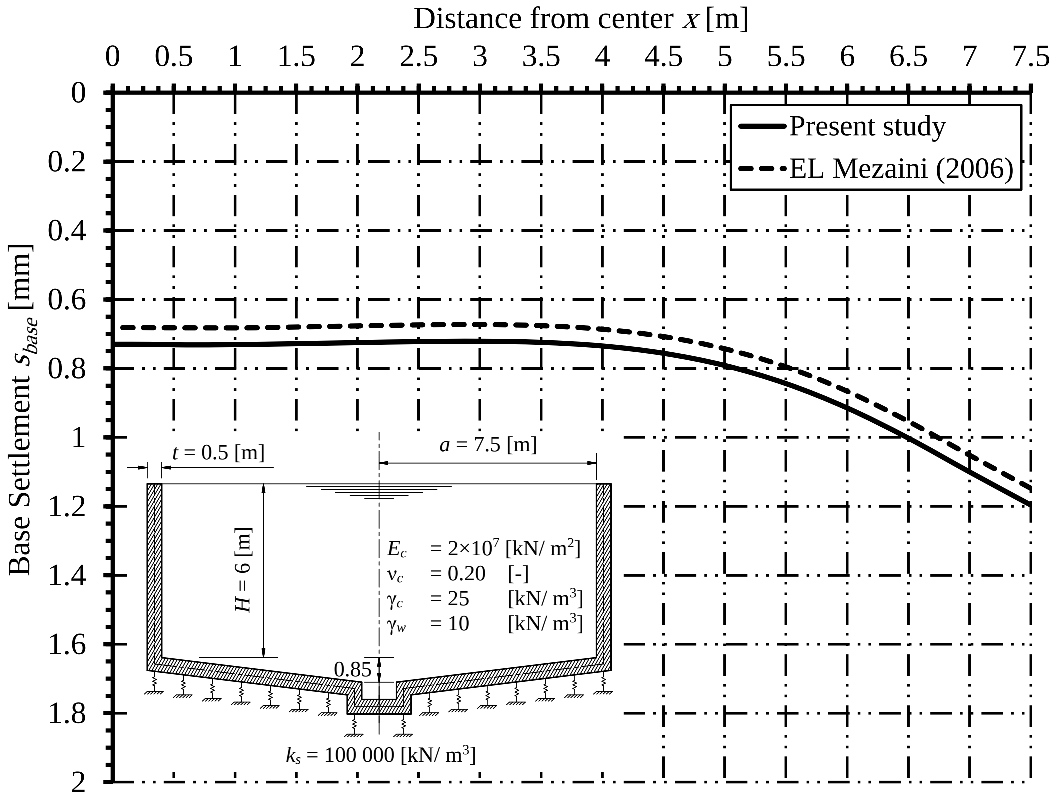

Figure 2.58 Conical base settlement s_{base}

2.16 Example 14: Tank resting on half space soil medium

2.16.1 Description of the problem

A differential quadrature solution for the flexure behavior of a circular cylindrical storage tank resting on an isotropic elastic half space soil medium is presented by *Kukreti/ Siddiqi* (1997). The interface between the base and the soil half space is considered to be perfectly smooth and continuous. The differential quadrature solution takes into account the interaction between the tank wall and the base using slope and moment compatibility. It also takes into account the interaction between the base and the soil medium using the contact pressure equation for the elastic half space. *Kukreti/ Siddiqi* (1997) verified their results with those of energy solution of the base by *Kukreti* (1992) and finite element model of *Booker/ Small* (1983).

To verify analysis of cylindrical storage tank resting on half space soil medium, results of the analysis using differential quadrature solution by *Kukreti/ Siddiqi* (1997), energy solution of the base plate by *Kukreti* (1992) and finite element model of *Booker/ Small* (1983) are compared with those obtained by the finite element analysis of *ELPLA* using circular cylindrical shell elements.

A circular cylindrical tank of an inner diameter of d = 18 [m] and a height of H = 7.5 [m] is considered as shown in Figure 2.59. The thickness of the tank wall and base is t = 0.36 [m]. The tank is filled with water. Figure 2.45 shows the storage tank with dimensions, while the tank material and unit weight of the water are listed in Table 2.17. The data of soil medium under the base of the tank are shown in Table 2.18.

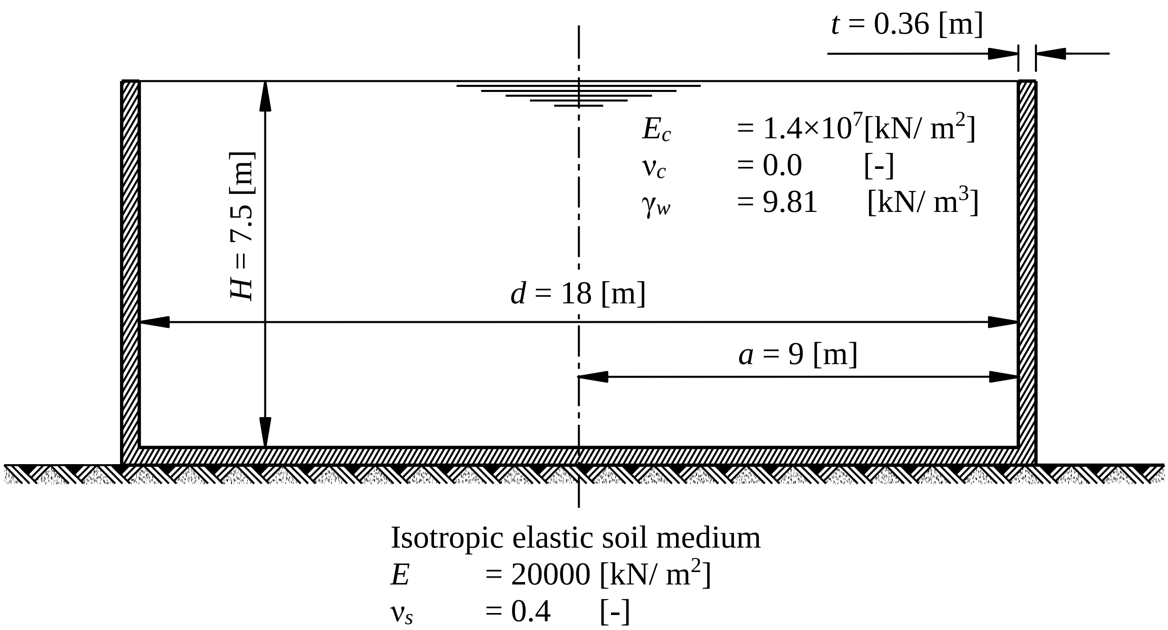

Figure 2.59 Circular cylindrical tank resting on an isotropic elastic soil medium

Table 2.17 Tank material and water unit weight

Modulus of Elasticity of the tank material	E_c	$= 1.4\times10^7$	[kN/ m^2]
Poisson's ratio of the tank material	ν_c	= 0.0	[-]
Unit weight of the water	γ_w	= 9.81	[kN/ m^3]

Table 2.18 Soil data

Modulus of Elasticity of the soil medium	E	= 20000	[kN/m^2]
Poisson's ratio of the soil medium	ν_s	= 0.4	[-]

The unrealistic value $\nu_c = 0.0$ was selected because this parameter has a little effect on the results obtained and because comparison was possible with the results of the differential quadrature solution of *Kukreti/ Siddiqi* (1997) and also with the results of the finite element model of *Booker*/ *Small* (1983).

2.16.2 Numerical Analysis

In order to illustrate the comparison between different methods for analyzing water storage tanks resting on an isotropic elastic half space soil medium and that of *ELPLA*, this numerical example is analyzed. Internal forces and base settlement calculated by *ELPLA* were compared with those of *Kukreti/ Siddiqi* (1997), *Kukreti* (1992) and *Booker*/ *Small* (1983). The height of the tank is divided into 30 equal elements, each of 0.25 [m], as shown in Figure 2.60. The base of the tank is divided into 45 equal elements, each of 0.2 [m].

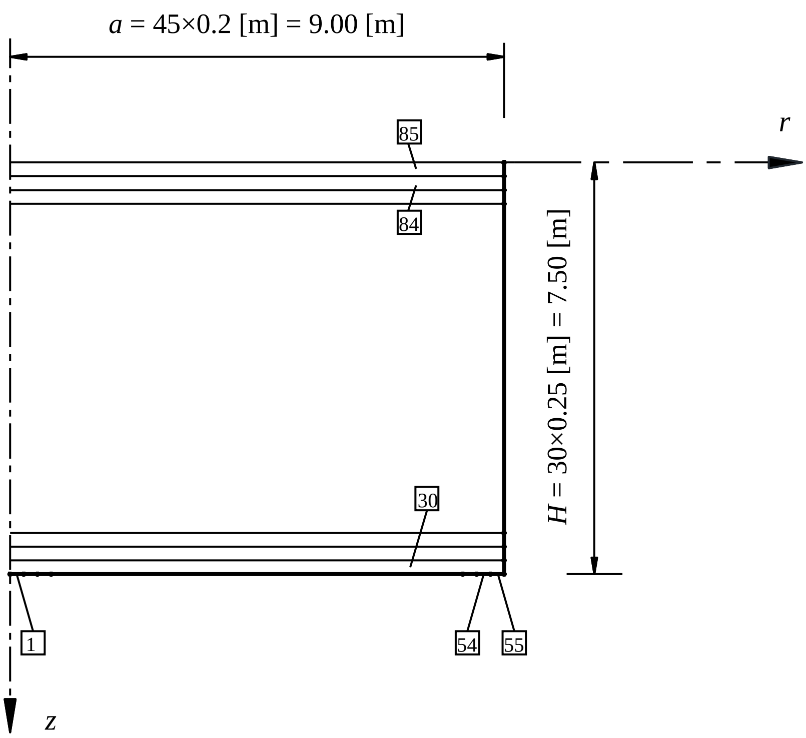

Figure 2.60 Finite element mesh of the tank

2.16.3 Results and discussions

The analysis of the considered tank was carried out by *ELPLA*, where the circular cylindrical tank and the base were simulated with a thin circular cylindrical shell element using finite element method. *Kukreti/ Siddiqi* (1997) analyzed the same tank using the differential quadrature method, while *Booker*/ *Small* (1983) used a finite element model to simulate the same tank. *Kukreti* (1992) solved the same tank with the energy method.

Figure 2.61 shows that the contact pressure within about 67 % of radius of the base is accurately predicted by the present analysis, with a maximum difference of less than 7 % from the other methods in the comparison. The results obtained by the differential quadrature method are the nearest to results obtained by the analysis of this study. In addition, the general shape of the distribution in the remaining part of the base is similar. The numerical difference continues to increase toward the base edge, due the fact that half space soil medium predicts infinity pressure at the edge.

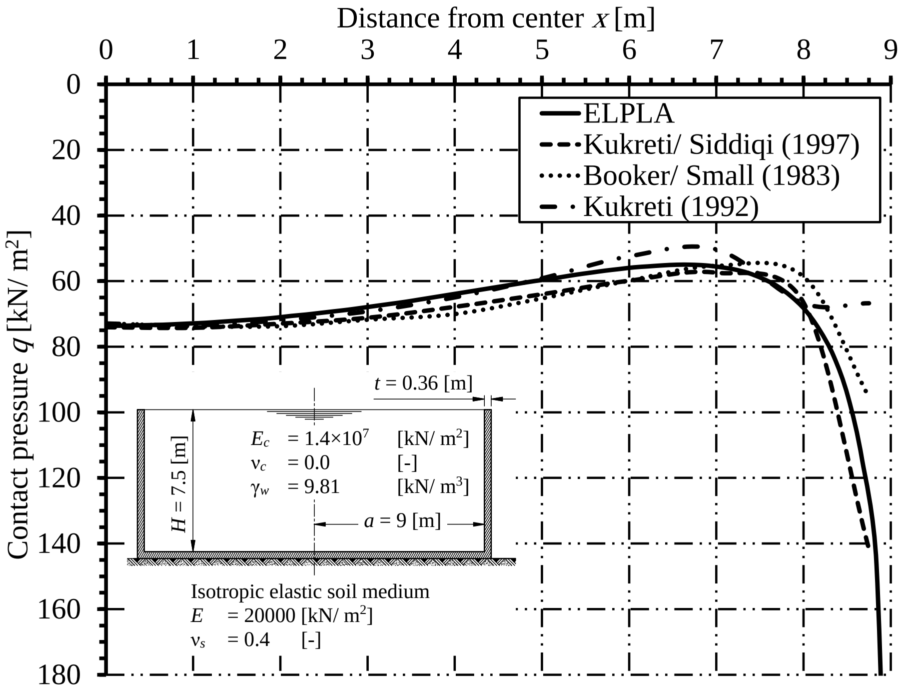

Figure 2.61 Variation of the contact pressure along the base

Differential deflection of the base with respect to the base -edge is shown in Figure 2.62. The maximum difference with the energy method of *Kukreti* (1992) is nearly 50 %, with finite element solution of *Booker*/ *Small* (1983) is approximately 39 % and with the differential quadrature method of *Kukreti/ Siddiqi* (1997) is less than 7 %. However, the overall deflected shape of the plate remains the same and the difference in central differential deflection is nearly 6 %.

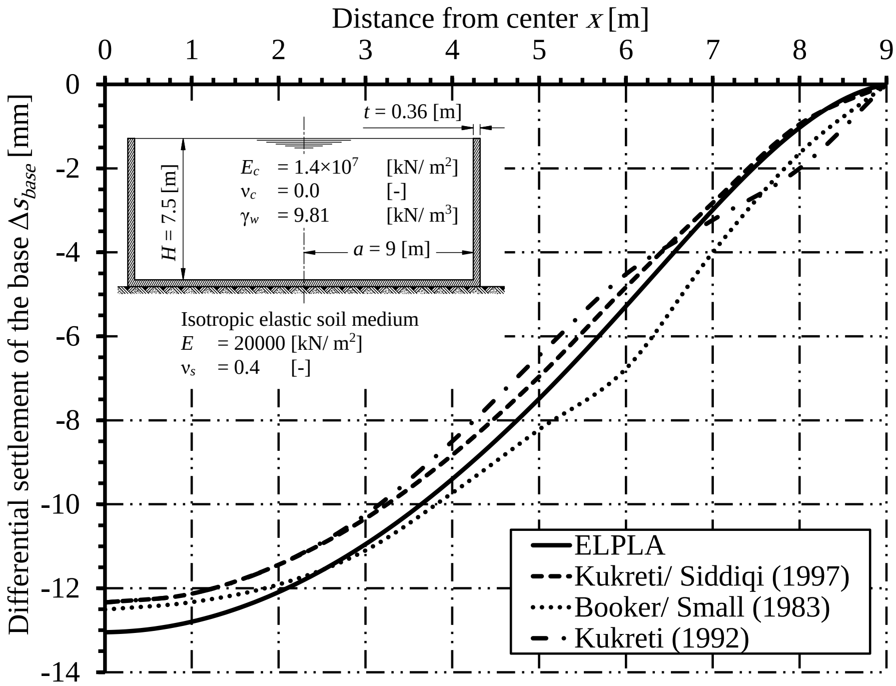

Figure 2.62 Differential deflection of the base

The base moment and the tank wall meridional moment are shown in Figure 2.63 and Figure 2.64, respectively. They are in close agreement with the finite element solution of *Booker/ Small* (1983). It is important to note that the differential quadrature method did not give any instability of solution in the outer quarter domain of the base, as it was experienced by the energy method reported by *Kukreti* (1992). Because high concentrations of moment often occur at the base center at the junction of the tank wall with the base the prediction of the central moment and the edge moment are of particular interest in structural analysis and design. The edge moment obtained from the present analysis is about 34.5 % more than the value predicted if the tank wall were assumed to be fixed at the bottom. Thus, any analysis based on the assumption that the tank wall is fixed at the base will give unconservative results. This justifies the necessity of including the interaction between the base, the soil medium, and the tank wall in the analysis.

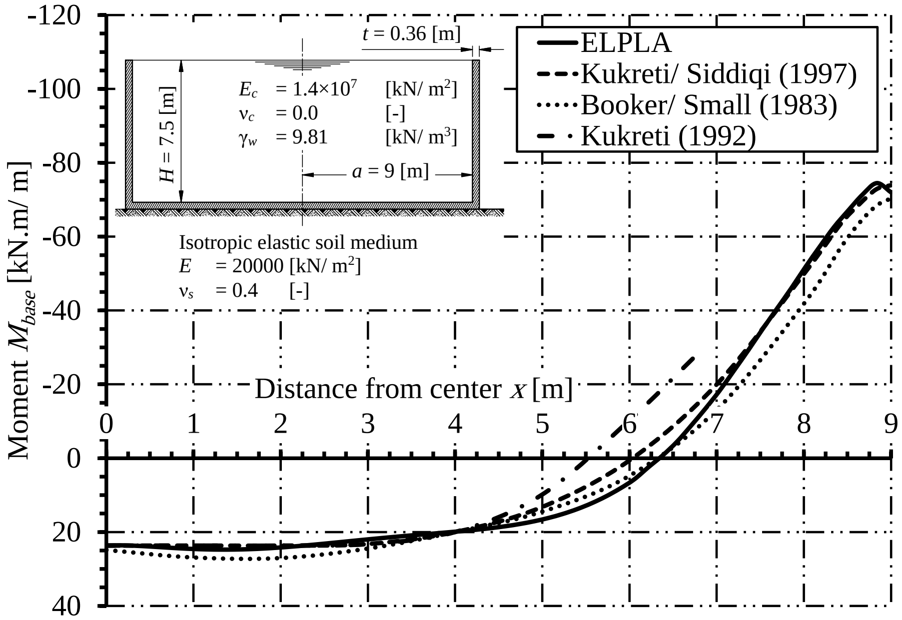

Figure 2.63 Meridional moment across the base raft M_{base}

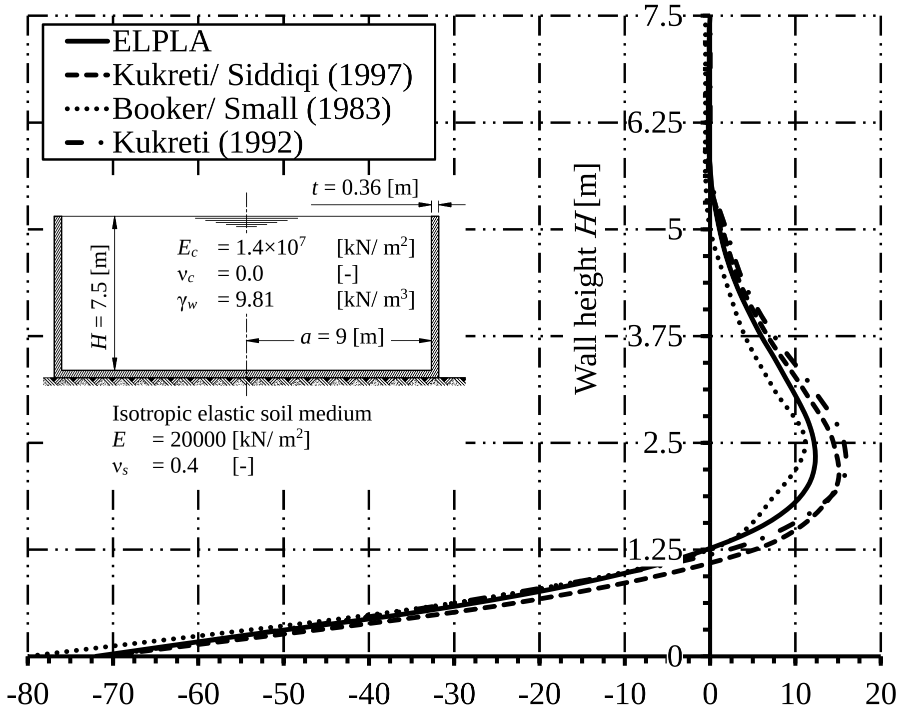

Figure 2.64 Meridional moment M_y along the wall height

The tank wall radial force variations along the height of the tank are shown in Figure 2.65. The results are in close agreement for the upper three quarters of the tank height (the maximum difference is 3.16 % with respect to the maximum magnitude of the force). In the differential quadrature method of *Kukreti/ Siddiqi* (1997) and the energy method of *Kukreti* (1992), the discrepancy in the value of the hoop tension near the base is due to the simplifying assumption made in this analysis that the base is infinitely stiff in the axial direction. The base, because of its assumed rigidity, does not allow the tank wall to displace radially at the base, making the value of the hoop force in the tank wall zero at this level. On the other hand; the finite element model of *Booker*/ *Small* (1983) and the analysis of this study give values of radial force and horizontal displacement at the base, because of taking in consideration the interaction between the wall and the base, and the interaction between the base and the soil.

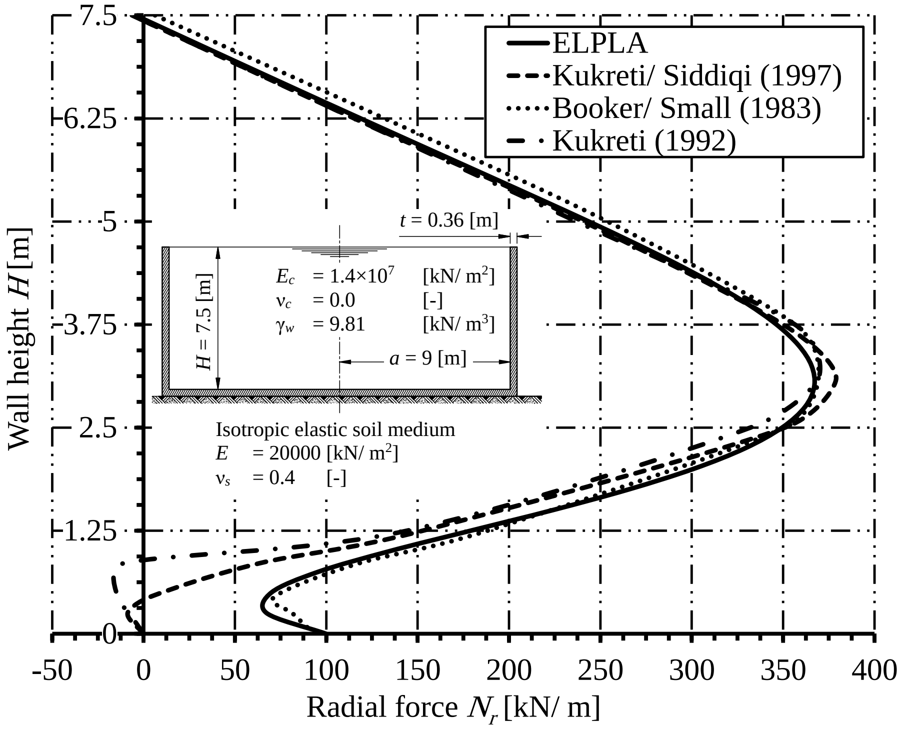

Figure 2.65 Radial force N_r along the wall height

Table 2.19, Table 2.20 and Table 2.21 show a comparison between results obtained from *ELPLA* and those obtained from *Kukreti/ Siddiqi* (1997) solution, *Booker*/ *Small* (1983) solution and *Kukreti* (1992) solution, respectively.

From these figures and tables, it can be concluded for the considered tank and soil that the difference in values is not more than 10 % and that illustrates a good accuracy for the program used in this research.

Table 2.19 Comparison between results obtained from differential quadrature solution of *Kukreti/ Siddiqi* (1997) and those obtained from *ELPLA* using circular cylindrical shell elements

Result	Type of analysis		Difference
	Differential quadrature method of *Kukreti/ Siddiqi* (1997)	*ELPLA*	
Contact pressure at the base center q	q [kN/ m^2]	q [kN/ m^2]	Δq [%]
	74.05	73.60	0.61
Maximum meridional moment on the wall M_y	M_y [kN.m/ m]	M_y [kN.m/ m]	ΔM_y [%]
	-71.16	-72.00	1.18
Maximum radial force on the wall N_r	N_r [kN/ m]	N_r [kN/ m]	ΔN_r [%]
	379.08	367.10	3.16
Maximum moment on the base M_{base}	M_{base} [kN.m/ m]	M_{base} [kN.m/ m]	ΔM_{base} [%]
	-73.94	-72.00	2.62
Differential deflection at the base center Δs_{base}	Δs_{base} [mm]	Δs_{base} [mm]	Δ (Δs_{base}) [%]
	-12.34	-13.05	5.75

Table 2.20 Comparison between results obtained from finite element solution of *Booker/ Small* (1983) and those obtained from *ELPLA* using circular cylindrical shell elements

Result	Type of analysis		Difference
	FEM of *Booker/ Small* (1983)	*ELPLA*	
Contact pressure at the base center q	q [kN/ m^2]	q [kN/ m^2]	Δq [%]
	72.91	73.60	0.95
Maximum meridional moment on the wall M_y	M_y [kN.m/ m]	M_y [kN.m/ m]	ΔM_y [%]
	-80.00	-72.00	10.00
Maximum radial force on the wall N_r	N_r [kN/ m]	N_r [kN/ m]	ΔN_r [%]
	369.38	367.10	0.62
Maximum moment on the base M_{base}	M_{base} [kN.m/ m]	M_{base} [kN.m/ m]	ΔM_{base} [%]
	-70.35	-72.00	2.35
Differential deflection at the base center Δs_{base}	Δs_{base} [mm]	Δs_{base} [mm]	Δ (Δs_{base}) [%]
	-12.51	-13.05	4.32

Table 2.21 Comparison between results obtained from energy method of *Kukreti* (1992) and those obtained from *ELPLA* using circular cylindrical shell elements

Result	Type of analysis		Difference
	Energy method of *Kukreti* (1992)	*ELPLA*	
Contact pressure at the base center q	q [kN/ m^2]	q [kN/ m^2]	Δq [%]
	72.91	73.60	0.95
Maximum meridional moment on the wall M_y	M_y [kN.m/ m]	M_y [kN.m/ m]	ΔM_y [%]
	-71.16	-72.00	1.18
Maximum radial force on the wall N_r	N_r [kN/ m]	N_r [kN/ m]	ΔN_r [%]
	369.38	367.10	0.62
Maximum moment on the base M_{base}	M_{base} [kN.m/ m]	M_{base} [kN.m/ m]	ΔM_{base} [%]
	-	-72.00	-
Differential deflection at the base center Δs_{base}	Δs_{base} [mm]	Δs_{base} [mm]	Δ (Δs_{base}) [%]
	-12.34	-13.05	5.75

2.17 Example 15: Tank with different base thickness on half space soil medium

2.17.1 Description of the problem

A finite element analysis for the flexure behavior of a circular cylindrical storage tank resting on an isotropic elastic half space soil medium is presented by *Melerski* (2006). The solution takes into account the interaction between the tank wall and the base using slope and moment compatibility. It also takes into account the interaction between the base and the soil medium.

To verify analysis of circular cylindrical storage tank resting on half space soil medium, results of the analysis using finite element analysis of *Melerski* (2006) were compared with those obtained by the finite element analysis of *ELPLA* using circular cylindrical shell elements.

A circular cylindrical tank of an inner diameter of d = 20 [m] and a height of H = 10 [m] is considered as shown in Figure 2.66. Thicknesses of the wall and the base are different. The thickness of the tank wall t_w = 0.2 [m] and that of the base is t_b = 0.5 [m]. The tank is filled with water. Figure 2.66 shows the storage tank, while the tank material and unit weight of the water are listed in 0. The data of soil medium under the base of the tank are shown in Table 2.23.

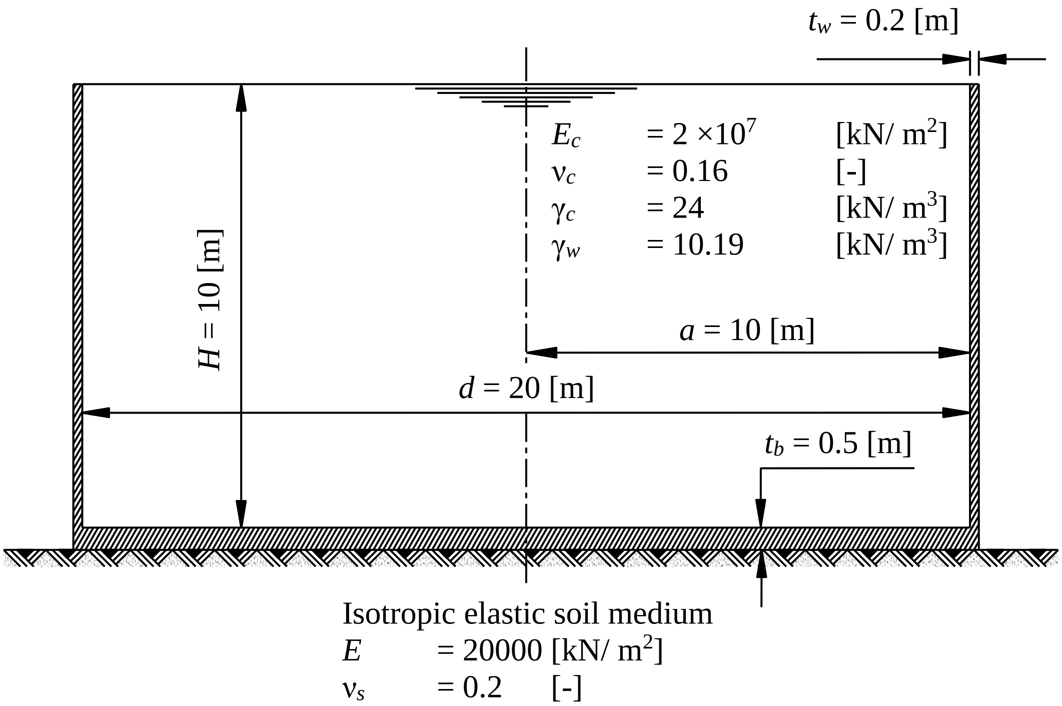

Figure 2.66 Circular cylindrical tank resting on an isotropic elastic soil medium

Table 2.22 Tank material and water unit weight

Modulus of Elasticity of the tank material	E_c	$= 2\times10^7$	[kN/ m^2]
Poisson's ratio of the tank material	ν_c	= 0.16	[-]
Unit weight of the tank material	γ_c	= 24	[kN/ m^3]
Unit weight of the water	γ_w	= 10.19	[kN/ m^3]

Table 2.23 Soil data

Modulus of Elasticity of the soil medium	E	= 20000	[kN/m^2]
Poisson's ratio of the soil medium	ν_s	= 0.2	[-]

2.17.2 Numerical Analysis

In order to illustrate the comparison between analyzing water storage tanks resting on an isotropic elastic half space soil medium and that of *ELPLA*, this example shown in Figure 2.66 is analyzed. Internal forces and displacements calculated by *ELPLA* were compared with those of *Melerski* (2006). The height of the tank is divided into 50 equal elements, each of 0.20 [m], as shown in Figure 2.67. The half base of the tank is divided into 50 equal elements, each of 0.20 [m].

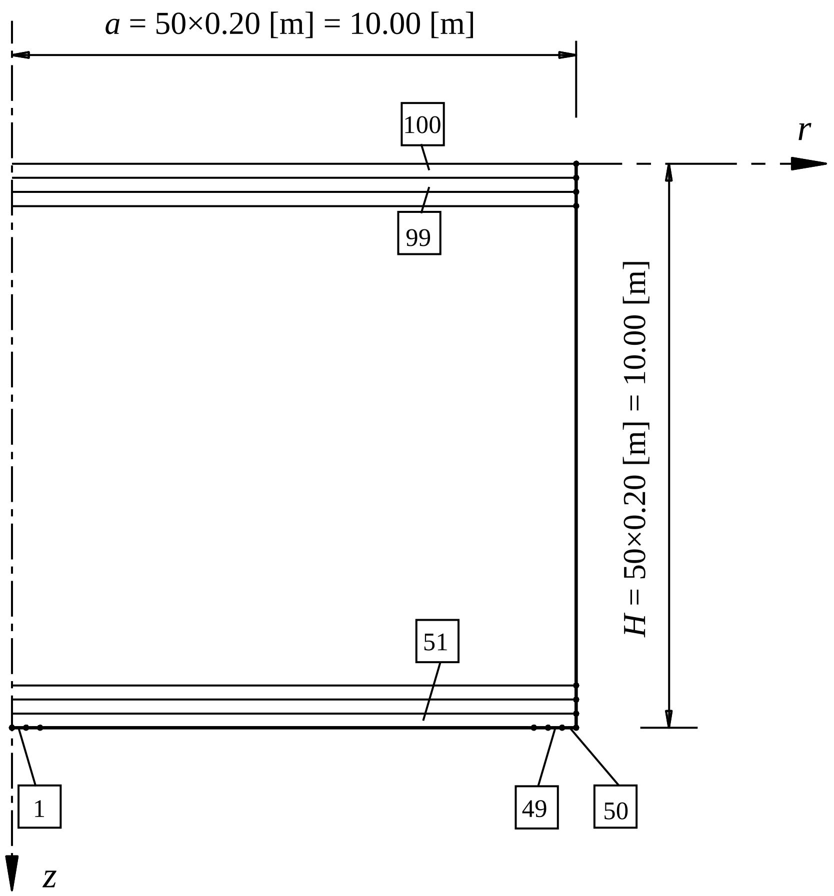

Figure 2.67 Finite element mesh of the tank

2.17.3 Results and discussions

The analysis of the considered tank is carried out by *ELPLA*, where the circular cylindrical tank and the base were simulated with a thin circular cylindrical shell element using finite element method. *Melerski* (2006) analyzed the same tank by a finite element method.

The tank is analyzed under the following two load cases:

(a) Empty tank (self-weight only).
(b) Full tank (self-weight and liquid pressure).

The base settlement in the two cases of loading are shown in Figure 2.68. They are in close agreement with the finite element solution of *Melerski* (2006). For case (a), the difference at the center is about 13%, while at the edge the value is fewer than *Melerski's* result with nearly 10% difference. For case (b), the values are more compatible, where the value of settlement at the center is greater with approximately 2%, while at the edge the difference becomes 6%.

The base moment is shown in Figure 2.69. Because high concentrations of moment often occur at the base center and at the junction of the tank wall with the base, the prediction of the central moment and the edge moment are of particular interest in structural analysis and design. For case (a), the edge moment obtained from the present analysis is about 7% less than the value of *Melerski* (2006), while the value of the moment at the center equals zero. For case (b), the edge moment is fewer than the value of *Melerski* (2006) with about 6%, while the moment at the center is bigger with about 1.8 %.

The wall meridional moment along the height of the tank is shown in Figure 2.70. For case (a), the moment at the wall-base junction is fewer than the value of *Melerski* (2006) with 1%. For case (b), the moment at the wall-base junction is bigger than the value of *Melerski* (2006), where the moment at the wall-base junction is not equal to the edge moment at the base for *Melerski* (2006) solution.

The tank wall radial force variations along the height of the tank is shown in Figure 2.71. The results are in close agreement with the finite element solution of *Melerski* (2006).

Figure 2.72 shows the horizontal displacement. It has the same diagrams as the radial force diagrams in the two cases of the analysis, where the horizontal displacement equal $v_h = N_\theta \, . \, a/ E \, t_w$.

where:

v_h	Horizontal displacement, [m].
N_r	Radial normal force in the wall, [kN/ m].
a	Tank radius, [m].
E	*Young's* modulus of elasticity, [kN/m^2].
t_w	Wall thickness, [m].

From these figures, it can be concluded for the considered tank and soil that the model used in the analysis illustrates a good accuracy for the program used in this research.

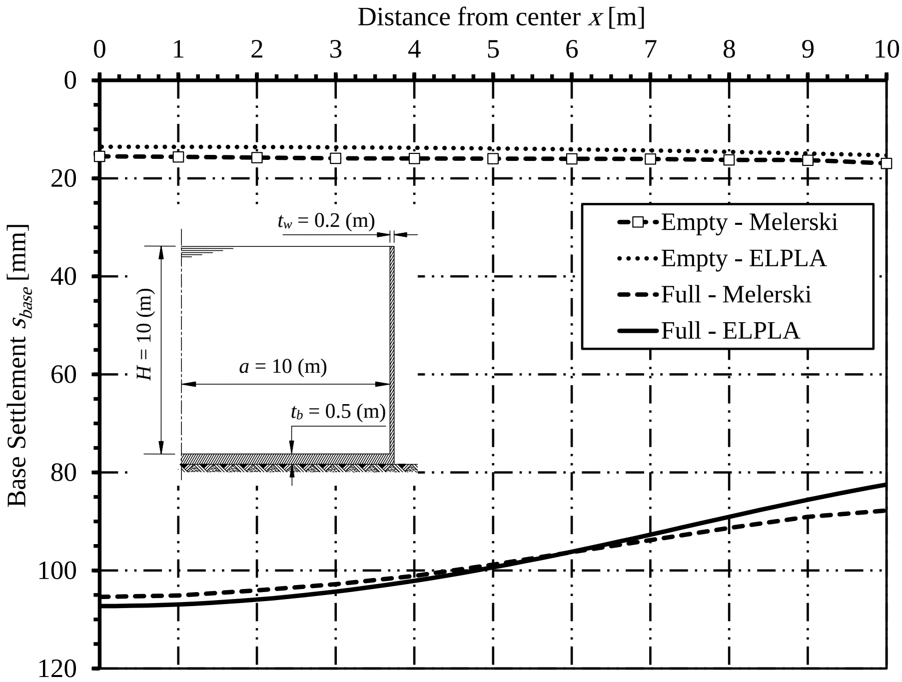

Figure 2.68 Variation of settlement s_{base} in the base plate

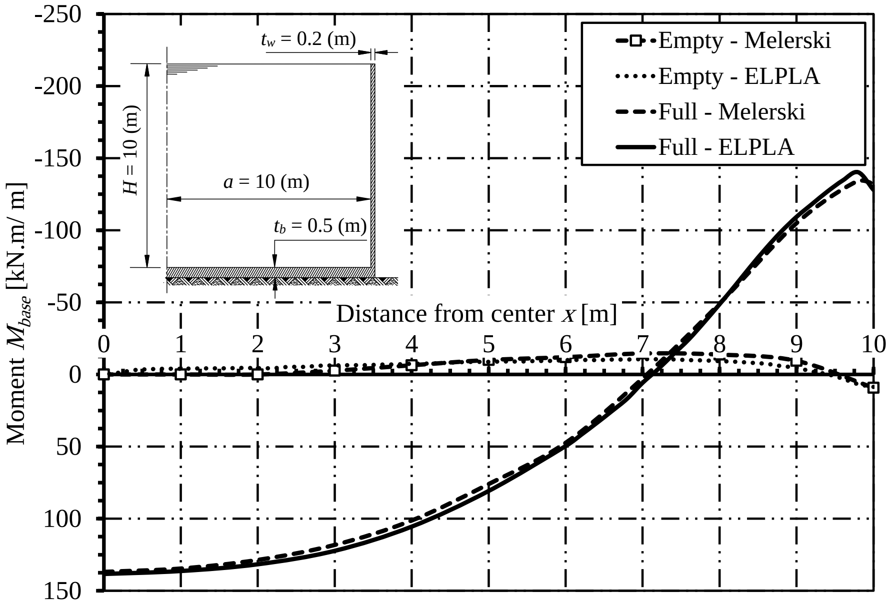

Figure 2.69 Variation of meridional moment M_{base} in the base plate

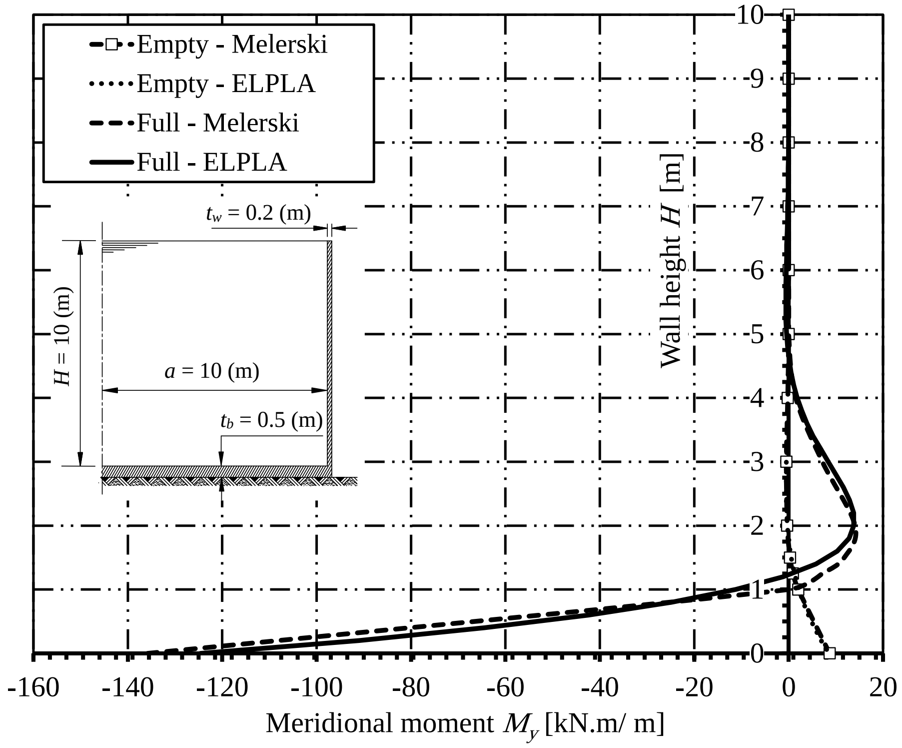

Figure 2.70 Meridional moment M_y along the wall height

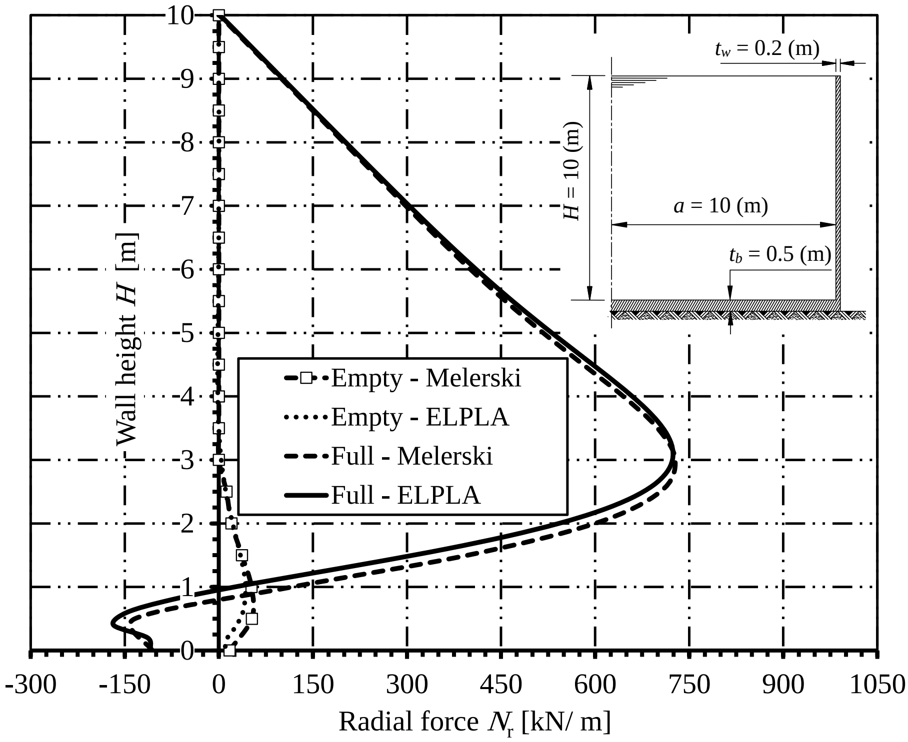

Figure 2.71 Radial force N_r along the wall height

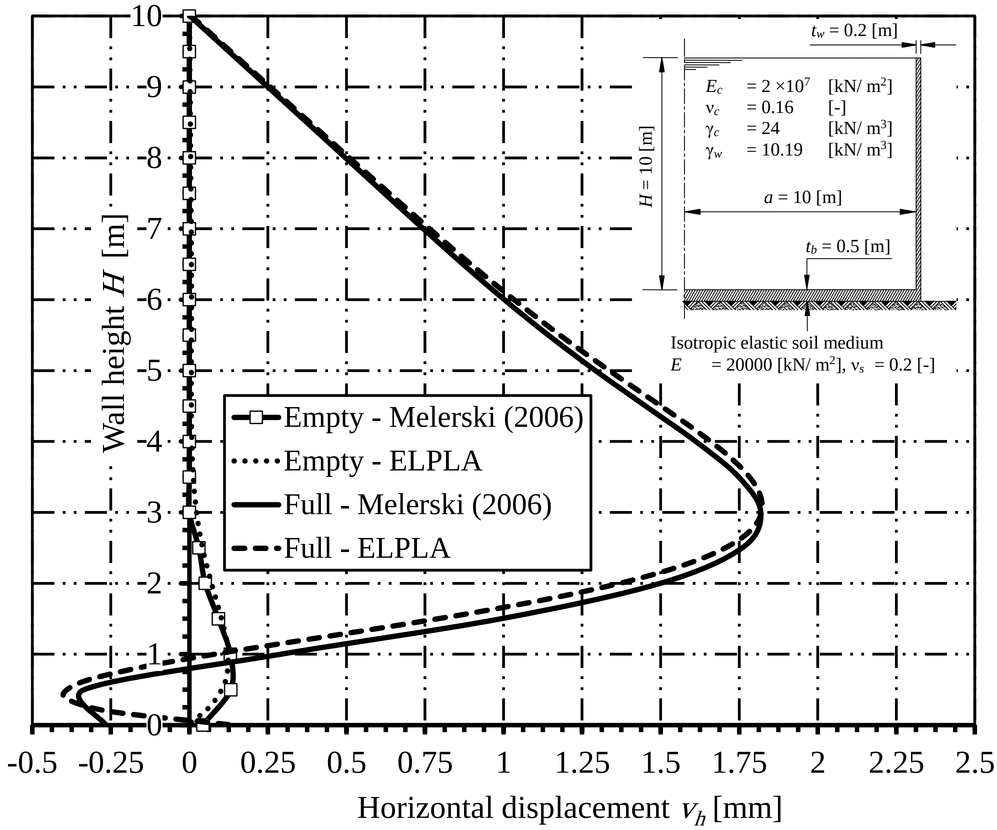

Figure 2.72 Horizontal displacement v_h along the wall height

2.18 Example 16: Water container with a conical base

2.18.1 Description of the problem

A finite element method for analyzing rational shells is available in the reference *Szilard et al.* (1986). To verify *ELPLA* for analyzing shell structures, the internal forces obtained by *Szilard et al.* (1986) for analyzing cylindrical water container with a conical base are compared with those obtained by *ELPLA*.

A cylindrical water container with a conical base of a radius of a = 3.0 [m] and a height of H = 12.0 [m] is considered as shown in Figure 2.73. Thickness of the container wall is 0.3 [m], while that for the conical base is 0.2 [m]. Figure 2.73 shows the container with dimensions and supports, while the container material and unit weight of the water are listed in Table 2.24.

Table 2.24 Container material and water unit weight

Modulus of Elasticity of the container material	E_c	= 10000	[kN/m^2]
Poisson's ratio of the container material	ν_c	= 0.17	[-]
Unit weight of the water	γ_w	= 10	[kN/m^3]

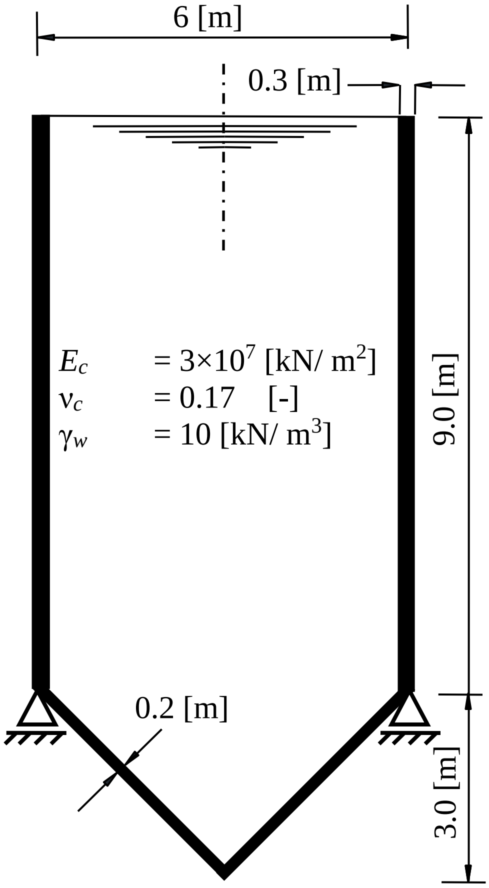

Figure 2.73 Cylindrical water container with dimensions and supports

2.18.2 Numerical Analysis

In the analysis, the height of the tank is divided into two main segments, the first one is divided into 30 elements (30×0.3 [m]), while the second is divided into 20 elements (20×0.15 [m]) as shown in Figure 2.74.

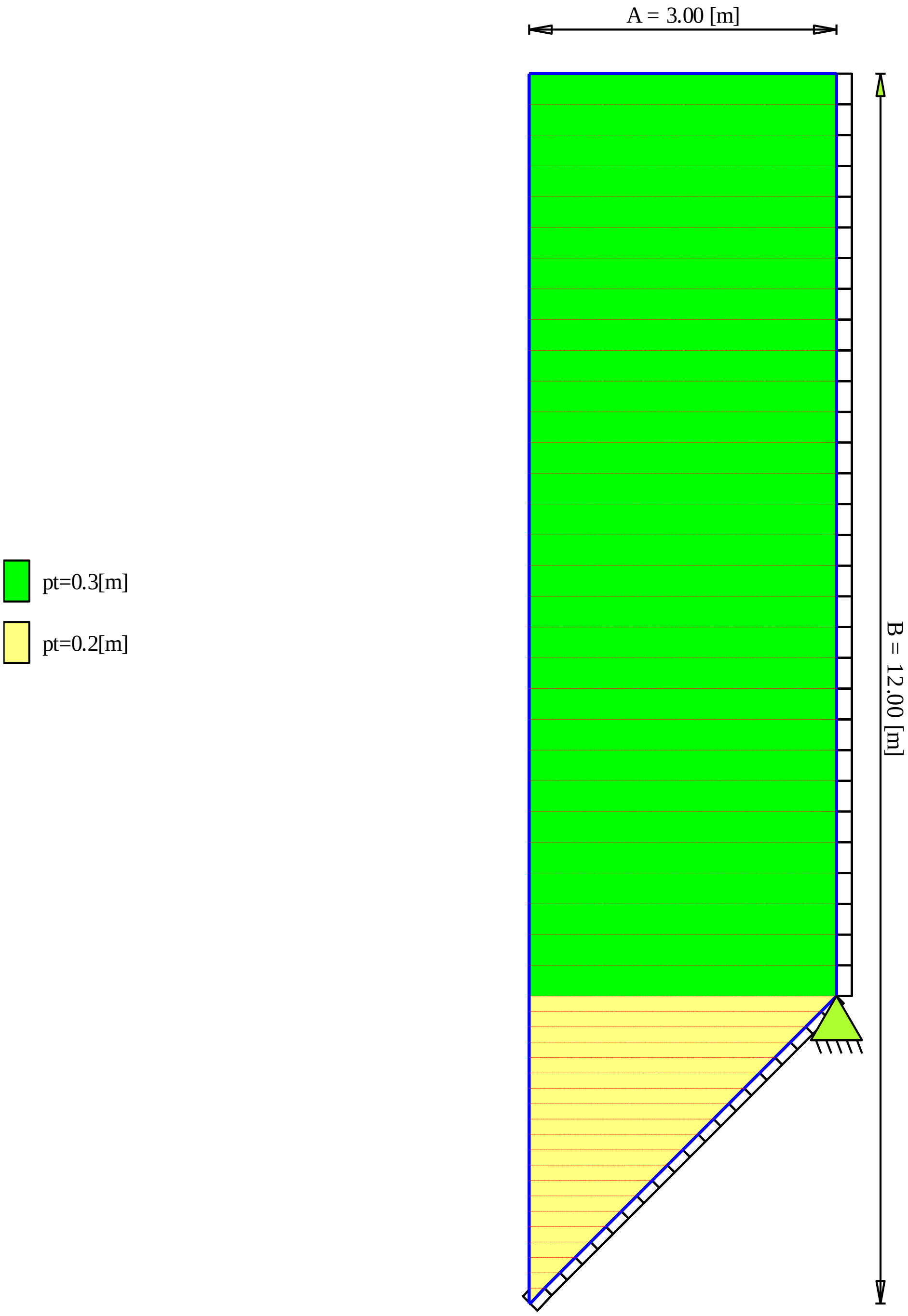

Figure 2.74 Finite element mesh of the container with boundary condition

2.18.3 Results and discussion

Results of *ELPLA* at segment ends are compared with those obtained by *Szilard et al.* (1986) in Table 2.25 to Table 2.27. These Tables show that results of *ELPLA* are in a good agreement with those of *Szilard et al.* (1986). Figure 2.75 to Figure 2.77 show the internal forces obtained by *ELPLA* along the wall height.

Table 2.25 Comparison between radial force N_r [kN/ m] obtained by *Szilard et al.* (1986) and those obtained by *ELPLA* at segment ends

Segment No.	Edge	Radial force N_r [kN/ m]		Absolute difference [kN/ m]
		Szilard et al. (1986)	*ELPLA*	
1	Start node	1.6767	1.6738	0.0029
	End node	-25.8878	-26.0930	0.2052
2	Start nod	9.0979	9.4414	0.3435
	End node	8.1024	9.5305	1.4281

Table 2.26 Comparison between meridional force N_y [kN/ m] obtained by *Szilard et al.* (1986) and those obtained by *ELPLA* at segment ends

Segment No.	Edge	Meridional force N_y [kN/ m]		Absolute difference [kN/ m]
		Szilard et al. (1986)	*ELPLA*	
1	Start node	-0.7139	-0.7274	0.0135
	End node	-3.8136	-3.8936	0.0800
2	Start nod	155.2807	155.2671	0.0136
	End node	14.1626	14.0693	0.0933

Table 2.27 Comparison between meridional moment M_y [kN.m/ m] obtained by *Szilard et al.* (1986) and those obtained by *ELPLA* at segment ends

Segment No.	Edge	Meridional moment M_y [kN.m/ m]		Absolute difference [kN.m/ m]
		Szilard et al. (1986)	*ELPLA*	
1	Start node	-0.0141	-0.0141	0.0000
	End node	-14.6691	-14.6653	0.0038
2	Start nod	-15.9102	-15.9074	0.0028
	End node	-0.6238	-0.7782	0.1544

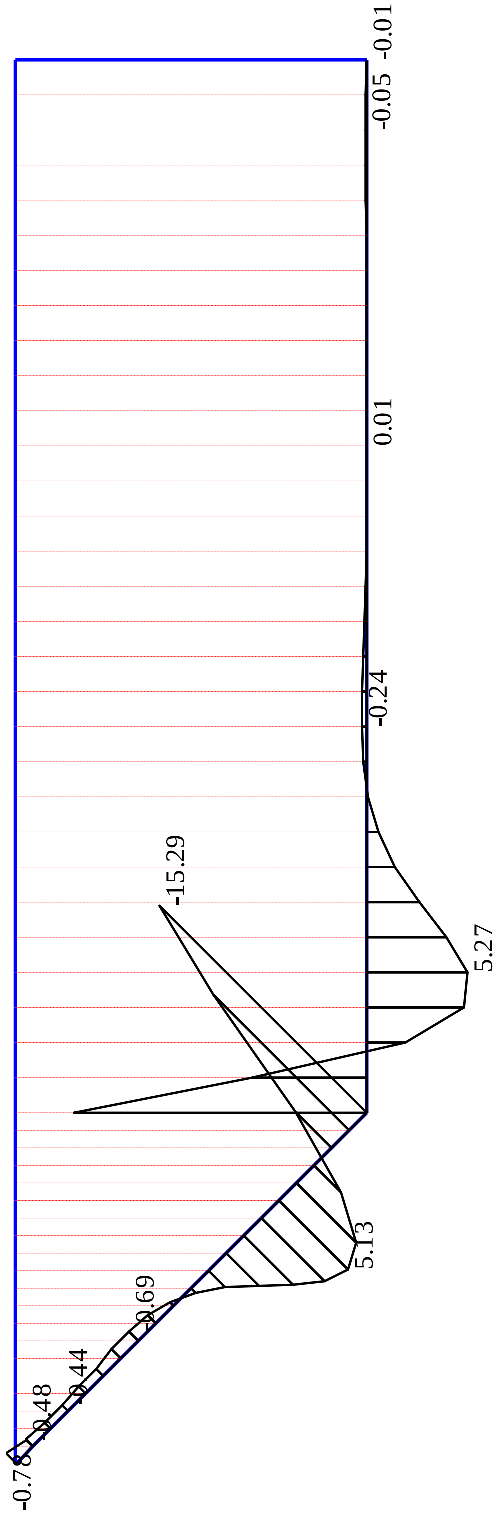

Figure 2.75 Meridional moment M_y [kN.m/ m] with wall height.

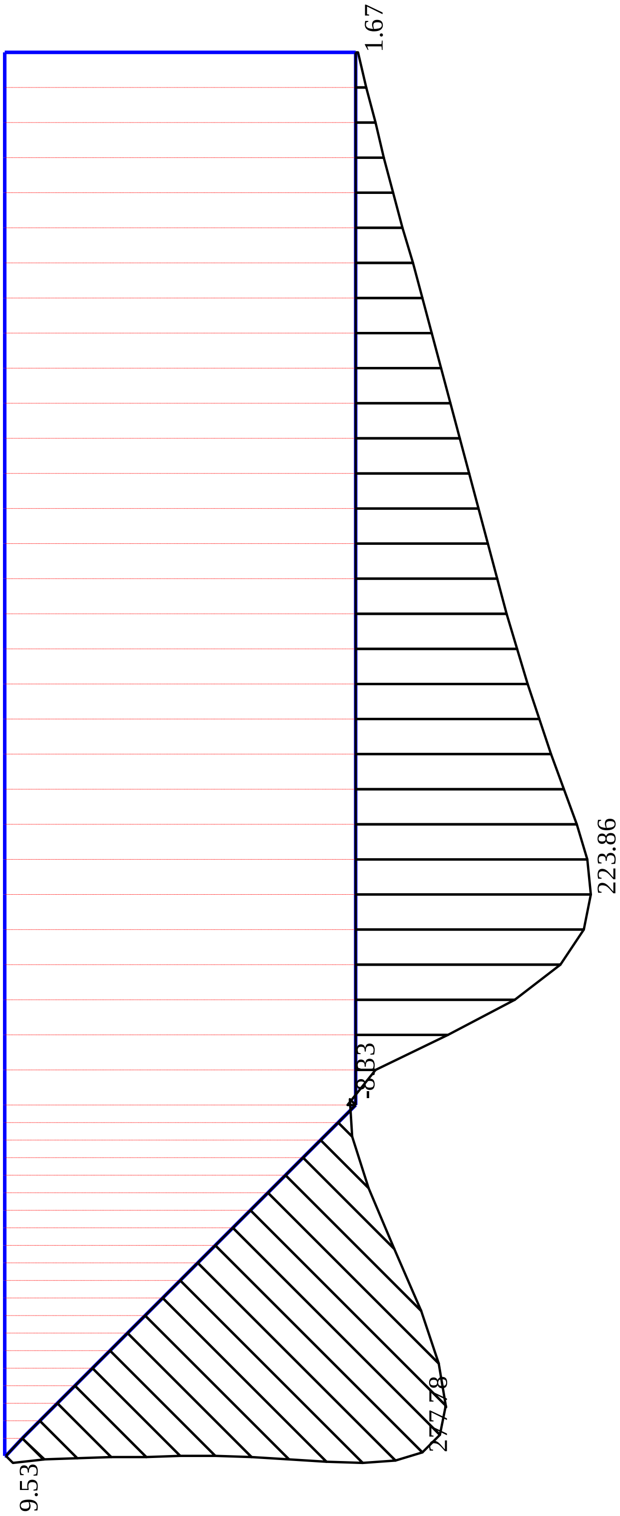

Figure 2.76 Radial force N_r [kN/ m] with wall height.

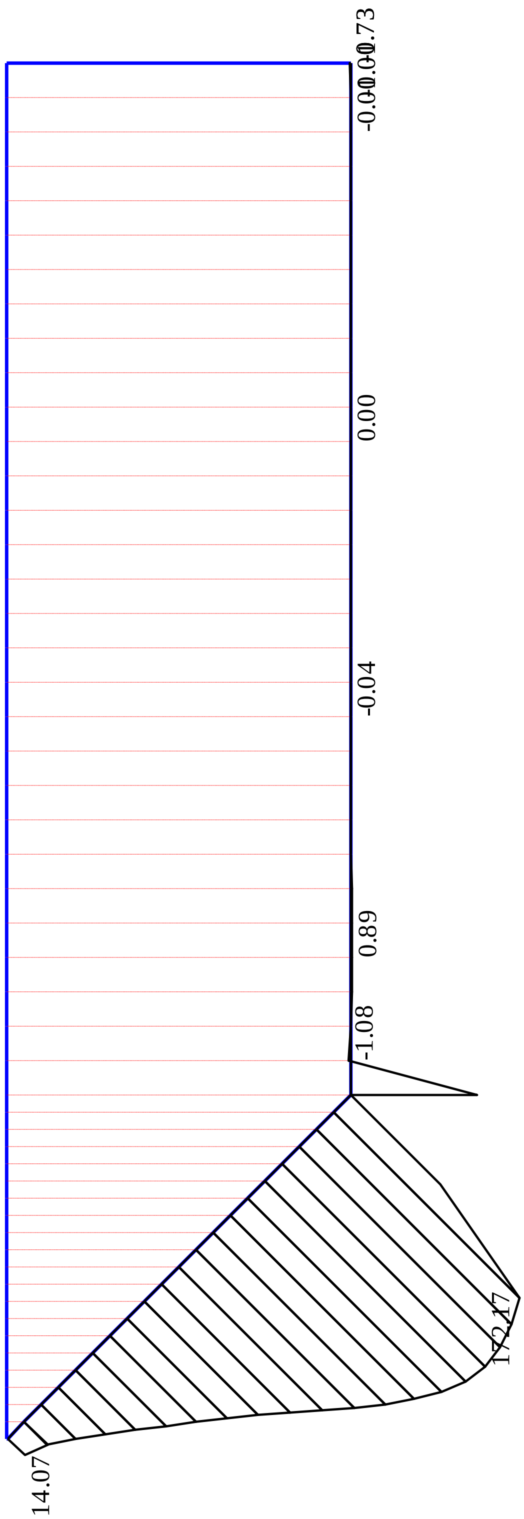

Figure 2.77 Meridional force N_y [kN/ m] with wall height.

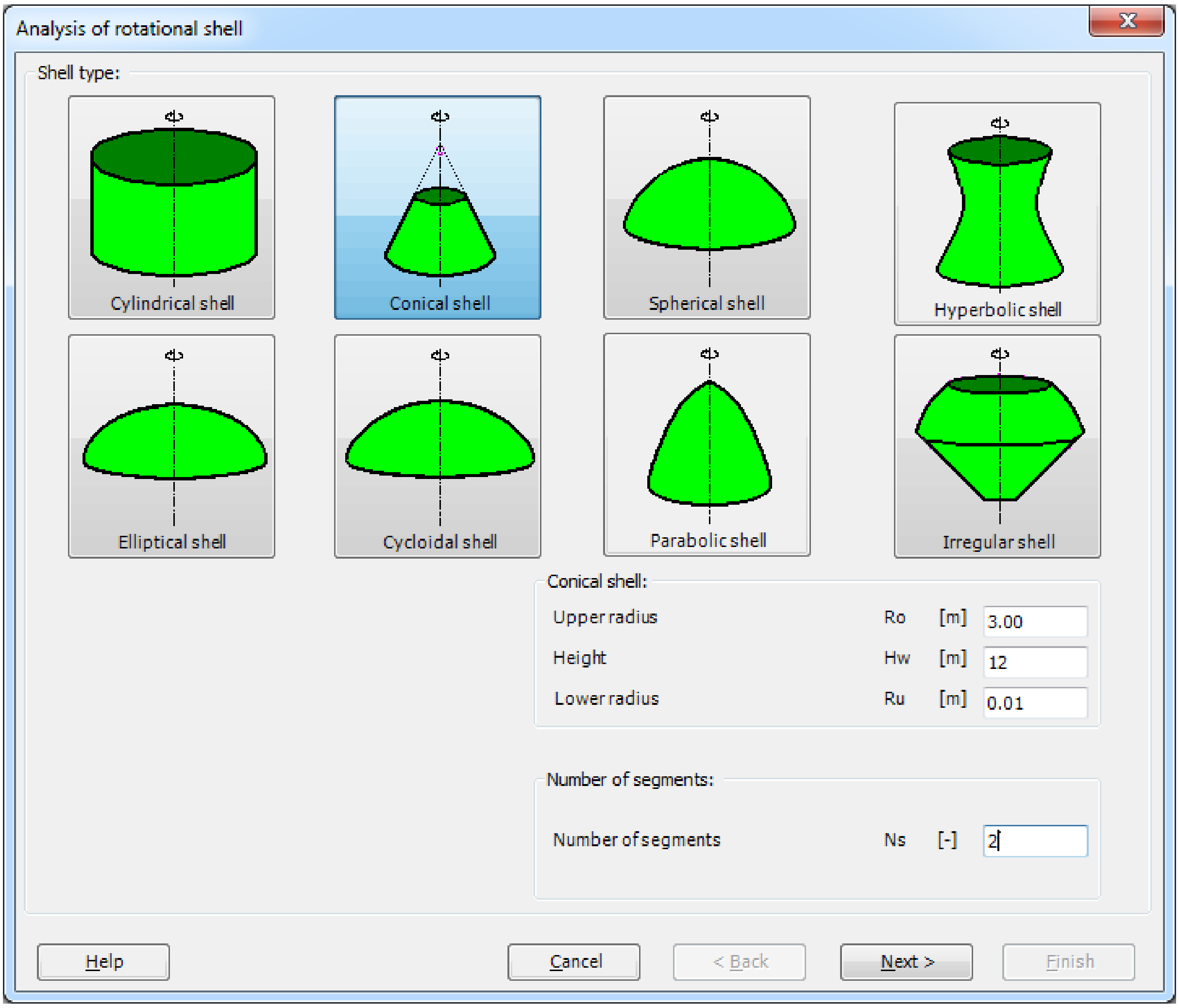

Figure 2.78 "Analysis of rotational shell" wizard

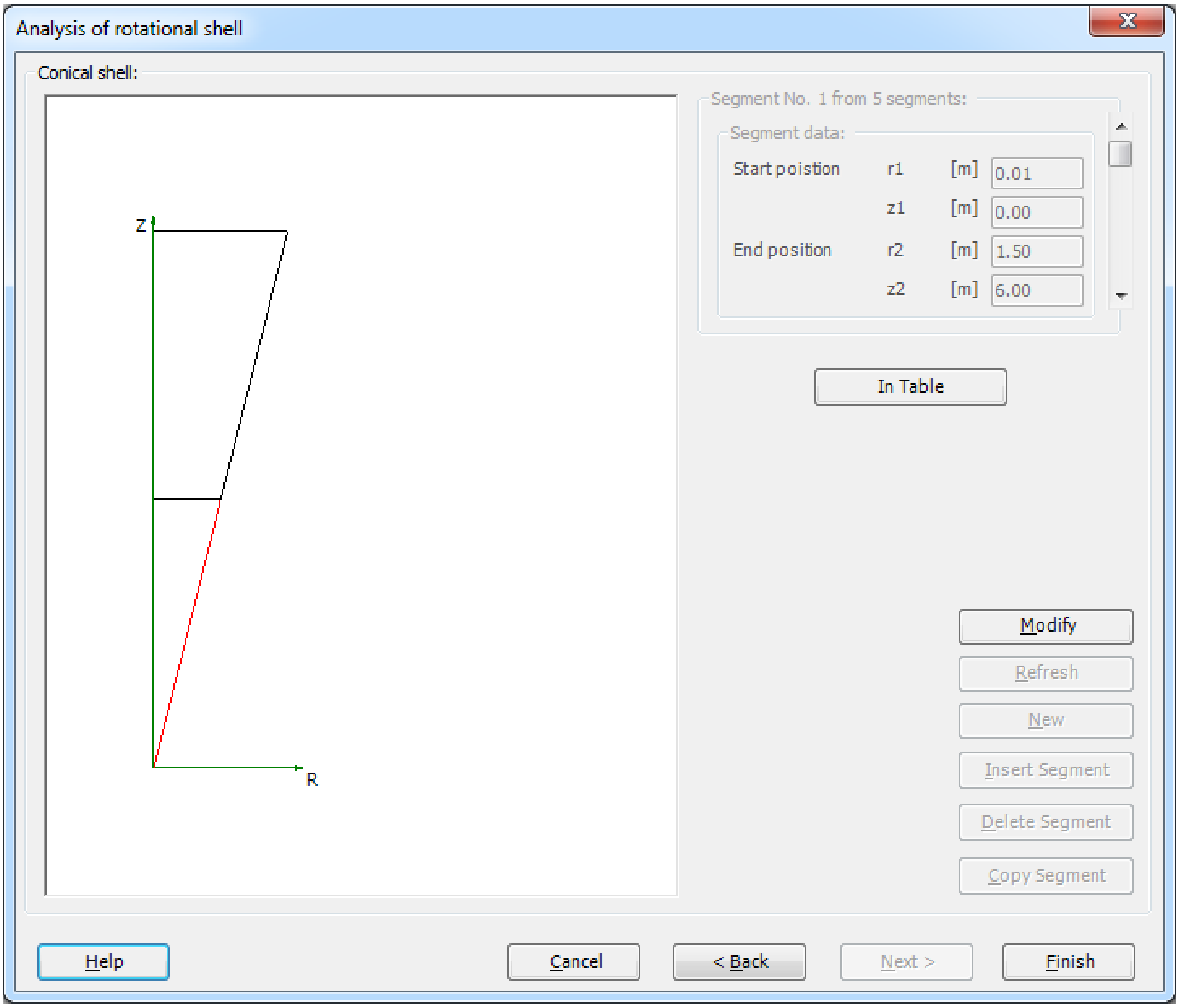

Figure 2.79 "Conical shell" form

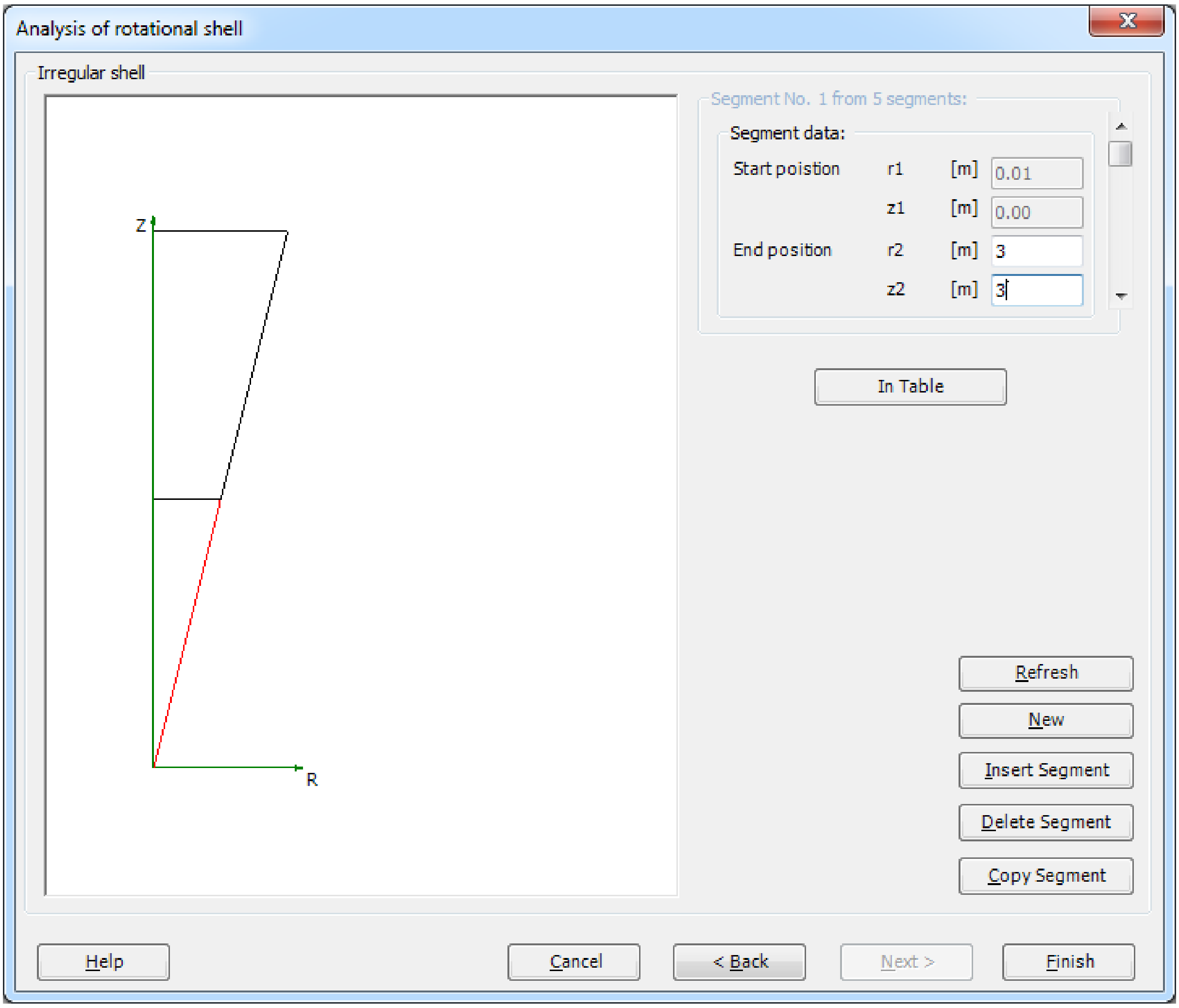

Figure 2.80 "Irregular shell" form

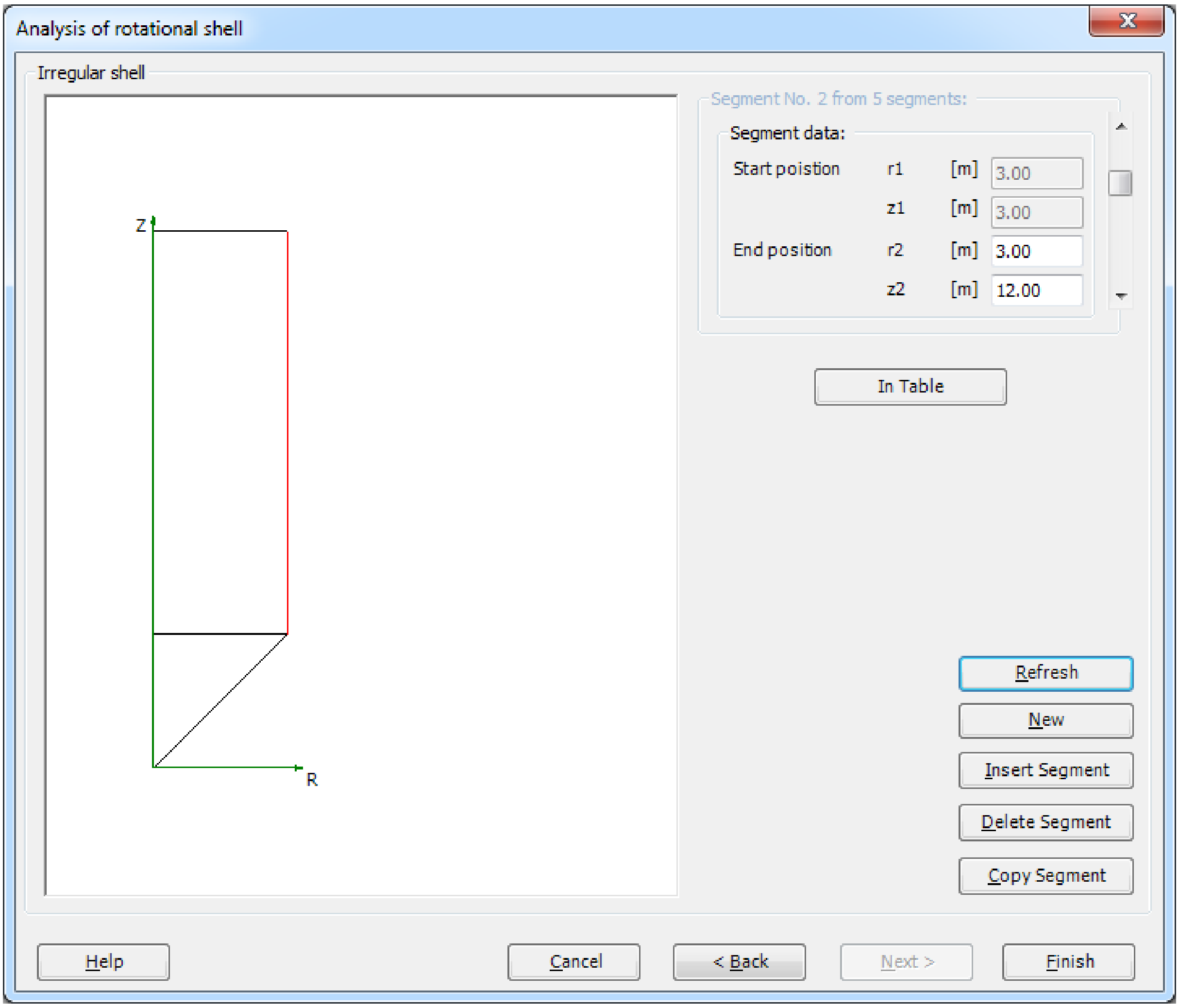

Figure 2.81 "Irregular shell" form

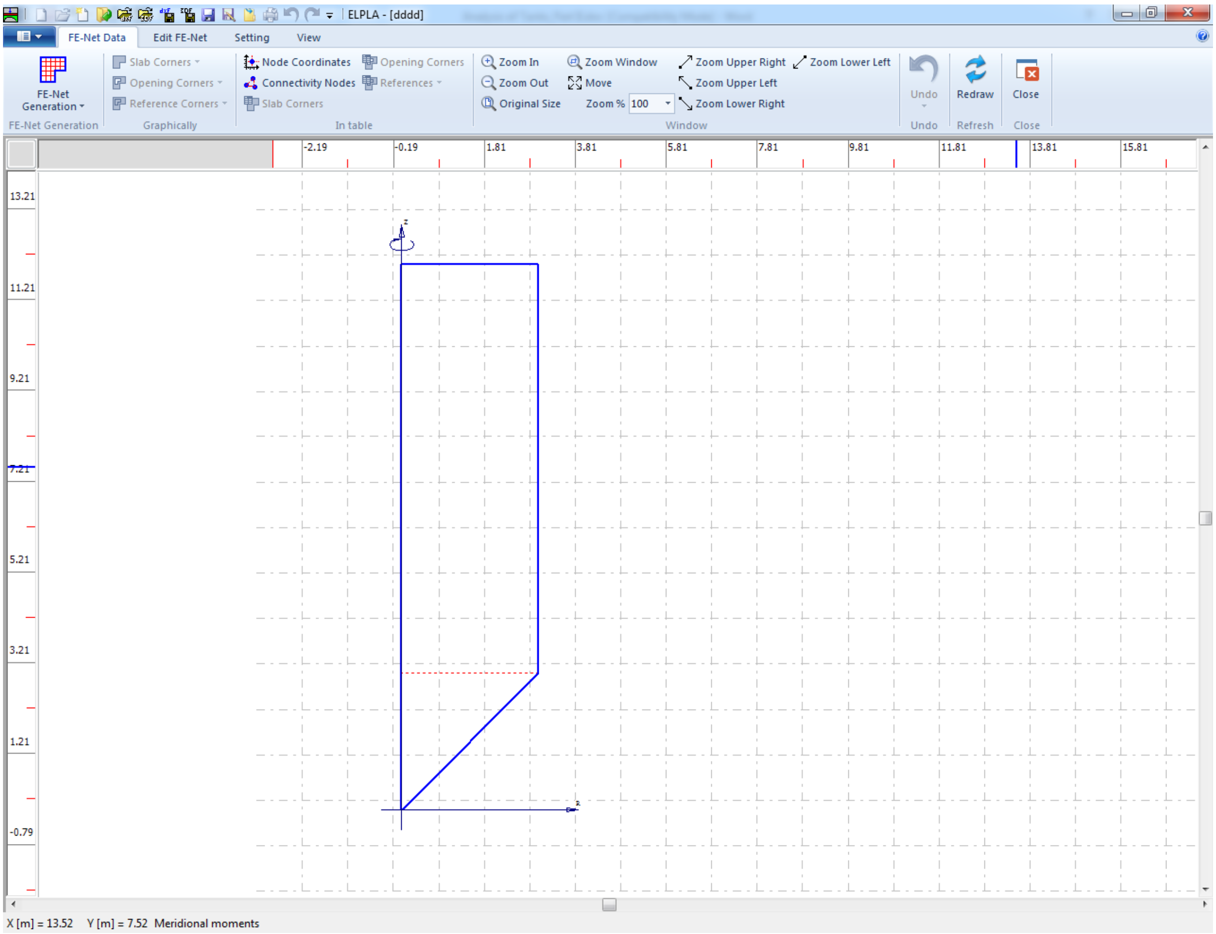

Figure 2.82 "FE-Net Data" window after generating the net

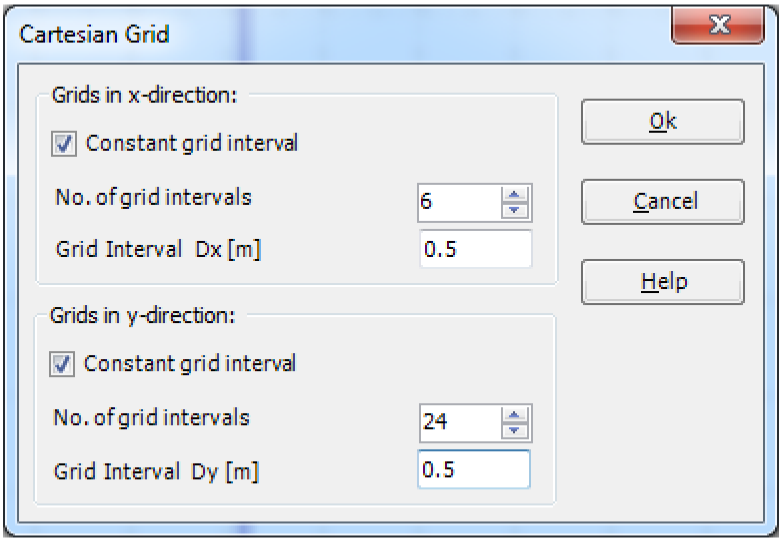

Figure 2.83 "Cartesian Grid" form

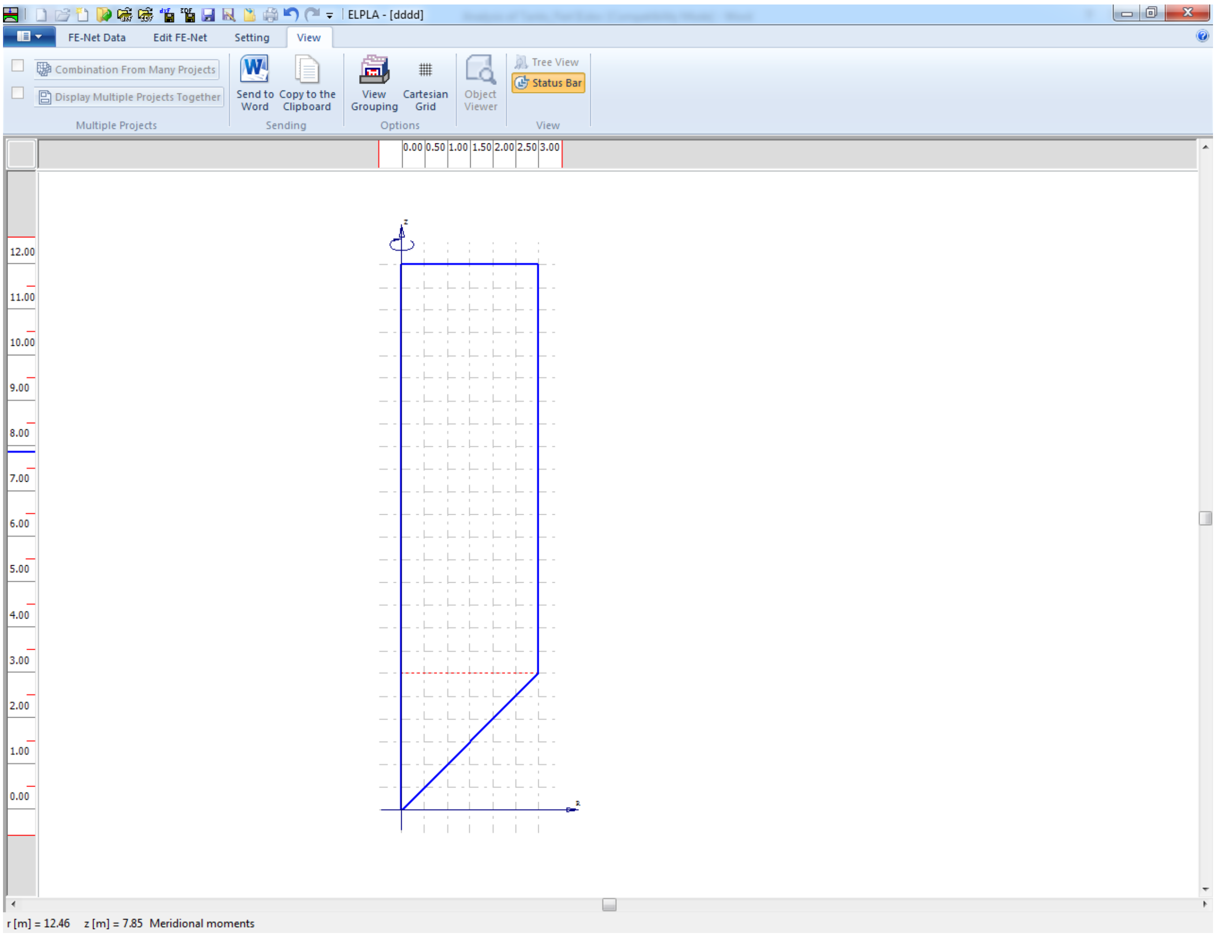

Figure 2.84 "FE-Net Data" window

2.19 Example 17: Hyperbolic shell under different loads

2.19.1 Description of the problem

A finite element method for analyzing rational shells is available in the reference *Szilard et al.* (1986). To verify *ELPLA* for analyzing shell structures, the internal forces obtained by *Szilard et al.* (1986) for analyzing hyperbolic shell under different loads are compared with those obtained by *ELPLA*.

Consider a hyperbolic shell of revolution with the following geometry:

Throat radius	R_o	= 18	[m]
Throat height	H_l	= 45	[m]
Lower radius	R_u	= 36	[m]
Total height	H	= 72	[m]
Thickness of the wall	t	=0.24	[m]

Meridian equation of the hyperbolic shell of revolution is given by:

$$r^2(\xi) = \frac{R_u^2 - R_o^2}{H_l^2}(\xi - H_l)^2 + R_o^2$$

$$r^2(\xi) = \frac{36^2 - 18^2}{45^2}(\xi - 45)^2 + 18^2$$

$$r^2(\xi) = 0.48(\xi - 45)^2 + 324$$

where r [m] is the radius at height ξ [m].

Figure 2.85 shows the geometry of the hyperbolic shell with dimensions and supports, while the shell material are listed in Table 2.28.

Table 2.28 hyperboloid shell material

Modulus of Elasticity of the shell material	E_c	$= 3\times10^7$	[kN/m^2]
Poisson's ratio of the shell material	ν_c	= 0.3	[-]

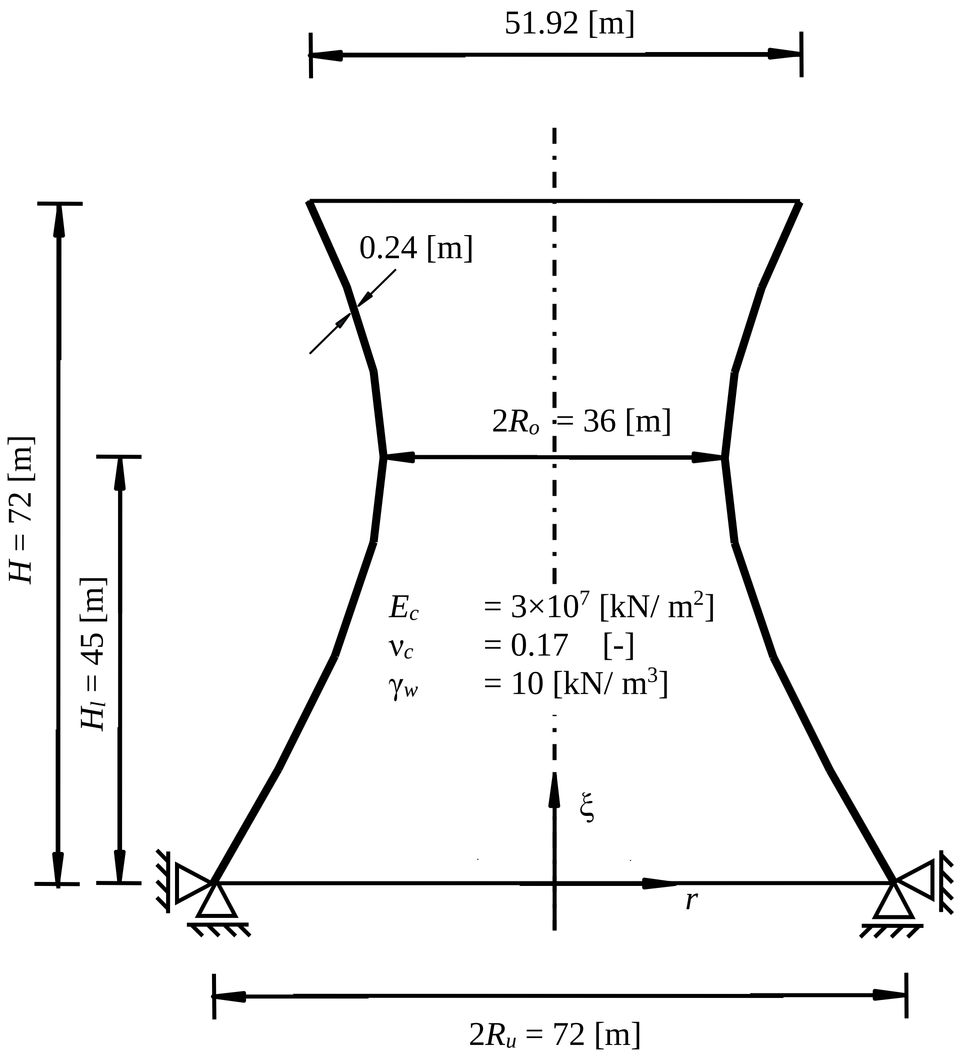

Figure 2.85 Geometry of the hyperbolic shell with dimensions and supports

2.19.2 Numerical Analysis

In the analysis, the height of the hyperbolic shell is divided into 7 main segments; each segment is divided into a number of elements. Segment dimensions and number of elements of each segment are shown in Figure 2.86.

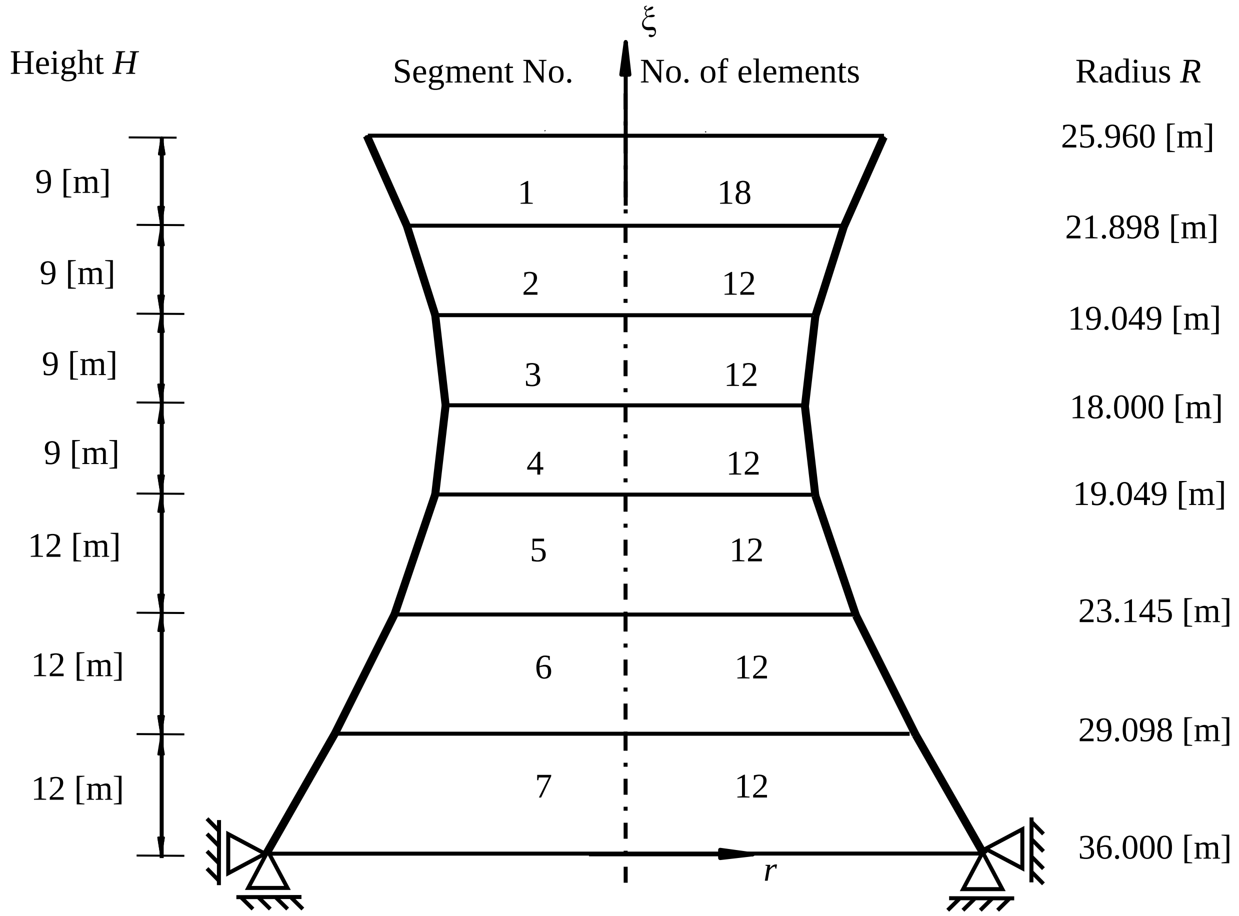

Figure 2.86 Segment dimensions and no. of elements in each segment

Internal forces are determined for the following load cases:

1. Self-weight of g = 6.0 [kN/m^2], Figure 2.87.

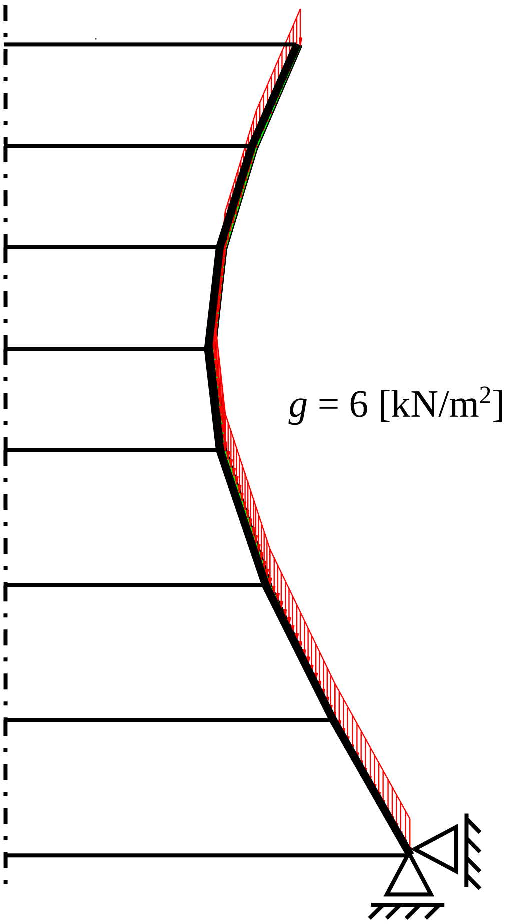

Figure 2.87 Shell with self-weight of g = 6.0 [kN/m^2]

2. Uniform external pressure of $p_s = -10$ [kN/m^2], Figure 2.88.

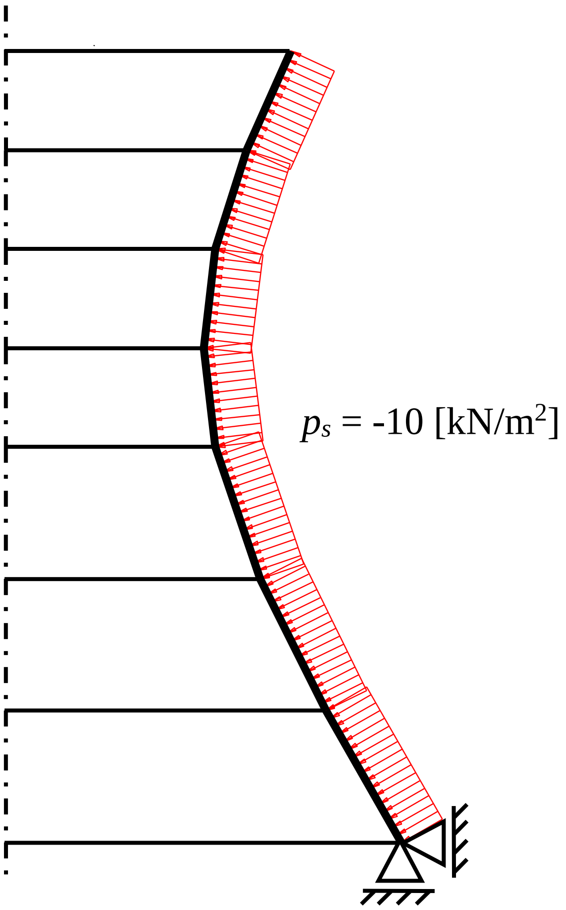

Figure 2.88 Shell with uniform external pressure of $p_s = -10$ [kN/m^2]

3. Horizontal line load of H_o = - 100 [kN/m] at the top edge of the shell, Figure 2.89.

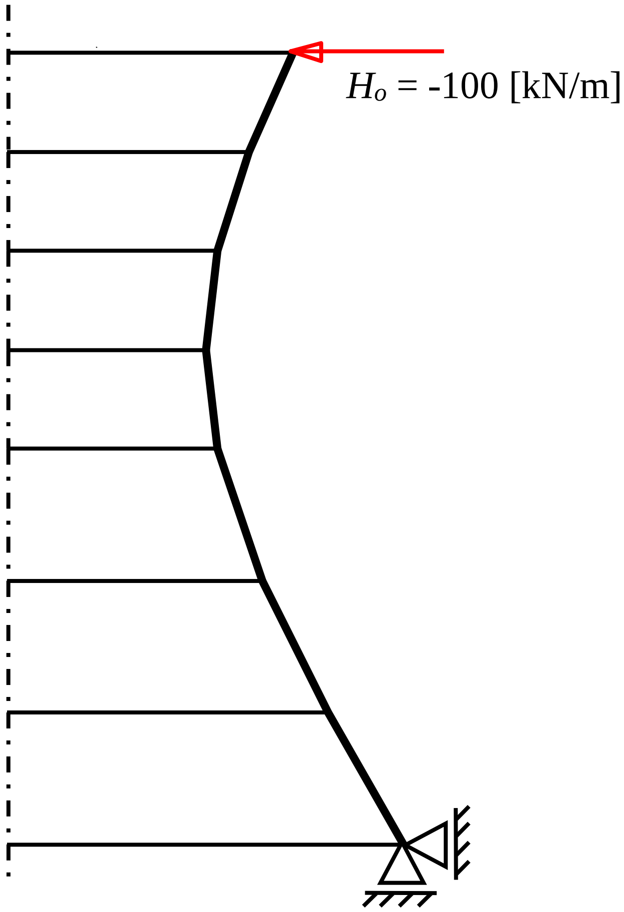

Figure 2.89 Shell with a horizontal line load of H_o = - 100 [kN/m]

2.19.3 Results and discussion

Results of *ELPLA* at segment ends for the three load of cases are compared with those obtained by *Szilard et al.* (1986) in Table 2.29 to Table 2.37. These Tables show that results of *ELPLA* are in a good agreement with those of *Szilard et al.* (1986). Figure 2.90 to Figure 2.98 show the internal forces obtained by *ELPLA* along the wall height.

Table 2.29 Comparison between radial force N_r [kN/ m] obtained by *Szilard et al.* (1986) and those obtained by *ELPLA* at segment ends. Load case 1.

Segment No.	Edge	Radial force N_r [kN/ m]		Absolute difference [kN/ m]
		Szilard et al. (1986)	*ELPLA*	
1	Start node	69.5724	69.5128	0.0596
	End node	0.5222	0.5287	-0.0065
2	Start node	-0.7700	-0.6579	-0.1121
	End node	-124.8571	-124.9916	0.1345
3	Start node	-125.8401	-126.0563	0.2162
	End node	-253.4129	-253.7656	0.3527
4	Start node	-254.4527	-254.8056	0.3529
	End node	-325.5648	-326.7562	1.1914
5	Start node	-328.2926	-329.0705	0.7779
	End node	-304.1353	-304.1556	0.0203
6	Start node	-305.9570	-305.8356	-0.1214
	End node	-240.7215	-241.4881	0.7666
7	Start nod	-241.9167	-242.4401	0.5234
	End node	-105.0295	-105.1321	0.1026

Table 2.30 Comparison between meridional force N_y [kN/ m] obtained by *Szilard et al.* (1986) and those obtained by *ELPLA* at segment ends. Load case 1.

Segment No.	Edge	Meridional force N_y [kN/ m]		Absolute difference [kN/ m]
		Szilard et al. (1986)	*ELPLA*	
1	Start node	-1.9396	-1.7369	0.2027
	End node	-68.0595	-68.0932	0.0337
2	Start node	-72.3711	-72.0512	0.3199
	End node	-139.5230	-139.2727	0.2503
3	Start node	-142.7999	-142.8207	0.0208
	End node	-202.3444	-202.4391	0.0947
4	Start node	-205.8094	-205.9064	0.0970
	End node	-250.8448	-250.9825	0.1377
5	Start node	-259.9382	-258.6959	1.2423
	End node	-294.5903	-294.0234	0.5669
6	Start node	-300.6625	-299.6241	1.0384
	End node	-325.4098	-325.1789	0.2309
7	Start nod	-329.3937	-328.3519	1.0418
	End node	-350.0983	-350.4408	0.3425

Table 2.31 Comparison between meridional moment M_y [kN.m/ m] obtained by *Szilard et al.* (1986) and those obtained by *ELPLA* at segment ends. Load case 1.

Segment No.	Edge	Meridional moment M_y [kN.m/ m]		Absolute difference [kN.m/ m]
		Szilard et al. (1986)	*ELPLA*	
1	Start node	-0.0009	-0.0011	0.0002
	End node	-3.1189	-3.1769	0.058
2	Start node	-2.9919	-3.0427	0.0508
	End node	-8.2363	-8.4232	0.1869
3	Start node	-8.4294	-8.4532	0.0238
	End node	-13.8129	-13.8321	0.0192
4	Start node	-14.0145	-14.0349	0.0204
	End node	-16.1447	-16.2391	0.0944
5	Start node	-15.0779	-15.514	0.4361
	End node	-12.3262	-12.6665	0.3403
6	Start node	-12.5098	-12.8408	0.331
	End node	-7.6055	-7.8502	0.2447
7	Start nod	-7.7253	-8.108	0.3827
	End node	-0.1248	-0.1125	0.0123

Table 2.32 Comparison between radial force N_r [kN/ m] obtained by *Szilard et al.* (1986) and those obtained by *ELPLA* at segment ends. Load case 2.

Segment No.	Edge	Radial force N_r [kN/ m]		Absolute difference [kN/ m]
		Szilard et al. (1986)	*ELPLA*	
1	Start node	-283.9419	-283.7302	0.2117
	End node	-201.7216	-201.7328	0.0112
2	Start node	-201.1569	-201.2161	0.0592
	End node	-107.0932	-107.0177	0.0755
3	Start node	-106.9399	-106.7979	0.1420
	End node	-59.5957	-59.4365	0.1592
4	Start node	-59.5928	-59.4335	0.1593
	End node	-97.5923	-97.2183	0.3740
5	Start node	-97.3619	-97.0933	0.2686
	End node	-225.6020	-225.7137	0.1117
6	Start node	-226.3025	-226.357	0.0545
	End node	-344.9325	-345.0061	0.0736
7	Start nod	-346.0169	-345.9579	0.0590
	End node	-20.2175	-21.1818	0.9643

Table 2.33 Comparison between meridional force N_y [kN/ m] obtained by *Szilard et al.* (1986) and those obtained by *ELPLA* at segment ends. Load case 2.

Segment No.	Edge	Meridional force N_y [kN/ m]		Absolute difference [kN/ m]
		Szilard et al. (1986)	*ELPLA*	
1	Start node	1.0249	0.9315	0.0934
	End node	46.8933	46.8819	0.0114
2	Start node	48.7761	48.6042	0.1719
	End node	84.5652	84.3615	0.2037
3	Start node	85.0767	85.0936	0.0169
	End node	99.1026	99.1436	0.041
4	Start node	99.1117	99.1535	0.0418
	End node	85.3395	85.3722	0.0327
5	Start node	86.1077	85.789	0.3187
	End node	33.8953	33.6757	0.2196
6	Start node	31.5603	31.5315	0.0288
	End node	-32.3984	-32.5001	0.1017
7	Start nod	-36.0127	-35.6723	0.3404
	End node	-67.3916	-70.6063	3.2147

Table 2.34 Comparison between meridional moment M_y [kN.m/ m] obtained by *Szilard et al.* (1986) and those obtained by *ELPLA* at segment ends. Load case 2.

Segment No.	Edge	Meridional moment M_y [kN.m/ m]		Absolute difference [kN.m/ m]
		Szilard et al. (1986)	*ELPLA*	
1	Start node	-0.0114	-0.0121	0.0007
	End node	2.2238	2.2645	0.0407
2	Start node	2.1246	2.1603	0.0357
	End node	5.0890	5.201	0.112
3	Start node	5.1616	5.1755	0.0139
	End node	6.9021	6.9114	0.0093
4	Start node	6.9034	6.9128	0.0094
	End node	5.6888	5.7224	0.0336
5	Start node	5.1782	5.3312	0.153
	End node	1.5604	1.5937	0.0333
6	Start node	1.4519	1.4886	0.0367
	End node	-0.6587	-0.682	0.0233
7	Start nod	-0.7019	-0.7397	0.0378
	End node	-2.4192	-2.2127	0.2065

Table 2.35 Comparison between radial force N_r [kN/ m] obtained by *Szilard et al.* (1986) and those obtained by *ELPLA* at segment ends. Load case 3.

Segment No.	Edge	Radial force N_r [kN/ m]		Absolute difference [kN/ m]
		Szilard et al. (1986)	*ELPLA*	
1	Start node	-2498.3086	-2506.92	8.6114
	End node	-6.1263	-6.1498	0.0235
2	Start node	-5.7148	-5.7743	0.0595
	End node	0.0550	0.0537	0.0013
3	Start node	0.0611	0.0594	0.0017
	End node	0.0047	0.0028	0.0019
4	Start node	0.0047	0.0028	0.0019
	End node	0.0039	0.0022	0.0017
5	Start node	0.0040	0.0022	0.0018
	End node	0.0024	0.0013	0.0011
6	Start node	0.0024	0.0013	0.0011
	End node	0.0011	0.0006	0.0005
7	Start nod	0.0011	0.0006	0.0005
	End node	0.0006	0.0003	0.0003

Table 2.36 Comparison between meridional force N_y [kN/ m] obtained by *Szilard et al.* (1986) and those obtained by *ELPLA* at segment ends. Load case 3.

Segment No.	Edge	Meridional force N_y [kN/ m]		Absolute difference [kN/ m]
		Szilard et al. (1986)	*ELPLA*	
1	Start node	-132.8555	-124.6019	8.2536
	End node	-1.2323	-1.1253	0.107
2	Start node	0.1393	0.1263	0.013
	End node	-0.0096	-0.0099	0.0003
3	Start node	0.0107	0.0092	0.0015
	End node	0.0034	0.0019	0.0015
4	Start node	0.0035	0.0019	0.0016
	End node	0.0033	0.0018	0.0015
5	Start node	0.0034	0.0019	0.0015
	End node	0.0029	0.0016	0.0013
6	Start node	0.0029	0.0016	0.0013
	End node	0.0024	0.0013	0.0011
7	Start nod	0.0024	0.0013	0.0011
	End node	0.0020	0.0011	0.0009

Table 2.37 Comparison between meridional moment M_y [kN.m/ m] obtained by *Szilard et al.* (1986) and those obtained by *ELPLA* at segment ends. Load case 3.

Segment No.	Edge	Meridional moment M_y [kN.m/ m]		Absolute difference [kN.m/ m]
		Szilard et al. (1986)	*ELPLA*	
1	Start node	10.5182	9.664	0.8542
	End node	-1.4044	-1.3918	0.0126
2	Start node	-1.0173	-1.0361	0.0188
	End node	-0.0059	-0.006	0.0001
3	Start node	-0.0054	-0.0055	1E-04
	End node	0.0002	0.0001	0.0001
4	Start node	0.0002	0.0001	0.0001
	End node	0.0002	0.0001	0.0001
5	Start node	0.0002	0.0001	0.0001
	End node	0.0001	0.0001	0
6	Start node	0.0001	0.0001	0
	End node	0.0001	0	0.0001
7	Start nod	0.0001	0	0.0001
	End node	0.0000	0	0

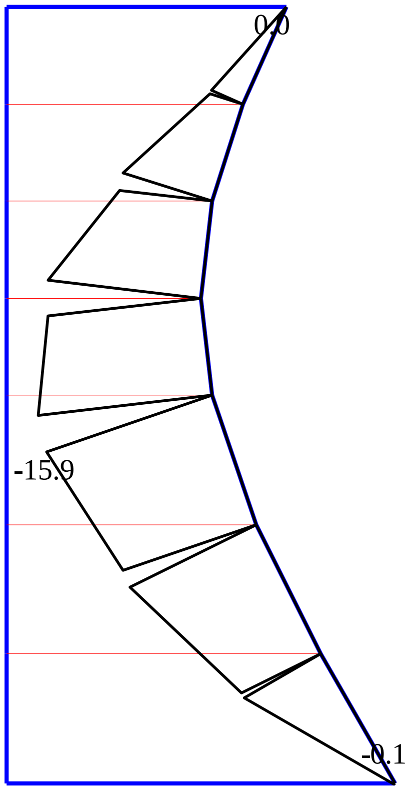

Figure 2.90 Meridional moment M_y [kN.m/ m] with shell height. Load case 1

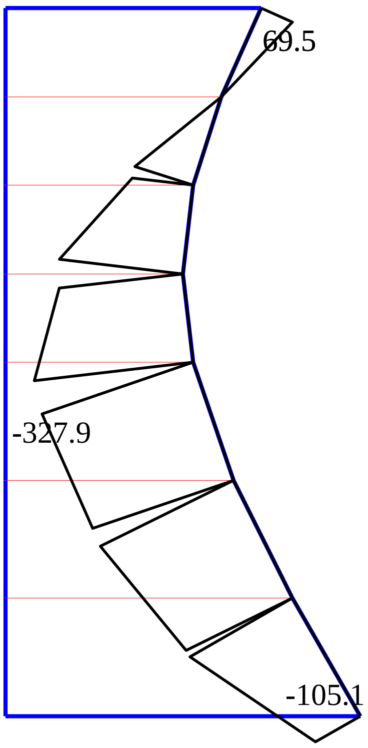

Figure 2.91 Radial force N_r [kN/ m] with shell height. Load case 1

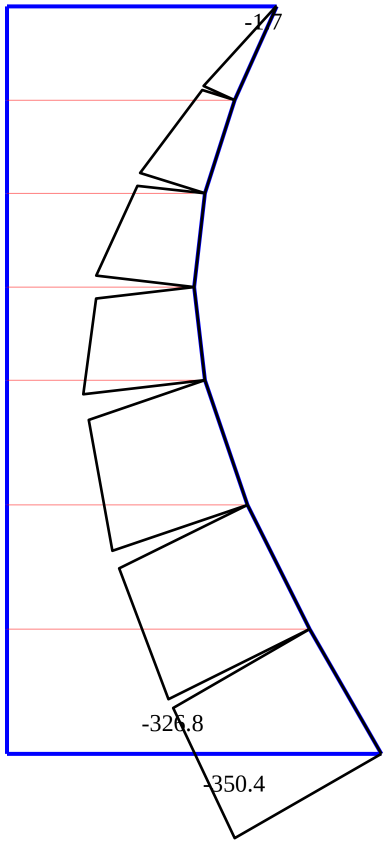

Figure 2.92 Meridional force N_y [kN/ m] with shell height. Load case 1

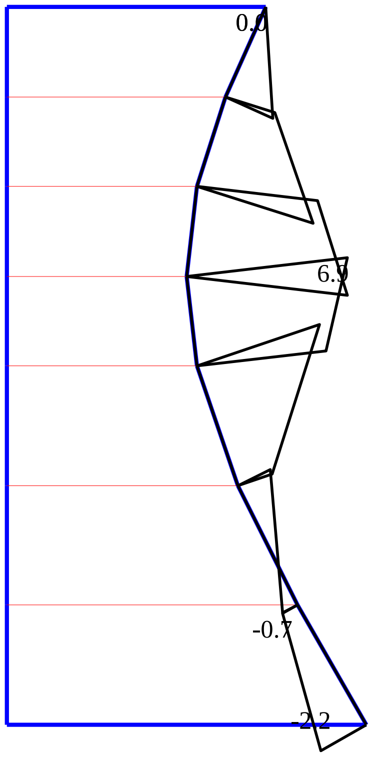

Figure 2.93 Meridional moment M_y [kN.m/ m] with shell height. Load case 2

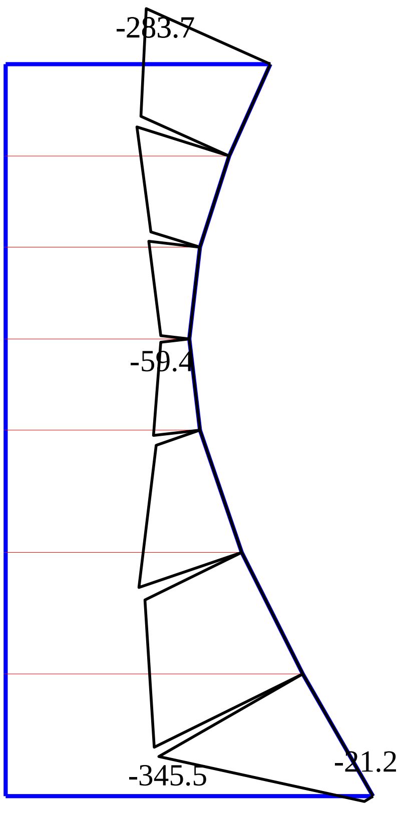

Figure 2.94 Radial force N_r [kN/ m] with shell height. Load case 2

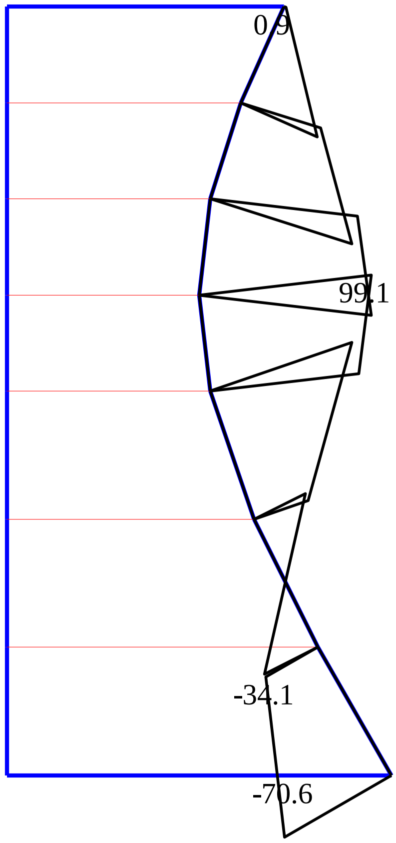

Figure 2.95 Meridional force N_y [kN/ m] with shell height. Load case 2

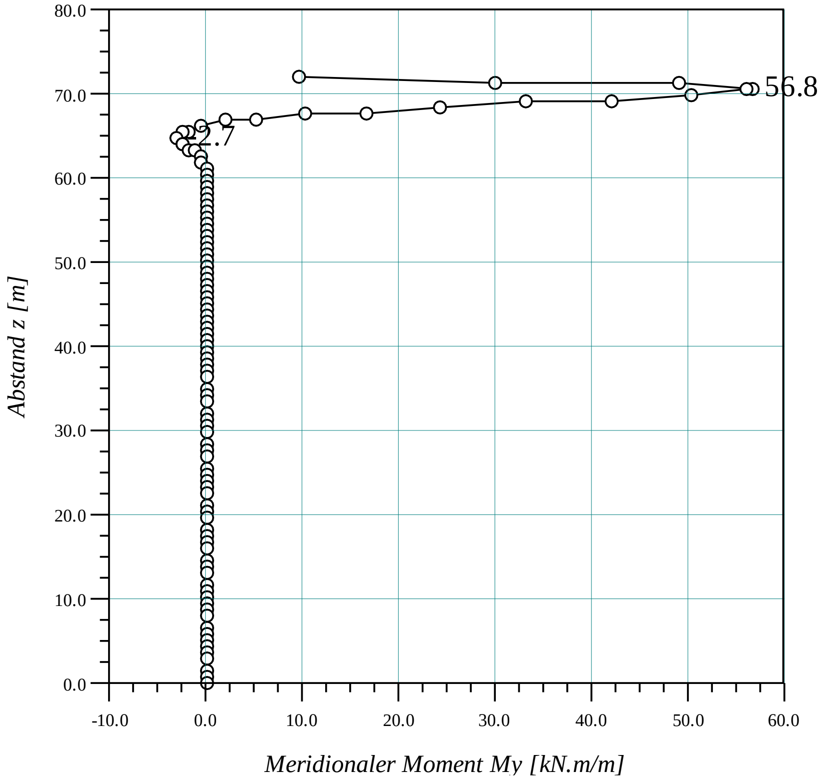

Figure 2.96 Meridional moment M_y [kN.m/ m] with shell height. Load case 3

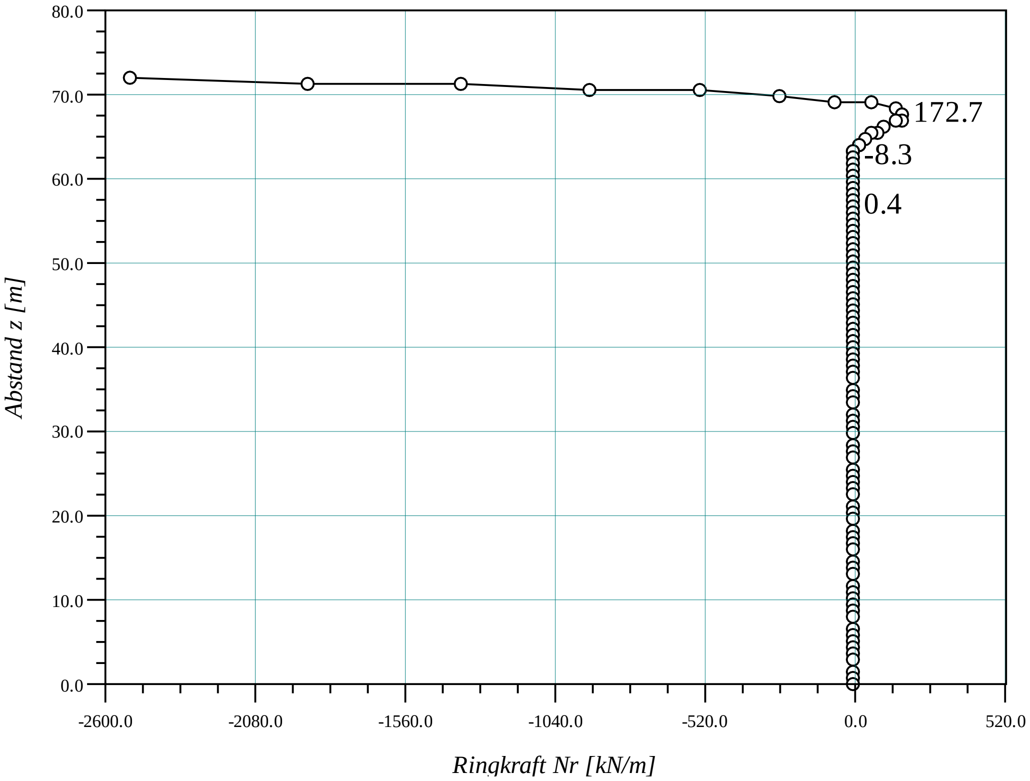

Figure 2.97 Radial force N_r [kN/ m] with shell height. Load case 3

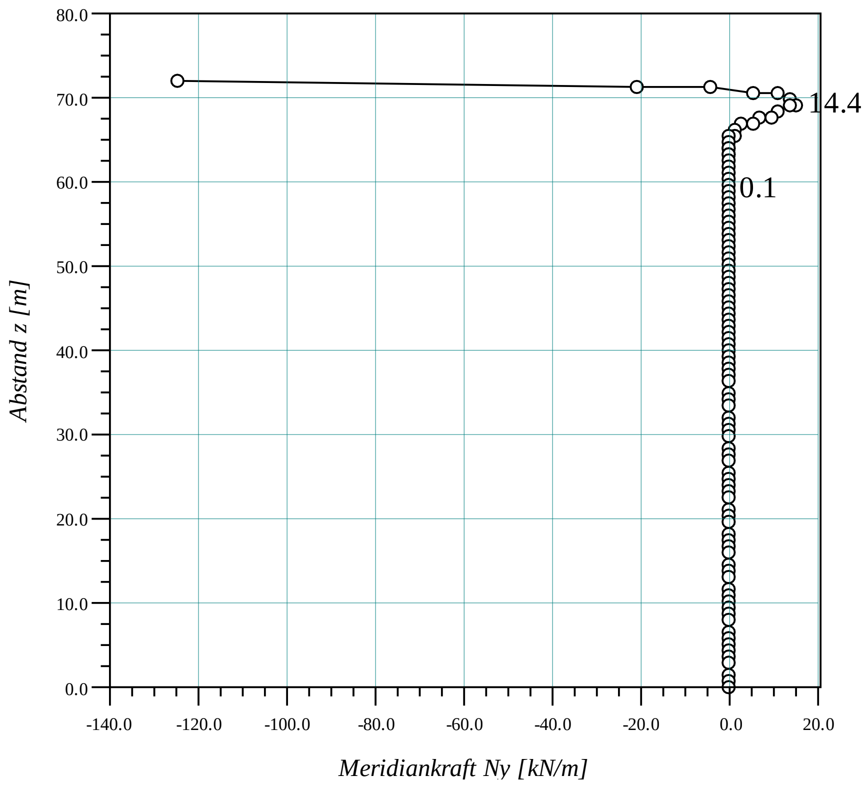

Figure 2.98 Meridional force N_y [kN/ m] with shell height. Load case 3

2.20 Example 18: A Silo filled with cement

2.20.1 Description of the problem

Analysis and design of silos using finite element method is available in the reference *Mansour* (2018). To verify *ELPLA* for analyzing silos for storing granular materials, the hoop tension obtained by *Mansour* (2018) for analyzing a silo filled with cement is compared with that obtained by *ELPLA*.

A circular concrete silo having a conical hopper at the bottom part and a conical roof at the upper part is considered. The main height of the silo is 8 [m] and its diameter is 4 [m]. The stored material is cement of a unit weight of 15.5 [kN/m^2]. The angle of internal friction of cement is 25 [°] and the angle of wall friction is 25 [°]. The thickness of the roof and the wall is 0.28 [m], while the thickness of the hopper is 0.25 [m]. The conical hopper bottom slope is 45 [°], opening at the bottom is 0.5 [m] and hopper bottom height is 3 [m]. Figure 2.85 shows the geometry of the silo with dimensions and support, while the silo shell material is listed in Table 2.38.

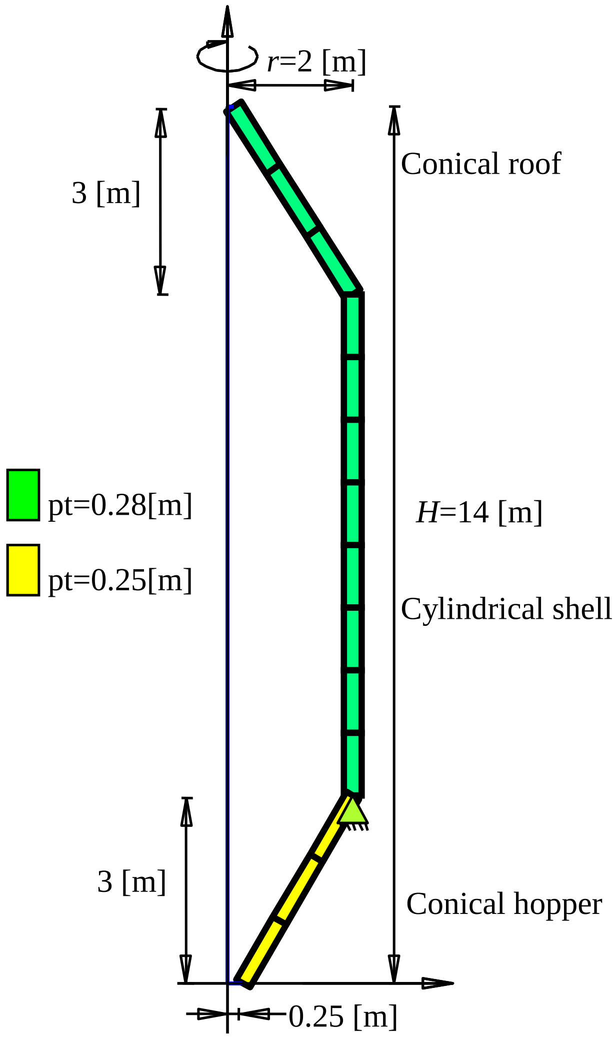

Figure 2.99 Geometry of the silo with dimensions and support

Table 2.38 Silo shell material

Modulus of Elasticity of the shell material	E_c	$= 2.486\times10^7$	[kN/m^2]
Poisson's ratio of the shell material	ν_c	= 0.2	[-]
Unit weight of the shell material	γ_c	= 23.563	[kN/m^3]

2.20.2 Pressure on the silo wall

According to *Janssen's* silo theory (1895), the horizontal pressure P_h [kN/m^2] on the silo wall at a depth h [m] below the free surface of the stored material is given by:

$$P_h = \frac{\gamma_s\ R}{\mu}\left[1 - \mathrm{Exp}\left(\frac{-\mu\ k\ h}{R}\right)\right]$$

in which k is the ratio of horizontal to vertical pressures, usually assumed equal to *Rankine's* coefficient of active earth pressure

$$k = \frac{1 - \sin\varphi}{1 + \sin\varphi}$$

h	Depth from the material top to the calculation section, [m]
k	Wall pressure coefficient, [-]
φ	Angel of internal friction of the stored material, [°]
γ_s	Unit weight of the stored material, [kN/m^3]
$R=A/U$	Hydraulic radius of the net horizontal cross section, [m]
$\mu=\tan\delta$	Friction coefficient between the silo wall and the stored material
δ	Angle of the wall friction, [°]
$A=\pi D^2/4$	Cross-sectional area of the silo, [m^2]
$U=\pi D$	Parameter of the silo, [m]
D	Diameter of the silo, [m]

Using the above relations and equations, the lateral pressure P_h on the main silo wall various depth is determined and presented in Table 2.39.

Table 2.39 Lateral pressure P_h on the main silo wall

Height from the top h [m]	Lateral pressure on the silo wall P_h [kN/m2]
1	5.731
2	10.475
3	14.400
4	17.648
5	20.337
6	22.562
7	24.403
8	25.926

2.20.3 Numerical Analysis

The wall of the silo is divided into three parts:
1. The roof part where no lateral pressure is applied on it
2. The main silo part where the lateral pressure p_h is applied.
3. The hopper part where no lateral pressure is applied on it

In the analysis, these three parts are divided into 14 segments; each segment is 1.0 [m]. Then these segments are divided into a number of elements, each element is 0.2 [m]. Segment dimensions and number of segments are shown in Figure 2.100.

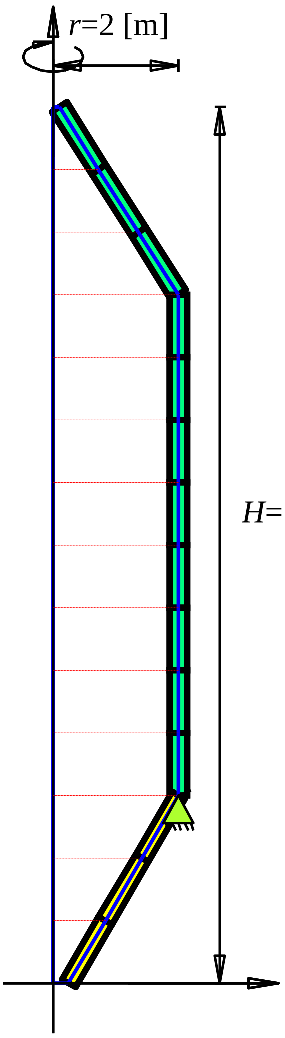

Figure 2.100 Segment dimensions

2.20.4 Results and discussion

Table 2.29Figure 2.101 shows the redial force obtained by *ELPLA*. The maximum redial force obtained by *ELPLA* is *Nr* =48.4 [kN/m], while that of *Mansour* (2018) is *Nr* =51.3 [kN/m]. They are in a good agreement.

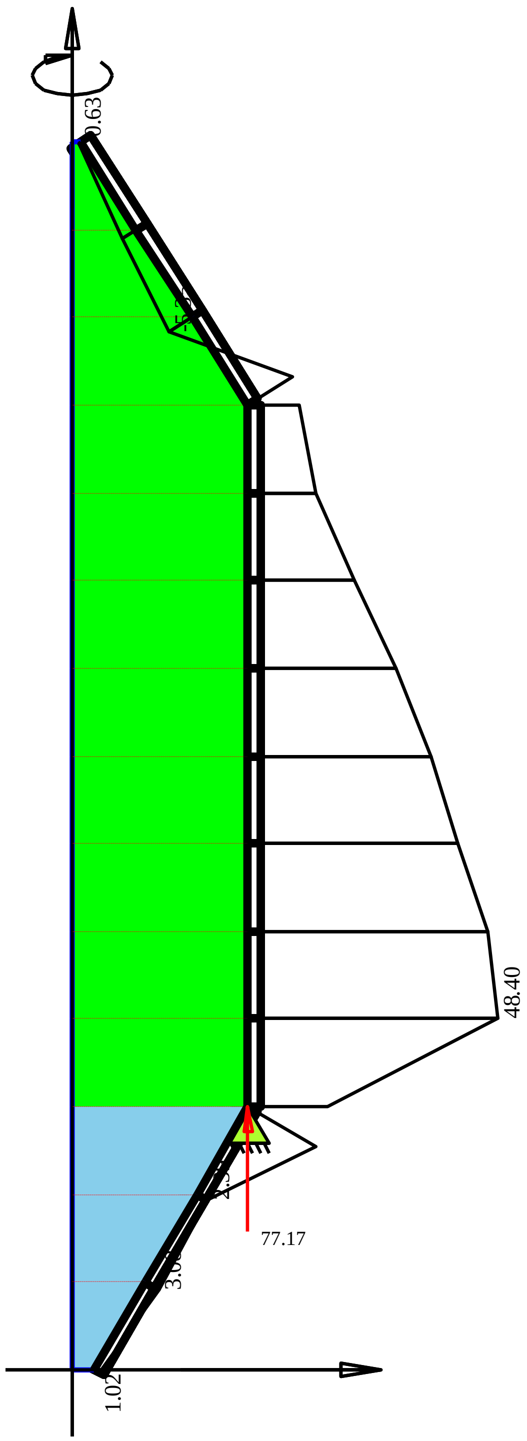

Figure 2.101 Redial force *Nr* [kN/m]

2.21 References

[1] *Ahrens, H.* and *Winselmann, D.* (1984): "Eine iterative Berechnung von Flächengründungen nach dem Steifemodulverfahren". Finite Elemente Anwendungen in der Baupraxis Verlag W. Ernst & Sohn, München.

[2] *Bakhoum, M.* (1992): "Structural Mechanics". Cairo, Egypt.

[3] *Booker, J. R.* and *Small, J. C.* (1983): "The analysis of liquid storage tanks on deep elastic foundation". Int. J. Numer. Anal. Methods Geomech. 7, 187-207.

[4] *Borowicka, H.* (1939): Druckverteilung unter elastischen Platten, Ingenieur-Archiv, Band 10, S. 113-125.

[5] *Das, B. M.* (1997): "Advanced soil mechanics", 2nd ed., USA, Tailor & Francis.

[6] *El Gendy M.* and *El Gendy A.* (2015): "Analysis and Design of Slab Foundations by FE-Method- Program *ELPLA* 10". GEOTEC Software Inc., Canada.

[7] *El Gendy, M.* (2003): "Numerical Modeling of Rigid Circular Rafts on Consolidated Clay Deposits". Int. Workshop on Geotechnics of Soft Soils-Theory and Practice. Vermeer, Schweiger, Karstunen & Cudny (eds.).

[8] *El Gendy, M.* (2006): "Developing stress coefficients for raft-deformation on a thick clay layer". Vol. 41, No. 3, September 2006, pp. 73-108. Scientific Bulletin, Faculty of Engineering, Ain Shams University, Cairo, Egypt.

[9] *El Gendy, O.* (2016): "Behavior of Tanks under Static and Cyclic Loading". MSc Thesis, Port Said University.

[10] *EL Mezaini, N.* (2006): "Effects of soil-structure interaction on the analysis of cylindrical tanks". Practice periodical on structural design and construction, Vol. 11, No. 01, Pages 50 -57.

[11] *Ghali, A.* (2000): "Circular storage tanks and silos – 2nd edition", by E & FN spon – 11 New Fetter Lane, London EC4P 4EE.

[12] *Godbout, S./ Marquis, A./ Fafard, M./ Picard, A.* (2003): Analytical determination of internal forces in a cylindrical tank wall from soil, liquid, and vehicle loads, Canadian Biosystems Engineering/Le géniedes biosystèmes au Canada 45: 5.7-5.14.

[13] *Grafton, P. E.* and *Strome, D. R.* (1963): "Analysis of Axis-Symmetric Shells by the Direct Stiffness Method," AIAA Journal, Vol. 1, No. 10, pp. 2342-2347.

[14] *Graßhoff, H.* (1955): "Setzungsberechnungen starrer Fundamente mit Hilfe des kennzeichnenden Punktes". Der Bauingenieur, S. 53-54.

[15] *Hauso, A.* (2014): "Analysis methods for thin concrete shells of revolution", M.Sc. Thesis, Faculty of Engineering, Norwegian University of Science and Technology.

[16] *Hemsley, J. A.* (1998): "Elastic analysis of raft foundations", Thomas Telford Ltd, 1 Heron Quay, London.

[17] *Hibbitt, Karlsson* and *Sorenson* (2008): "ABAQUS 6.8: A computer software for finite element analysis", *Hibbitt, Karlsson and Sorenson Inc*., Rhode Island, USA.

[18] *Houchmand Naïmi* (1957): Beiträge zur Anwendung der Schalentheorie bei Bogenstaumauern, Promotionsarbeit, Eidgenössischen Technischen, Hochschule in Zürich.

[19] *Janssen, H. A.* (1895): "Versuche über Getreidedruck in Silozellen". VDI, Zeitschrift, Düsseldorf, Band 39, Aug. 31, 1885, S. 1045-1049.

[20] *Kany, M.* (1974): "Berechnung von Flächengründungen", 2. Auflage Verlag Ernst & Sohn, Berlin.

[21] *Kany, M.*, *El Gendy M.* and *El Gendy A.* (2008): "Analysis and Design of Slab Foundations by FE-Method- Program *ELPLA* 9.2". GEOTEC Software, Zirndorf, Germany.

[22] *Karaşin, H./ Gülkan, P./ Aktas, G.* (2014): A Finite Grid Solution for Circular Plates on Elastic Foundations, KSCE Journal of Civil Engineering (2015) 19(4):1157-1163.

[23] *Kukreti, A. & Siddiqi, Z.* (1997): "Analysis of fluid storage tanks including foundation-superstructure interaction using differential quadrature method". Appl. Math. Modeling 1997, 21:193-205, April.

[24] *Kukreti, A., Zaman, M.* and *Issa, A.* (1993): "Analysis of fluid storage tanks including foundation-superstructure interaction". Appl. Math. Modelling 1993, Vol. 17, December.

[25] Mathworld.wolfram.com

[26] *Mansour, I.* (2018): "Analysis and Design of Silos Using Finite Elements". M.Sc., Sudan University of Science and Technology

[27] *Melerski, E. S.* (1991), "Simple elastic analysis of axisymmetric cylindrical storage tanks", Journal of Structural Engineering, Vol. 117, No. 11, Pages 3239-3260.

[28] *Melerski, E.* (2006): "Design analysis of beams, circular plates and cylindrical tanks on elastic foundations – 2nd edition". Taylor & Francis group, London, UK.

[29] *Mistríková, Z & Jendželovský, N* (2012): "Static analysis of the cylindrical tank resting on various types of subsoil", Journal of civil engineering and management, Vol. 18(5): 744-751.

[30] *Mobarak, W.* (2010): "Effect of Tie Girders on Piled Footing in Port Said", M.Sc. Thesis, Faculty of Engineering, Suez Canal University.

[31] *Nishida, Y.* (1956): "A brief note on compression index of soils". Journal of SMFE Div., ASCE, July, p 1027 (1-14).

[32] *Ohde, J.* (1942): "Die Berechnung der Sohldruckverteilung unter Gründungskörpern Der Bauingenieur". Heft 14/16, S. 99-107 - Heft 17/18 S. 122-127.

[33] *Percy, J. H., Pian, T. H. H., Klein, S.,* and *Navaratna, D. R.* (1965): "Application of matrix displacement method to linear elastic analysis of shells of revolution." AIAA Journal, Vol. 3, No. 11, pp. 2138-2145.

[34] *Reda, A.* (2009): "Optimization of Reinforced Concrete Piled Raft", M.Sc. Thesis, Faculty of Engineering, Suez Canal University.

[35] *Rockey, K. C., Evans, H. R., Griffiths, D. W.* and *Nethercot, D. A.* (1975): "The Finite Element Method- A Basic Introduction for Engineers", by Crospy Lockwood Staples, London.

[36] *Samangany, A.Y., Naderi R., Talebpur M. H. and Shahabi H.* (2013): "Static and Dynamic Analysis of Storage Tanks Considering Soil-Structure Interaction", International Research Journal of Applied and Basic Sciences, Vol. 6(4), 515-532.

[37] *Szilard, R., Ziesing* and *Pickhardt* (1986): "Basic- Programme für Baumechanik und Statik". Wilhelm Ernst und Sohn Verlag für Architektur und technische Wissenschaften, Berlin.

[38] *Terzaghi, K., Peck, R.B.* and *Mesri, Gh.* (1996), "Soil mechanics in engineering practice", 3rd Ed., John Wiley, New York.

[39] *Timoshenko, S. & Woinowsky-Krieger S.* (1959): "Theory of plates and shells". McGraw- Hill Book Co. Singapore.

[40] *Utku, M.,* and *Inceleme, I.* (2000): The Analysis of the Stability of General Slip Surfaces, Geotechnique, 15(1): 79-93.

[41] *Ventsel, E.* and *Krauthammer, T.* (2001): "Thin Plates and Shells: Theory, Analysis and Applications". Marcel Dekker, INC., New York.

[42] *Vichare, S. & Inamdar, M.* (2010): "An analytical solution for cylindrical concrete tank on deformable soil", International journal of advanced structural engineering, Vol. 2, No. 1, Pages 71-93, Islamic Azad university, south Tehran branch.

[43] *Winkler, E.* (1867): " Die Lehre von der Elastizität und Festigkeit". Dominicus, Prag.

[44] www.wolframalpha.com/entities/plane_curves.

[45] *Zaman, M.* and *Koragappa, N.* (1989): "Analysis of tank-foundation-half-space interaction using an energy approach". Appl. Math. Modelling, Vol. 13, February.

[46] *Zienkiewicz, O. C.* and *Cheung, Y. K.* (1965): "Plates and Tanks on Elastic Foundations - an Application of Finite Element Method". International Journal of Solids Structures Vol. 1, pp. 451-461, Pergamon.

[47] *Zienkiewicz, O. C.* and *Cheung, Y. K.* (1967): "The Finite Element Method in Structural and Continuum Mechanics". Berkshire, England, by McGraw-Hill Publishing Company Limited.

[48] *Zienkiewicz, O. C.* and *Taylor, R. L.* (1967): "The Finite Element Method – Vol. 2: Solid Mechanics". Berkshire, England, by McGraw-Hill Publishing Company Limited.

[49] *Zingoni, A.* (1997): "Shell Structures in Civil and Mechanical Engineering". Thomas Telford publisher, Thomas Telford services Ltd, 1 Heron Quay, London E14 4JD